



NATIONAL TECHNICAL UNIVERSITY OF ATHENS

SCHOOL OF CIVIL ENGINEERING

DEPARTMENT OF WATER RESOURCES & ENVIRONMENTAL ENGINEERING

Diploma Thesis:

**“MATHEMATICAL SIMULATION OF THE EFFECT
OF SEDIMENT ON FLOOD FLOWS”**



Author: Leventis Pantelis

Supervisor: A. I. Stamou, Professor, NTUA

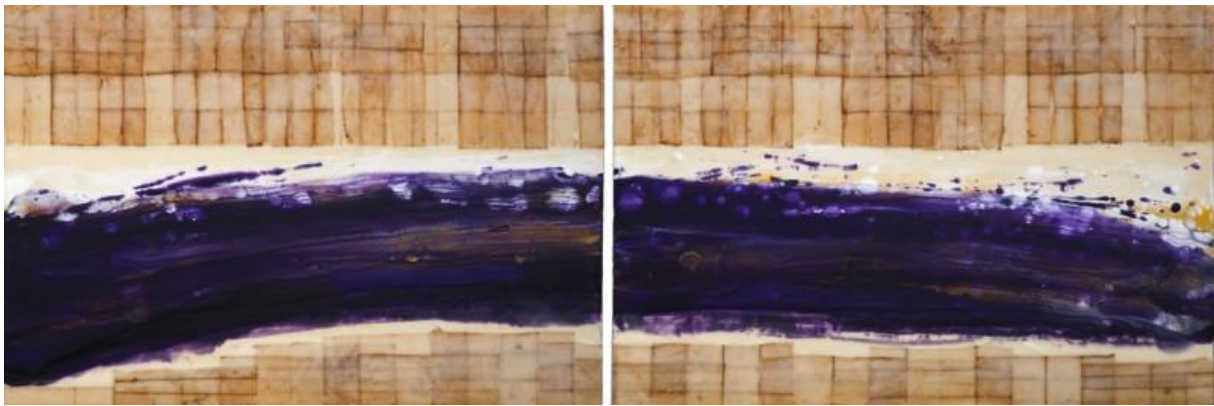
Athens, November 2018



ΕΘΝΙΚΟ ΜΕΤΣΟΒΙΟ ΠΟΛΥΤΕΧΝΕΙΟ
ΣΧΟΛΗ ΠΟΛΙΤΙΚΩΝ ΜΗΧΑΝΙΚΩΝ
ΤΟΜΕΑΣ ΥΔΑΤΙΚΩΝ ΠΟΡΩΝ ΚΑΙ ΠΕΡΙΒΑΛΛΟΝΤΟΣ

Διπλωματική Εργασία:

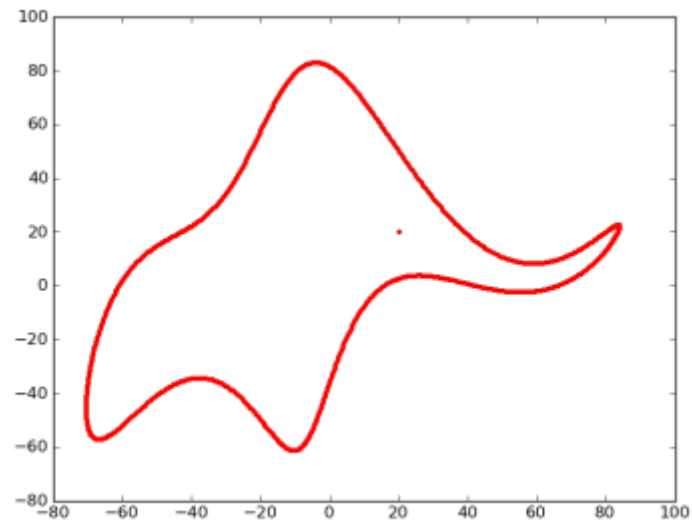
“ΜΑΘΗΜΑΤΙΚΗ ΠΡΟΣΟΜΟΙΩΣΗ ΤΗΣ ΕΠΙΔΡΑΣΗΣ ΤΩΝ ΦΕΡΤΩΝ ΥΛΙΚΩΝ ΣΕ ΠΛΗΜΜΥΡΙΚΕΣ ΡΟΕΣ”



Φοιτητής: Λεβέντης Παντελής

Επιβλέπων: Α. Ι. Στάμου, Καθηγητής, ΕΜΠ

Αθήνα, Νοέμβριος 2018



With four parameters I can fit an elephant, and with five I can make him wiggle his trunk.

John von Neumann

Ευχαριστίες/ Acknowledgements (in Greek)

Τελειώνοντας τις σπουδές μου θέλω να ευχαριστήσω όσους με στήριξαν σε αυτή την προσπάθεια.

Αρχικά θέλω να ευχαριστήσω τους γονείς μου, Νίκο και Ελένη, για όσα μου έχουν προσφέρει και γιατί αποτελούν για μένα πρότυπο εργατικότητας, τιμιότητας και ηθικής.

Ευχαριστώ επίσης τον επιβλέποντα καθηγητή, κύριο Αναστάσιο Στάμου, χάρις στον οποίο γνώρισα το αντικείμενο της Υπολογιστικής Ρευστομηχανικής, για την ανάθεση του πολύ ενδιαφέροντος θέματος της διπλωματικής μου εργασίας και για την άριστη συνεργασία.

Ευχαριστώ θερμά το νέο ερευνητή Ανδρέα Παπαδημητρίου, ο οποίος με βοήθησε στην εγκατάσταση και χρήση του λογισμικού που χρησιμοποίησα, καθώς και στη συγγραφή κώδικα.

Ευχαριστίες οφείλονται και στο συνάδελφο Γιώργο Μαρκόπουλο, ο οποίος ανέπτυξε, στα πλαίσια της δικής του διπλωματικής εργασίας, το υδροδυναμικό μοντέλο της πλημμύρας της Μάνδρας που χρησιμοποίησα.

Τέλος, ευχαριστώ τη γραφίστρια Μαρία Κρητικού για τη βοήθεια στην εκμάθηση προγράμματος επεξεργασίας εικόνας. Το πρόγραμμα χρησιμοποιήθηκε για την ενσωμάτωση εικόνων από τα πειραματικά δεδομένα στα γραφήματα υπολογιστικών αποτελεσμάτων.

Λεβέντης Παντελής

Abstract

In the present study TELEMAC-MASCARET system was used to simulate the effect of sediment transport and geomorphological changes on the November 15th, 2017 Mandra flood. SISYPHE module was used for the sediment transport/morphological model, fully coupled with a TELEMAC-2D hydrodynamic model. Flash floods (FF) are strong and fast flows that occur from a few minutes to several hours after rainfall (Grutfest & Huber, 1991). They have been associated with intense soil erosion, which results in sediment and debris transport. These occur mainly within catchments in arid and semi-arid areas lacking vegetation, as are many cases in the Mediterranean basin. Climate change has been suggested by recent studies to increase the incidence and the severity of rainfall events as well as the desertification rate of vast areas (IPCC, 1995). The last is expected to lead to an increase in the erosion rate in these areas and consequently the effect of solid materials in flood flows. 2D mathematical models are widely used for flood simulations, where the depth averaged values can be considered. This renders the simulations of natural meandering rivers and channel bends a challenge, due to the fact that the secondary current effects play an important role in both the hydrodynamic flow regime, and the sediment transport/geomorphological processes. In order to study this effect, several simulations of the Yen and Lee (1995) experiments were conducted. The models were calibrated (A. Mendoza et al., 2017) and the predictions of 12 widely used sediment transport formulas were compared to the experimental data. Van Rijn sediment transport formula (1989) predicted a final riverbed morphology that was consistent with the experimental measurements and was incorporated in the Mandra flood model.

Keywords: Flash Flood; Hydrodynamics; Sediment transport; Geomorphology; Benchmark; Numerical Modelling; Attica; Mandra; TELEMAC-2D; SISYPHE.

Εκτενής Περίληψη/ Extended Abstract (in Greek)

1. Εισαγωγή

Οι Ξαφνικές Πλημμύρες (ΞΠ) είναι (Grutfest & Huber, 1991) γρήγορες ροές στην επιφάνεια της Γης και προκαλούνται από έντονη βροχόπτωση σε μικρό χρονικό διάστημα. Είναι από τα πιο καταστροφικά φυσικά φαινόμενα και έχουν ως αποτέλεσμα την απώλεια ανθρώπινων ζώων, αλλά και οικονομικές επιπτώσεις σε παγκόσμια κλίμακα (E. Gaume et al., 2008). Το μέσο ετήσιο κόστος των φυσικών καταστροφών, παγκοσμίως, ανέρχεται σε 40 εκατ. € (Munich Re, 2003). Ένα σημαντικό μέρος αυτών οφείλεται σε ΞΦ. Ένα μόνο επεισόδιο ΞΠ προξένησε καταστροφές αξίας 1.2 εκατ. € στην περιοχή της Gard, στη νότια Γαλλία, το 2002, ενώ στην περίπτωση της πλημμύρας του ποταμού Aude, το 1999, προκλήθηκαν καταστροφές αξίας 3.3 εκατ. € (Huet et al., 2003). Όσο μεγάλες και αν είναι οι επιπτώσεις στην οικονομία, δεν μπορούν να συγκριθούν με τις απώλειες ανθρώπινων ζώων. Οι τελευταίες, είναι σημαντικές τόσο στις μεσογειακές χώρες, αλλά και ευρύτερα. Χαρακτηριστικό είναι το παράδειγμα της πλημμύρας της Βαρκελώνης (1962), που στοίχισε τη ζωή σε πάνω από 400 κατοίκους (L. Bustow et al., 1964). Αντίστοιχης έντασης ήταν και τα φαινόμενα στο Piemonte της Ιταλίας, το 1968 και 1994, με 72 και 69 νεκρούς αντίστοιχα (Ferro, 2005/ Guzzetti et al., 2005). Η ανά χείρας διπλωματική εργασία παρουσιάζει πτυχές της μεγάλης ΞΠ που έπληξε την περιοχή της Μάνδρας στις 15 Νοεμβρίου του 2017 και στοίχισε τη ζωή σε 23 ανθρώπους.

Τα τελευταία χρόνια, αρκετές μελέτες προτείνουν συσχέτιση μεταξύ των πολύ έντονων βροχοπτώσεων, και κατ' επέκταση των ΞΠ, με την κλιματική αλλαγή (IPCC, 1995). Αυτό αναμένεται να οδηγήσει σε αύξηση της συχνότητας εμφάνισης ΞΠ, κάτι που εκτιμάται ότι θα έχει ιδιαίτερα δυσμενείς επιπτώσεις σε ξηρές περιοχές, όπως η λεκάνη της Μεσογείου (Alpert et al., 2002). Οι ΞΠ τείνουν να είναι πιο καταστροφικές όταν εκδηλώνονται σε αστικό περιβάλλον, το οποίο χαρακτηρίζεται από αδιαπέρατες επιφάνειες (Davis, 2001). Ένας ακόμα παράγοντας που συνταλεί σε αυτό είναι το ότι η μεγέθυνση των πόλεων δεν συνοδεύεται πάντα από έργα αντιπλημμυρικής προστασίας (C. Parathanasiou et al., 2012). Τα έργα υποδομής αναπτύσσονται πολλές φορές για να καλύψουν συγκεκριμένες ανάγκες που προκύπτουν από την κοινωνικοοικονομική μεγέθυνση αγνοώντας τις ενδεχομένως αρνητικές επιπτώσεις που αυτά θα έχουν στην παροχέυτηση των πλημμυρικών ροών (C. Parathanasiou et al., 2015). Τέτοια είναι η περίπτωση έργων που προκαλούν υδρομορφολογική αλλοίωση σε μια λεκάνη απορροής ή αυξάνουν τις αδιαπέρατες επιφάνειες.

Οι ΞΠ σχετίζονται με έντονες γεωμορφολογικές αλλοιώσεις (Εικόνα 1), που προκύπτουν από τη συμπάρασυρση και απόθεση στερεών από τις πλημμυρικές ροές. Αναμένεται ότι οι γεωμορφολογικές αλλοιώσεις θα αυξηθούν στο μέλλον, λόγω της ερημοποίησης περιοχών που φτάνουν ως και το 35% της επιφάνειας της στεριάς, οι οποίες θα είναι πιο επιρρεπείς στη διάβρωση (UNEP). Η επίδραση των στερεών στα υδροδυναμικά χαρακτηριστικά των πλημμυρικών ροών δεν λαμβάνεται υπόψη στα διάφορα μοντέλα, ως σήμερα.



Εικόνα 1. Εναπόθεση φερτών σε ρέματα κατά τις πλημμύρες του Αυγούστου του 2005 σε περιοχές της Ελβετίας. (πηγή: wileyonlinelibrary.com/journal/espl).

2. Βιβλιογραφική έρευνα

Ο σκοπός της βιβλιογραφικής έρευνας είναι η επιλογή του MM που θα χρησιμοποιηθεί για τη διπλωματική εργασία. Αυτό θα πρέπει να πληροί τα ακόλουθα κριτήρια:

1. Να είναι ελεύθερα διαθέσιμο στο διαδίκτυο
2. Να έχει χρησιμοποιηθεί επαρκώς και να θεωρείται αξιόπιστο
3. Να διαθέτει ανοιχτό κώδικα που να επιτρέπει στον χρήστη τυχούσες αλλαγές
4. Να μπορεί να λειτουργήσει με μια πληθώρα εξισώσεων στερεομεταφοράς για την μελέτη και σύγκρισή των αποτελεσμάτων τους με πειραματικά δεδομένα

Τα Μαθηματικά Μοντέλα (MM) είναι βασικό εργαλείο για προσομοιώσεις ΞΠ. Η ανάπτυξη της τεχνολογίας στη σύγχρονη εποχή συντέλεσε στο να καταστήσει οικονομικά εφικτή η αγορά προσωπικού υπολογιστή από ένα σημαντικό μέρος του πληθυσμού. Αυτό οδήγησε στην επέκταση της χρήσης των MM, τα οποία μέχρι πρότινος χρησιμοποιούνταν για ερευνητικούς σκοπούς, στον κλάδο των μελετητών μηχανικών. Οι κύριες μέθοδοι που χρησιμοποιούνται για τη διακριτοποίηση του χώρου είναι οι μέθοδος των πεπερασμένων διαφορών (FDM), η μέθοδος των πεπερασμένων στοιχείων (FEM) και η μέθοδος των πεπερασμένων όγκων (FVM).

Τα MM χρησιμοποιούνται για ανάλυση κινδύνου τόσο στην υπάρχουσα κατάσταση, όσο και σε μελλοντικές καταστάσεις, αλλά έχουν και έναν ευρύτερο ρόλο (Van Duivedijk, 2005). Πιο συγκεκριμένα, χρησιμοποιούνται για τον έλεγχο της αποτελεσματικότητας αντιπλημμυρικών έργων, για την εκτίμηση των αποτελεσμάτων της πλημμύρας στα έργα μιας περιοχής, καθώς και για κατάστρωση χαρτών πλημμυρικού κινδύνου. Χρησιμοποιούνται τέλος και για την ανάπτυξη Συστημάτων Έγκαιρης Προειδοποίησης (ΣΕΠ) που στόχο έχουν την ενημέρωση των πολιτών για τυχούσα επερχόμενη πλημμύρα.

Τα MM για την προσομοίωση ΞΠ μπορεί να είναι στοχαστικά, να βασίζονται δηλαδή στην ανάλυση της συχνότητας της πλημμύρας και ντετερμινιστικά, δηλαδή να βασίζονται στις φυσικές ιδιότητες των παραμέτρων που επηρεάζουν μια ΞΠ (Mambretti et al., 2008). Τα ντετερμινιστικά MM είναι συχνά μοντέλα διόδευσης πλημμύρας, που εκτιμούν την εξέλιξη του υδρογραφήματος της διατομής εισόδου κατά μήκος μιας κοίτης ποταμού ή μιας πλημμυρικής λεκάνης. Τα υδροδυναμικά μοντέλα 1D επιλύουν 2 εξισώσεις για να προβλέψουν την εξέλιξη του υδρογραφήματος: την εξίσωση της συνέχειας και την εξίσωση της διατήρησης της γραμμικής ορμής. Υπολογίζουν 2 μεταβλητές της ροής, την μέση ταχύτητα (U) και τη στάθμη του νερού (H).

Τα μοντέλα διόδευσης πλημμύρας μπορεί να είναι υδρολογικά ή υδροδυναμικά. Τα υδρολογικά μοντέλα επιλύουν την εξίσωση διατήρησης της μάζας και μια εμπειρική σχέση για τον υπολογισμό του υδρογραφήματος εξόδου. Είναι πιο απλουστευτικά από τα υδροδυναμικά και θεωρούνται ακατάλληλα για την περίπτωση ταχέως ανυψούμενων υδρογραφημάτων εισόδου, όπως συμβαίνει με τις ΞΠ, γιατί αμελούν την επίδραση από τα ανάντη. Στα υδροδυναμικά μοντέλα αντίθετα, λαμβάνονται υπόψη αυτά τα φαινόμενα και γι' αυτό ενδείκνυνται για προσομοιώσεις ΞΠ. Αυτά επιλύουν τις εξισώσεις Navier Stokes για να υπολογίσουν την παροχή, την ταχύτητα και τις στάθμες σε θέσεις της ροής.

Στις μέρες μας, τα υδροδυναμικά μοντέλα 1D και 2D χρησιμοποιούνται στις περισσότερες περιπτώσεις για ανάλυση πλημμυρικού κινδύνου (Kvočka et al., 2017), παρότι τα περισσότερα προγράμματα διαθέτουν και μοντέλα 3D. Είναι σημαντικό να βρεθεί μια μέση λύση μεταξύ της απαιτούμενης ακρίβειας των αποτελεσμάτων και των διατιθέμενων υπολογιστικών δυνατοτήτων. Η επιλογή των διαστάσεων του μοντέλου εξαρτάται από το μέγεθος της περιοχής μελέτης (Huybrechts et al., 2010). Τα μοντέλα 1D χρησιμοποιούνται κυρίως για περιοχές μεγάλης έκτασης σε αντίθεση με τα 3D μοντέλα που ενδείκνυνται για μικρές περιοχές μελέτης. Τα 2D χρησιμοποιούνται σε ενδιάμεσες περιπτώσεις. Τα μοντέλα 2D χρησιμοποιούνται για τη προσομοίωση ΞΠ για τον επιπρόσθετο λόγο ότι υπολογίζουν τα μέσα καθ' ύψος μεγέθη, που θεωρείται ικανοποιητική σύμβαση για τις περιπτώσεις όπου η επιφάνεια που καταλαμβάνεται απ' την πλημμύρα είναι πολύ μεγαλύτερη από το βάθος του νερού.

Διάφορα προγράμματα διατίθενται σήμερα, που μπορούν να χρησιμοποιηθούν για προσομοιώσεις ΞΠ. Κάποια από τα πιο γνωστά είναι το CCHE2D-Flow που αναπτύχθηκε από το Πανεπιστήμιο του Μισισίπι, το HEC-RAS που είναι πιθανότατα το πιο διαδεδομένο και επάρχει σε εκδόσεις 1Δ, 2Δ και 3Δ, το MIKE FLOOD που είναι ένα πακέτο ειδικά σχεδιασμένο για την προσομοίωση πλημμυρικών φαινομένων. Τέλος υπάρχει και η πλατφόρμα λογισμικού TELEMAC-MASCARET, η οποία περιλαμβάνει διάφορα υπομοντέλα που καλύπτουν ένα μεγάλο εύρος εφαρμογών.

Η βιβλιογραφική έρευνα, που έγινε στα πλαίσια της διπλωματικής εργασίας, αφορά εκτός από τα διαθέσιμα MM και τις εξισώσεις στερεομεταφοράς. Με την πάροδο των χρόνων μια πληθώρα από εξισώσεις στερεομεταφοράς έχουν αναπτυχθεί με σκοπό την πρόβλεψη του ρυθμού στερεομεταφοράς. Ο ρυθμός αυτός αφορά συνεκτικό ή μη συνεκτικό ιζήμα ή μια μίξη αυτών. Η συνολική στερεομεταφορά μπορεί να αναλυθεί σε 2 συνιστώσες, την στερεομεταφορά σε σύρση και τη στερεομεταφορά σε αιώρηση. Η τελευταία είναι και η πιο σημαντική για την περίπτωση του μη συνεκτικού ιζήματος, το οποίο χρησιμοποιήθηκε στις προσομοιώσεις των μοντέλων της διπλωματικής εργασίας. Στον Πίνακα 1 παρουσιάζονται κάποιες βασικές παράμετροι των εξισώσεων στερεομεταφοράς, όπου: ρ_s η πυκνότητα του ιζήματος, ρ_w η πυκνότητα του νερού, g η επιτάχυνση της βαρύτητας, D_{50} η διάμετρος του κόκκου ιζήματος από την οποία το 50% των κόκκων του δείγματος έχει μικρότερη διάμετρο, τ_b η διατμητική τάση πυθμένα και ν η κινηματική συνεκτικότητα.

Πίνακας 1. Γενικές παράμετροι στερεομεταφοράς σε ποτάμιο περιβάλλον.

Γενικές Παράμετροι	
Σχετική πυκνότητα	$\Delta = \frac{\rho_s - \rho_w}{\rho_w}$
Αδιάστατη διάμετρος κόκκου ιζήματος	$D_* = \left(\frac{g\Delta}{\nu}\right)^{1/3} D_{50}$
Κρίσιμη παράμετρος Shields [Προσέγγιση καμπύλης Shields – Van Rijn (1993)]	$\theta_{cr} = \begin{cases} 0.24D_*^{-1}, & 1 \leq D_* \leq 4 \\ 0.14D_*^{-0.64}, & 4 < D_* \leq 10 \\ 0.04D_*^{-0.1}, & 4 < D_* \leq 20 \\ 0.013D_*^{0.29}, & 20 < D_* \leq 150 \\ 0.055, & D_* > 150 \end{cases}$
[Soulsby (1997)]	$\theta_{cr} = \frac{0.3}{1 + 1.2D_*} + 0.55[1 - \exp(-0.02D_*)]$
Επιφανειακή τριβή	$\mu = \frac{C'_F}{C_F}$, όπου $C'_F = 2 \left[\frac{k}{\log\left(\frac{12h}{k_s}\right)} \right]^2$, $k=0.40$ (von Karman)
Ταχύτητα καθίζησης μη συνεκτικού ιζήματος	$W_s = \begin{cases} \frac{(s-1)gD_{50}^2}{18\nu}, & D_{50} \leq 10^{-4}m, \\ \frac{10\nu}{D_{50}} \left[\sqrt{1 + 0.01 \frac{(s-1)gD_{50}^3}{\nu}} - 1 \right], & 10^{-4} < D_{50} \leq 10^{-3}m \\ 1.1\sqrt{(s-1)gD_{50}}, & D_{50} > 10^{-3}m \end{cases}$
Soulsby (1997)	$W_s = \frac{\nu}{D_{50}} [(10.36^2 + 1.049D_*^3)^{1/2} - 10.36]$
Παράμετρος Shields	$\theta = \frac{\tau_b}{(\rho_s - \rho_w)gD_{50}}$
Ταχύτητα διάτμησης	$U_* = \sqrt{\frac{\tau_b}{\rho_w}}$

Στην επόμενη σελίδα παρουσιάζονται μερικές ευρύτατα χρησιμοποιούμενες εξισώσεις στερεομεταφοράς, καθώς και το εύρος εφαρμογής τους. Η στερεοπαροχή Q_b εκφράζεται σε m^2/s , ενώ σε κάποιες περιπτώσεις υπολογίζεται πρώτα η αδιαστατοποιημένη παροχή στερεομεταφοράς Φ_b . Η στερεοπαροχή χρησιμοποιείται στη συνέχεια για την εκτίμηση της εξέλιξης πυθμένα μέσω της εξίσωσης Exner.

- Εξίσωση στερεομεταφοράς ιζήματος σε σύρση Rottner (1959)

$$Q_b = \sqrt{(s-1)gD_{50}^3} \left\{ \frac{\sqrt{U^2 + V^2}}{(s-1)gD_{50}} [0.0667 \left(\frac{D_{50}}{H}\right)^{2/3} - 0.14] - 0.778 \left(\frac{D_{50}}{H}\right) \right\}$$

- Εξίσωση στερεομεταφοράς ιζήματος σε σύρση Nielsen (1992)

$$Q_b = \sqrt{(s-1)gD_{50}^3} \left(\frac{12\tau_b}{\rho_w(s-1)gD_{50}} - 0.05 \right) \sqrt{\frac{\tau_b}{\rho_w(s-1)gD_{50}}}$$

- Εξίσωση στερεομεταφοράς ιζήματος σε σύρση Meyer-Peter & Muller (1947)

$$\Phi_b = \begin{cases} 0, \alpha\nu \theta < \theta_{cr} \\ 8(\theta - \theta_{cr})^{3/2}, \alpha\nu \theta > \theta_{cr} \end{cases}$$

$$Q_b = \Phi_b \sqrt{g(s-1)D_{50}^3}$$

- Εξίσωση στερεομεταφοράς ιζήματος σε σύρση Van Rijn (1993)

$$\Phi_b = \begin{cases} 0, \alpha\nu \theta < \theta_{cr} \\ 0.053D_*^{-0.3} \left(\frac{\theta - \theta_{cr}}{\theta_{cr}}\right)^{2.1}, \alpha\nu \theta > \theta_{cr} \end{cases}$$

$$Q_b = \Phi_b \sqrt{g(s-1)D_{50}^3}$$

- Εξίσωση στερεομεταφοράς ιζήματος σε σύρση Schoklich (1962)

$$q_{cr} = 0.21J^{-1.12} \sqrt{gD_{16}^3}, \text{ όπου } J \text{ η κλίση ενέργειας}$$

$$q = H\sqrt{U^2 + V^2} \text{ η παροχή}$$

$$Q_b = \begin{cases} 0, \alpha\nu q \leq q_{cr} \\ \frac{2.5}{s} J^{3/2} (q - q_{cr}), \alpha\nu q > q_{cr} \end{cases}$$

- Εξίσωση στερεομεταφοράς ιζήματος σε σύρση Cheng (2002)

$$\Phi_b = 13.0\theta^{1.5} \exp\left(-\frac{0.05}{\theta^{1.5}}\right)$$

$$Q_b = \Phi_b \sqrt{g(s-1)D_{50}^3}$$

- Εξίσωση συνολικής στερεομεταφοράς Karim-Kennedy (1983)

$$Q_t = k_1 \left[\frac{\sqrt{U^2 + V^2}}{\sqrt{g(s-1)D_{50}}} \right]^{2.97} \left(\frac{U_*}{W_s} \right)^{1.47} \sqrt{g(s-1)D_{50}^3} \text{ όπου } k_1 = 0.00139$$

- Εξίσωση συνολικής στερεομεταφοράς Engelund-Hansen

$$Q_b = 0.1 \sqrt{(s-1)gD_{50}^3} \left(\sqrt{\frac{\tau_b}{(\rho_s - \rho_w)gD_{50}}} \right)^5 / C_F, \text{ όπου } C_F \text{ ο συντελεστής τριβής.}$$

Ο παρακάτω πίνακας παρουσιάζει το συνιστώμενο εύρος εφαρμογών διαφόρων εξισώσεων στερεομεταφοράς σύμφωνα με τους Karamisheva et al. (2006).

Πίνακας 2. Εύρος εφαρμογών εξισώσεων στερεομεταφοράς (Karamisheva et al., 2006).

Εξίσωση στερεομεταφοράς	Βάθος (m)	Κλίση	D (mm)	V (m/s)
Meyer-Peter & Muller	0.01-1.20	0.0004-0.02	0.4-29.0	0.36-2.90
Scholkitch	0.01-0.22	0.00012-0.055	0.3-4.9	0.24-1.40
Engelund-Hansen	0.06-0.31	0.000055-0.019	0.19-0.93	0.19-1.90
Ackers-White	0.18-11.5	0.000022-0.0015	0.04-4.0	0.33-0.87
Yang	0.01-15.0	0.000043-0.028	0.15-1.7	0.24-1.95
Karim-Kennedy	0.03-5.20	0.00015-0.024	0.14-28.65	0.31-2.84
Van Rijn	0.10-16.0	NA	0.19-3.6	0.34-1.55
Molinas-Wu	1.50-62.2	0.000002-0.0025	0.02-2.6	0.2-2.42
Yang-lim	0.01-16.5	0.0003-0.013	0.02-57.0	NA

3. Η πλατφόρμα λογισμικού TELEMAC-MASCARET

Η πλατφόρμα λογισμικού TELEMAC-MASCARET επιλέχθηκε για τη διπλωματική εργασία γιατί πληροί τα κριτήρια που τέθηκαν προηγουμένως. Πρόκειται για ένα ανοικτό σύστημα από επιμέρους υπομοντέλα που καλύπτουν ένα μεγάλο εύρος εφαρμογών και βασίζεται σε διακριτοποίηση χώρου πεπερασμένων στοιχείων (FEM):

- SISYPHE είναι το υπομοντέλο στερεομεταφοράς και εξέλιξης πυθμένα.
- Το NESTOR αξιοποιεί τα δεδομένα από βυθοκορήσεις σε ποταμούς για προσομοιώσεις μεταβολών του πυθμένα.
- Το MASCARET 1 είναι το υδροδυναμικό μοντέλο 1Δ για προσομοιώσεις με ελεύθερη επιφάνεια
- Το ARTEMIS χρησιμοποιείται για προσομοιώσεις που σχετίζονται με ανεμογενή κύματα σε ακτές και λιμένες.
- Το TELEMAC-2D είναι το υδροδυναμικό μοντέλο 2Δ που χρησιμοποιείται σε προσομοιώσεις που χαρακτηρίζονται από μικρό σε σχέση με την επιφάνεια βάθος.
- Το TELEMAC-3D χρησιμοποιείται για προσομοιώσεις που αφορούν σχετικά μικρής έκτασης περιοχή μελέτης στις οποίες δεν μπορούν να χρησιμοποιηθούν τα μέσα καθ' ύψος μεγέθη.

Για τα μοντέλα που προσομοιώθηκαν στη διπλωματική εργασία χρησιμοποιήθηκε το SISYPHE για την μοντελοποίηση των διεργασιών της στερεομεταφοράς/εξέλιξης πυθμένα άμεσα συζευγμένο με το TELEMAC-2D για το υδροδυναμικό καθεστώς.

Ο κώδικας του TELEMAC-2D επιλύει το ακόλουθο σύστημα διαφορικών εξισώσεων:

$$\frac{\partial h}{\partial t} + u \nabla (h) + h \operatorname{div}(u) = S_h \quad \text{Εξίσωση συνέχειας} \quad (3.1)$$

$$\frac{\partial u}{\partial t} + u \nabla (u) = -g \frac{\partial Z}{\partial x} + S_x + \frac{1}{h} \operatorname{div}(h v_t \nabla u) \quad \text{Εξίσωση διατήρησης ορμής κατά x} \quad (3.2)$$

$$\frac{\partial v}{\partial t} + u \nabla (v) = -g \frac{\partial Z}{\partial y} + S_y + \frac{1}{h} \operatorname{div}(h v_t \nabla v) \quad \text{Εξίσωση διατήρησης ορμής κατά y} \quad (3.3)$$

$$\frac{\partial T}{\partial t} + u \nabla (T) = S_T + \frac{1}{h} \operatorname{div}(h v_t \nabla T) \quad \text{Εξίσωση διατήρησης ιχνοθετών} \quad (3.4)$$

όπου:

- h (m) το βάθος ροής
- u, v (m/s) οι συνιστώσες της ταχύτητας
- t (m/l or °C) παθητικός ιχνοθέτης
- g (m/s²) επιτάχυνση της βαρύτητας
- v_t, v_T (m²/s) σταθερές ορμής και ιχνοθέτη
- Z (m) στάθμη ελεύθερης επιφάνειας
- t (s) χρόνος
- x, y (m) οριζόντιες συντεταγμένες
- S_h (m/s) πηγή του υγρού
- S_T (m/s) πηγή του ιχνηθέτη
- H, u and T είναι οι άγνωστοι

Σε προσομοιώσεις αργά εξελισσόμενων φαινομένων, όπως η παράκτια διάβρωση, το μορφολογικό μοντέλο δεν είναι συζευγμένο με το υδροδυναμικό, σε αντίθεση με τα πλημμυρικά φαινόμενα, που η διάβρωση γίνεται ταυτόχρονα με την προώθηση των γρήγορων επιφανειακών ροών. Αρχικά γίνεται ο υπολογισμός της στερεοπαροχής και στη συνέχεια το SISYPHE επιλύει την εξίσωση Exner για την εξέλιξη του πυθμένα:

$$(1-p) \frac{\partial Z_b}{\partial t} + \frac{\partial(\delta_c c_b)}{\partial t} + \frac{\partial(qt, x)}{\partial x} + \frac{\partial(qt, y)}{\partial y} + n_e - n_d = 0 \quad (3.5)$$

όπου:

- Z_b η στάθμη πυθμένα
- p το πορώδες του πυθμένα
- c_b η συγκέντρωση σε ίζημα της στρώσης ιζήματος σε σύρση

4. Προσομοιώσεις των πειραμάτων Yen & Lee (1995)

Τα πειράματα των Yen και Lee (1995) είναι από τα πιο γνωστά πειράματα στερεομεταφοράς και εξέλιξης πυθμένα και μοντέλα τους προσομοιώθηκαν, στα πλαίσια της διπλωματικής εργασίας, γιατί παρουσιάζουν τα ακόλουθα χαρακτηριστικά:

1. Κεκλιμένο κανάλι με καμπύλο τμήμα και αλουβιακές αποθέσεις στον πυθμένα.
2. Μεταβαλλόμενη ροή.
3. Ίζημα με συγκεκριμένη κοκκομετρική διαβάθμιση (μη ομοιόμορφο).

Τα χαρακτηριστικά που επιλέχθηκαν προσομοιάζουν εκείνα των ΞΠ. Οι μηχανισμοί που σχετίζονται με τη στερεομεταφορά και την εξέλιξη πυθμένα είναι στην πραγματικότητα πολύ πιο σύνθετοι από αυτούς σε ευθύγραμμο κανάλια, λόγω της εγκάρσιας συνιστώσας της ροής σε στροφές και κατ' επέκταση της εγκάρσιας στερεομεταφοράς.

Η πειραματική διάταξη αποτελείται από ένα κανάλι πλάτους 1m, με ευθύγραμμο τμήματα μήκους 11.5m ανάντη και κατόντη του ημικυκλίου με ακτίνα 4.5m. Η κατά μήκος κλίση είναι 0.2% και η εγκάρσια θ στην αρχική φάση. Ο πυθμένας είναι στρωμένος με 20cm ιζήματος μέσης διαμέτρου κόκκων 1mm και τυπικής απόκλισης 2.5. Κατά τη διάρκεια του πειράματος το κανάλι δεν εφοδιάζεται με επιπλέον ίζημα από τη διατομή εισόδου. Αρχικά η παροχή και το βάθος ροής εισόδου είναι σταθερά, 0.02m³/s και 5.44 cm αντίστοιχα και στη συνέχεια αυτά αυξάνονται γραμμικά, με την εφαρμογή ενός υδρογραφήματος στη διατομή εισόδου, ενώ έπειτα μειώνονται ξανά μέχρι να φτάσουν τις αρχικές τιμές. Τα χαρακτηριστικά των 5 πειραμάτων που διενεργήθηκαν από τους Yen και Lee (1995) παρουσιάζονται στον παρακάτω πίνακα. Η αδιαστατοποιημένη, με το αρχικό βάθος ροής, μεταβολή του πυθμένα μετρήθηκε και παρουσιάστηκαν τα αποτελέσματα στις διατομές μέγιστης διάβρωσης και απόθεσης (Πίνακας 4 και Πίνακας 5).

Πίνακας 3. Χαρακτηριστικά των 5 πειραμάτων των Yen και Lee (1995).

Run	Q _p (m ³ /s)	h _p (m)	T _d (min)
1	0.0750	0.129	180
2	0.0685	0.121	204
3	0.0613	0.113	240
4	0.0530	0.103	300
5	0.0436	0.091	420

Πίνακας 4. Αδιαστατοποιημένη μεταβολή πυθμένα στη θέση μέγιστης επίχωσης.

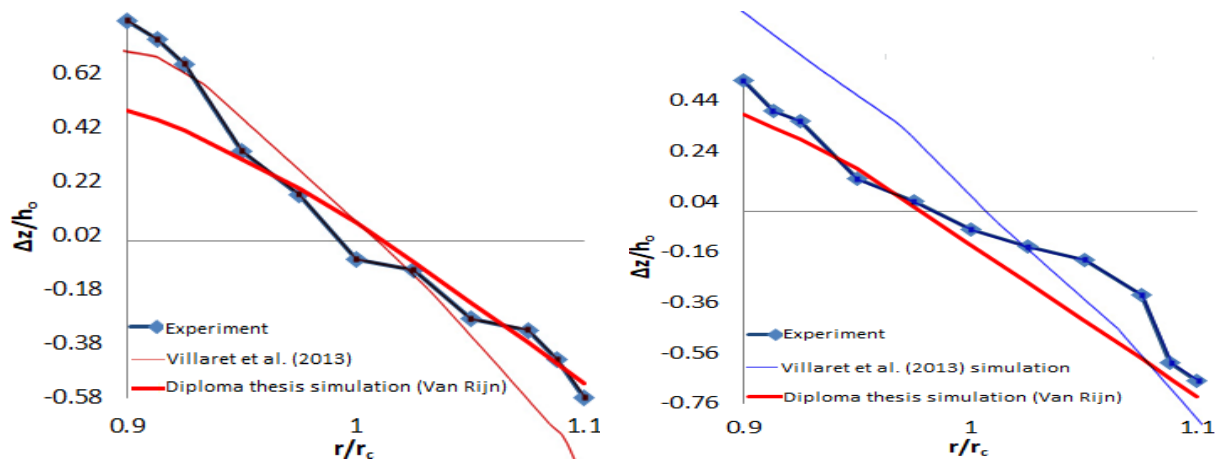
Run	Section	r/r _c										
		0.900	0.913	0.925	0.950	0.975	1.000	1.025	1.050	1.075	1.088	1.100
1	75°	1.13	1.03	0.99	0.86	0.75	0.55	0.30	-0.50	-1.25	-1.47	-1.54
2	75°	0.92	0.81	0.70	0.57	0.35	0.03	-0.11	-0.33	-0.79	-0.88	-1.00
3	75°	0.88	0.81	0.74	0.53	0.30	-0.06	-0.18	-0.24	-0.47	-0.57	-0.65
4	90°	0.81	0.74	0.65	0.33	0.17	-0.07	-0.11	-0.29	-0.33	-0.44	-0.58
5	90°	0.75	0.72	0.63	0.29	-0.02	-0.07	-0.07	-0.13	-0.42	-0.42	-0.40

Πίνακας 5. Αδιαστατοποιημένη μεταβολή πυθμένα στη θέση μέγιστης διάβρωσης.

Run	r/r _c										
	0.900	0.913	0.925	0.950	0.975	1.000	1.025	1.050	1.075	1.088	1.100
1	0.86	0.80	0.73	0.53	0.37	0.29	0.06	-0.66	-1.34	-1.77	-2.06
2	0.83	0.66	0.61	0.51	0.28	0.16	-0.03	-0.35	-1.04	-1.43	-1.62
3	0.82	0.69	0.62	0.40	0.28	0.07	-0.21	-0.66	-0.96	-1.39	-1.55
4	0.52	0.40	0.36	0.13	0.04	-0.07	-0.14	-0.19	-0.33	-0.60	-0.67
5	0.32	0.18	0.08	-0.03	-0.09	-0.08	-0.07	-0.18	-0.24	-0.35	-0.42

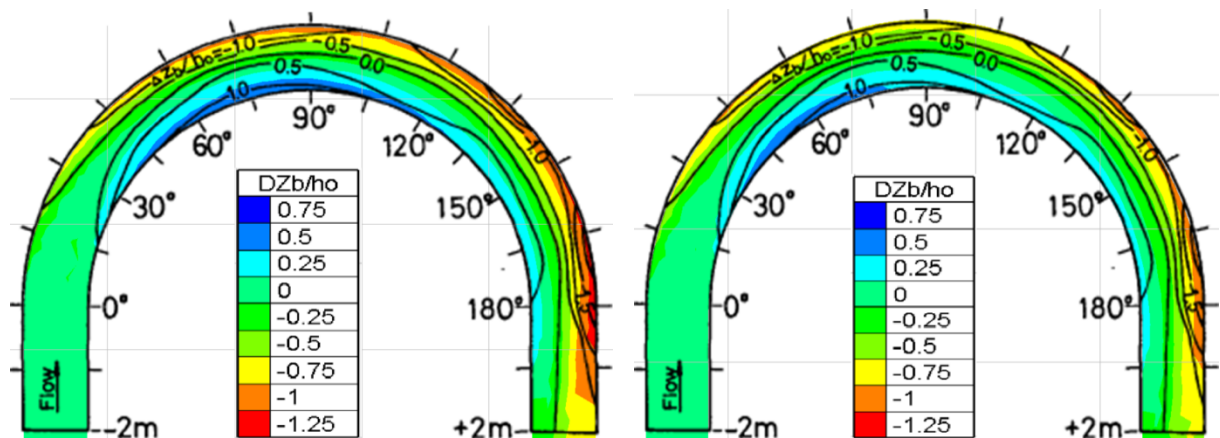
Χρησιμοποιήθηκαν διάφορα μοντέλα για τις προσομοιώσεις των πειραμάτων των Yen & Lee (1995). Αξιοποιήθηκαν όλες οι διαθέσιμες από το λογισμικό εξισώσεις στερεομεταφοράς και προστέθηκαν 7 ακόμα, σε γλώσσα FORTRAN. Αρχικά δομήθηκαν 12 μοντέλα με ισάριθμες εξισώσεις στερεομεταφοράς και με αυτά προσομοιώθηκε το πείραμα 4 (Run-4) με ίζημα ομοιόμορφης κοκκομετρίας. Τα 6 από αυτά που έδωσαν τα καλύτερα αποτελέσματα χρησιμοποιήθηκαν για τις προσομοιώσεις και των 5 πειραμάτων με μη ομοιόμορφο ίζημα.

Ένα σημαντικό κομμάτι των προσομοιώσεων αυτών των μοντέλων ήταν το καλιμπράρισμά τους, ούτως ώστε να λαμβάνεται υπόψη η εγκάρσια συνιστώσα της ταχύτητας και η εγκάρσια στερεομεταφορά. Τα 2D μοντέλα υστερούν σε αυτό το σημείο γιατί θεωρούν μέσες καθ' ύψος τιμές των μεγεθών. Γι' αυτό τον λόγο γίνεται διόρθωση, τόσο ως προς τη διεύθυνση της στερεομεταφοράς, όσο και ως προς τον ρυθμό της. Επιλέχθηκε η προσέγγιση Talmon et al. για τη διεύθυνση της στερεομεταφοράς και εκείνη των Koch & Flokstra για τον ρυθμό της. Η παράμετρος A της δευτερεύουσας ροής στο υδροδυναμικό μοντέλο επιλέχθηκε 12 και η παράμετρος β_2 για τη διόρθωση της διεύθυνσης στερεομεταφοράς επιλέχθηκε 1.6 (A. Mendoza et al., 2017). Τα αποτελέσματα με αυτές τις παραμέτρους ήταν ενθαρυντικά και για το 4^ο πείραμα συγκεκριμένα καλή εκτίμηση έδωσε το μοντέλο με την εξίσωση στερεομεταφοράς Van Rijn (1989). Στην Εικόνα 2 τα αποτελέσματα συγκρίνονται με εκείνα προσομοίωσης με ομοιόμορφο ίζημα 1mm (Villaret et al., 2013), τη μέθοδο του Engelund (1974) για την επίδραση της δευτερεύουσας ροής και την εξίσωση στερεομεταφοράς των Meyer-Peter & Mueller.



Εικόνα 2. Σύγκριση των αποτελεσμάτων μοντέλου με εξίσωση Van Rijn (1989) και μοντέλου με εξίσωση Meyer-Peter & Mueller (Villaret et al., 2013) στις θέσεις μέγιστης απόθεσης (αριστερά) και μέγιστης διάβρωσης (δεξιά) με τα πειραματικά δεδομένα.

Η διερεύνηση αφορούσε τις διαθέσιμες από το λογισμικό εξισώσεις στερεομεταφοράς: Meyer-Peter & Mueller, Einstein-Brown, Hunziker, Engelund-Hansen και Engelund-Hansen & Cholley-Cunge. Σε αυτές προστέθηκαν οι: Cheng, Karim-Kennedy, Ackers-White, Frijlink, Yag Lim, Nielsen και Reid. Η Engelund-Hansen & Cholley-Cunge έδωσε τα καλύτερα αποτελέσματα στις προσομοιώσεις με ομοιόμορφο ίζημα. Αντίθετα στις προσομοιώσεις με μη ομοιόμορφο ίζημα καλά αποτελέσματα έδωσαν οι Meyer-Peter & Mueller, Van Rijn, Cheng, και Reid. Τα αποτελέσματα των δύο τελευταίων παρουσιάζονται στην Εικόνα 3.



Εικόνα 3. Οι ισοϋψείς των αποτελεσμάτων μεταβολής ύψους πυθμένα από τα μοντέλα των εξισώσεων Cheng και Reid σε σχέση με τα πειραματικά δεδομένα για το Πείραμα-1.

5. Χαρακτηριστικά της πλημμύρας της Μάνδρας

Η πόλη της Μάνδρας βρίσκεται στο Θριάσειο Πεδίο, στη Δυτική Αττική και περιβάλλεται από την Πάρνηθα στο βορρά, το όρος Αιγάλεω ανατολικά, το όρος Πατέρας δυτικά και την παραλία της Ελευσίνας στο νότο. Αποτελεί την έδρα του δήμου Μάνδρας-Ειδυλλίας, με επιφάνεια 426197 km² και 17885 μόνιμους κατοίκους σύμφωνα με την τελευταία απογραφή (Ελληνική Στατιστική Αρχή, 2011). Βρίσκεται σε λεκάνη απορροής έκτασης περίπου 75 km², την οποία διατρέχουν διάφορα ρέματα, τα οποία συγκλίνουν στα 2 κύρια, το Σούρες και την Αγία Αικατερίνη, με λεκάνες απορροής 23 και 22km² αντίστοιχα. Η κοίτη των ρεμάτων έχει υποστεί εκτεταμένες μορφολογικές αλλοιώσεις τις τελευταίες δεκαετίες, με συνέπεια τη μείωση της παροχетеυτικότητάς τους.

Η συχνότητα εμφάνισης πλημμυρικών φαινομένων στην περιοχή της Μάνδρας και η ανάγκη μετριασμού των επιπτώσεών τους στη τοπική κοινωνία, οδήγησαν στην εκπόνηση της τελικής μελέτης των έργων αντιπλημμυρικής προστασίας τον Ιούλιο του 2012. Οι περιβαλλοντικοί όροι της μελέτης εγκρίθηκαν 2 χρόνια αργότερα, τον Ιούλιο του 2014 και οι κοίτες των ρεμάτων οριοθετήθηκαν τον Ιανουάριο του 2016. Τα έργα αυτά αποτελούνται από:

1. τη διευθέτηση του ρέματος Σούρες (μήκος 1.74 km, παροχή σχεδιασμού 91-125 m³/s και διατομή 24.0-34.4 m²)
2. τη μερική εκτροπή του ρ. Αγίας Αικατερίνης προς το ρ. Σούρες (μήκος 1.52 km, παροχή σχεδιασμού 47 m³/s και διατομή 12.5-24.0 m²). Κατάντη της εκτροπής, η Αγία Αικατερίνη μετά από ένα υπογειοποιημένο τμήμα (μήκος 2.27 km, παροχή 10 m³/s και διατομή 3.4 m²) εκβάλλει στο ρ. Σούρες. Το ρ. Σούρες διέρχεται από το υπάρχον διευθετημένο τμήμα του με δίδυμο κανάλι (4.0X3.0 m²).

Η βροχόπτωση που προξένησε την ΞΠ της 15^{ης} Νοεμβρίου 2017 ξεκίνησε από το απόγευμα της 14^{ης} και κορυφώθηκε τις πρώτες πρωινές ώρες. Αρχικά ήταν ήπιας έντασης, ωστόσο κατά τη διάρκεια της νύχτας εκδηλώθηκαν καταιγίδες βόρεια της Μάνδρας και της Νέας Περάμου, που διήρκεσαν περίπου 8 h. Η βροχόπτωση ξεπέρασε τα 200 mm μέσα σε 6 h, το μεγαλύτερο μέρος της οποίας μεταξύ 5:00 και 8:00, σύμφωνα με το Εθνικό Αστεροσκοπείο Αθηνών. Οι παροχές εκτιμήθηκε ότι αντιστοιχούν σε βροχόπτωση με περίοδο επαναφοράς 50 χρόνων. Ένα από τα χαρακτηριστικά του φαινομένου είναι η έντονη στερεομεταφορά που παρατηρήθηκε, λόγω της διάβρωσης των αλλουβιακών αποθέσεων που είχαν συσσωρευτεί στο τμήμα της λεκάνης απορροής ανάντη της Μάνδρας (E. Lekkas et al., 2017). Οι δυσμενείς επιπτώσεις της πλημμύρας οφείλονται εκτός από τη δριμύτητα των καιρικών φαινομένων και στην μεγέθυνση της πόλης της Μάνδρας, η οποία αναπτύχθηκε κάθετα στη διεύθυνση των ρεμάτων. Η περιοχή έχει πληγεί από πλημμυρικά φαινόμενα μικρότερης κλίμακας αρκετές φορές, με πιο πρόσφατη εκείνη του Ιουνίου του 2018. Σύμφωνα με τους κατοίκους, οι πλημμυρικές ροές της μεγάλης πλημμύρας του Νοέμβρη του 2017 έφτασαν στα όρια της πόλης, με έντονη την παρουσία φερτών, γύρω στις 6:00 π.μ..

Η ομάδα που ασχολήθηκε με τη μελέτη της πλημμύρας της Μανδρας, αποτελούμενη από προπτυχιακούς και μεταπτυχιακούς φοιτητές της Σ.Π.Μ. Ε.Μ.Π., επισκέφτηκε 4 φορές την περιοχή, το φθινόπωρο του 2018. Οι πρώτες 2 επισκέψεις έγιναν για τη συλλογή πληροφοριών απαραίτητων για το ΜΜ που χρησιμοποιήθηκε για τις προσομοιώσεις. Πιο συγκεκριμένα μετρήθηκαν τα πλάτη των κοιτών, οι διαστάσεις των οχετών, αλλά και οι μέγιστες στάθμες των πλημμυρικών ροών. Οι τελευταίες χρησιμοποιήθηκαν για την επιβεβαίωση των αποτελεσμάτων του υδροδυναμικού μοντέλου και η μέτρησή τους ήταν εφικτή μήνες μετά την πλημμύρα λόγω της ύπαρξης λεπτόκοκκου ιζήματος που άφησε ίχνη στους τοίχους της πόλης. Οι 2 τελευταίες επισκέψεις έγιναν για την διανομή και συλλογή ερωτηματολογίων, σχετικών με το σχεδιασμό ενός Συστήματος Έγκαιρης Προειδοποίησης στην περιοχή.

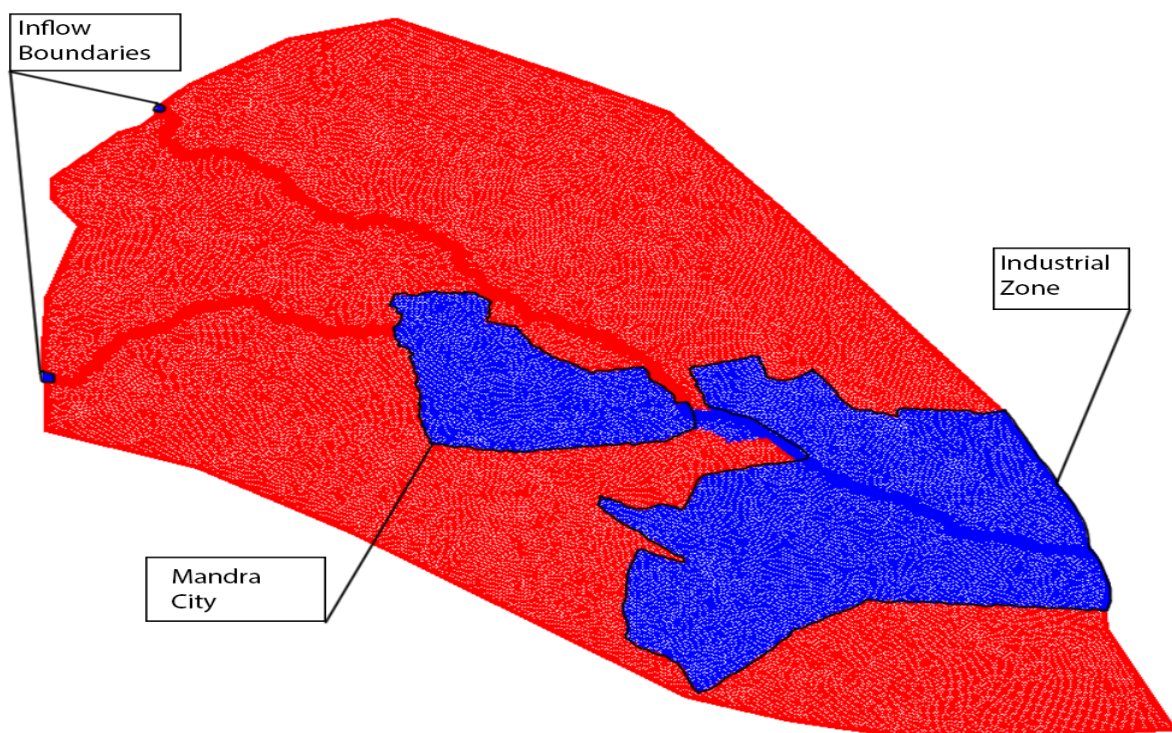
6. Το MM της πλημμύρας της Μάνδρας

Το υπολογιστικό πλέγμα που χρησιμοποιήθηκε για το μοντέλο της Μάνδρας αποτελείται από 85753 σημεία και 167051 τριγωνικά στοιχεία. Παράχθηκε μέσω του λογισμικού Blue Kenue. Το Blue Kenue διαθέτει 2 επιλογές για υπολογιστικά πλέγματα: το T3 Mesh Generator και το T3 Channel Mesher. Το τελευταίο χρησιμοποιήθηκε για την παραγωγή των υπολογιστικών πλεγμάτων των 2 ρεμάτων, τα οποία στη συνέχεια ενοποιήθηκαν με το εξωτερικό πλέγμα, μέσω του T3 Mesh Generator. Στη συνέχεια, έγινε ενσωμάτωση ενός αρχείου υψομέτρων στο υπολογιστικό πλέγμα, καθώς και ενός αρχείου επιφανειακής τραχύτητας που βασίστηκε σε χάρτες κάλυψης γης (Corine Land Cover). Στο μοντέλο έγινε και εισαγωγή αρχείου με τα τεχνικά έργα που σχετίζονται με την παροχέυτωση των πλημμυρικών ροών.

Το υπολογιστικό πλέγμα του MM περιλαμβάνει 4 ανοιχτά όρια. Τα 2 είναι όρια εισόδου και βρίσκονται στο ανώταρο άκρο του ρ. Σούρες και του ρ. Αγία Αικατερίνη. Τα 2 όρια εξόδου βρίσκονται στην εκβολή του ρ. Σούρες στο ρ. Σαρανταπόταμος και στο ρ. Μικρό Κατερίνη ανάντη της πόλης της Ελευσίνας. Τα υδρογραφήματα που χρησιμοποιήθηκαν στις διατομές εισόδου είναι του Tsakiris (2017)

Το ολοκληρωμένο μοντέλο που χρησιμοποιήθηκε για τη προσομοίωση της πλημμύρας της Μάνδρας βασίζεται σε 2D υδροδυναμικό μοντέλο, πλήρως συζευγμένο με το γεωμορφολογικό/μοντέλο στερεομεταφοράς. Το τελευταίο χρησιμοποιεί την εξίσωση στερεομεταφοράς των Engelund-Hansen & Cholley-Cunge και έπειτα υπολογίζει την εξέλιξη της μορφολογίας του πυθμένα με την εξίσωση Exner.

Για το γεωμορφολογικό/μοντέλο στερεομεταφοράς χρησιμοποιήθηκε αρχείο στο οποίο ορίστηκαν οι μη διαβρώσιμες περιοχές. Σε αυτό περιλαμβάνονται επίσης τα αρχεία της γεωμετρίας και της επιφανειακής τραχύτητας. Ορίστηκαν 2 μη διαβρώσιμες περιοχές. Η πρώτη αποτελεί την επιφάνεια που καλύπτει η πόλη της Μάνδρας, ενώ η άλλη την έκταση που καταλαμβάνει η βιομηχανική περιοχή (Εικόνα 4). Προστέθηκαν και 2 μικρές μη διαβρώσιμες περιοχές στα ανοιχτά όρια εισόδου για των περιορισμό των ανεξέλεγκτων διαβρώσεων που προκαλούσαν οι μεγάλες ταχύτητες λόγω υπολογιστικών αστάθειών σε εκείνες τις περιοχές.



Εικόνα 4. Οι μη διαβρώσιμες περιοχές στο υπολογιστικό πλέγμα του MM της Μάνδρας.

7. Αποτελέσματα και σχολιασμός

Μελετήθηκε η επίδραση των πλημμυρικών ροών στη γεωμορφολογική αλλοίωση της κοίτης ποταμών. Χρησιμοποιήθηκε η πλατφόρμα λογισμικού TELEMAC-MASCARET (Galand et al., 1991; Hervouet and Van Haren, 1996) για ένα πλήρως συζευγμένο μοντέλο TELEMAC-2D/SISYPHE για τη μελέτη της πλημμύρας της Μάνδρας. Το μοντέλο, που βρίσκεται σε προκαταρκτικό στάδιο, χρησιμοποιεί την εξίσωση στερεομεταφοράς των Engeland-Hansen & Chollet-Cunge. Η τελευταία έδωσε καλά αποτελέσματα στην προσομοίωση του πειράματος των Yen & Lee (1995) για ομοιόμορφο ίζημα. Για την προσομοίωση της στερεομεταφοράς και της γεωμορφολογικής αλλοίωσης χρησιμοποιήθηκε ομοιόμορφο ίζημα που βρίσκεται στο όριο μεταξύ λεπτής άμμου και ιλύος (0.63mm), λόγω έλλειψης ιζηματολογικών δεδομένων. Η προσέγγιση των A. Mendoza et al. (2017) δεν ακολουθήθηκε γιατί δεν παρατηρήθηκε έντονη επίδραση της δευτερεύουσας ροής. Τα αποτελέσματα της προσομοίωσης ήταν τα ακόλουθα:

1. Στο ανάντη τμήμα του ρ. Σούρες παρουσιάστηκε έντονη μορφολογική αλλοίωση που έφτασε τα 2 m διάβρωση και το 1.5 m επίχωση. Οι τιμές αυτές εμφανίστηκαν σε περιορισμένη επιφάνεια περίπου 4.5 h από την έναρξη της προσομοίωσης.
2. Στο ανάντη τμήμα του ρ. Αγία Αικατερίνη η γεωμορφολογική αλλοίωση ήταν λιγότερο έντονη λόγω της μικρότερης κλίσης πυθμένα. Οι μέγιστες τιμές που προέκυψαν ήταν 1.2 m και 1 m για τη διάβρωση και την επίχωση αντίστοιχα. Οι ακραίες τιμές εμφανίστηκαν περίπου 5 h από την έναρξη της προσομοίωσης και ήταν σε περιορισμένη επιφάνεια.
3. Στο ρ. Σούρες παρουσιάστηκε διάβρωση στις όχθες και επίχωση στο μέσο των διατομών. Το φαινόμενο αυτό ήταν λιγότερο έντονο στο ρ. Αγία Αικατερίνη.
4. Παρατηρήθηκε χρονική υστέρηση μεταξύ της εμφάνισης των μέγιστων ταχυτήτων και της μέγιστης διάβρωσης που έφτασε την 1h.
5. Τα αποτελέσματα του μοντέλου για την επιφάνεια της πλημμύρας είναι μια καλή προσέγγιση της αντίστοιχης επιφάνειας που μετρήθηκε.
6. Η επίδραση των γεωμορφολογικών αλλοιώσεων στην έκταση της πλημμύρας της Μάνδρας δεν ήταν σημαντική.

8. Συμπεράσματα και προτάσεις

Τα αποτελέσματα του μοντέλου της Μάνδρας θεωρήθηκαν λογικά. Ωστόσο, το μοντέλο βρίσκεται ακόμα σε προκαταρκτικό στάδιο και τα αποτελέσματά του πρέπει να επιβεβαιωθούν με σχετικές μετρήσεις πεδίου. Μερικές προτάσεις για τη βελτίωση των μαθηματικών προσομοιώσεων της πλημμύρας της Μάνδρας είναι οι εξής:

1. Η περαιτέρω διερεύνηση της επίδρασης των γεωμορφολογικών αλλοιώσεων στις πλημμυρικές ροές. Πιο συγκεκριμένα προτείνεται η εξαγωγή χρονοσειρών για τα βάθη ροής του υδροδυναμικού και του ολοκληρωμένου μοντέλου σε διατομές των ρεμάτων και η μεταξύ τους σύγκριση.
2. Οι πλημμυρικές ροές που εμφανίστηκαν στην περίπτωση της Μάνδρας χαρακτηρίστηκαν από τη μεταφορά και απόθεση αδρομερών υλικών, κάτι που δεν μπορεί να προσομοιωθεί με το TELEMAC-MASCARET. Γι'αυτό το λόγο προτείνεται και η προσομοίωση ενός άλλου μοντέλου που θα λαμβάνει το φαινόμενο αυτό υπόψη του.
3. Προτείνεται η προσομοίωση με μη ομοιόμορφο ίζημα, όταν υπάρξει πρόσβαση σε ιζηματολογικά δεδομένα. Σε αυτή τη περίπτωση συνιστάται η χρήση μοντέλου με την εξίσωση του Van Rijn (1989), η οποία έδωσε τα καλύτερα αποτελέσματα στην προσομοίωση του πειράματος των Yen & Lee (1995) με μη ομοιόμορφο ίζημα.
4. Προτείνεται η διερεύνηση σεναρίου με συνεκτικό και μη συνεκτικό ίζημα για να μελετηθεί και η συνεισφορά του ιζήματος σε αιώρηση.
5. Προτείνεται τέλος η επέκταση του υπολογιστικού πεδίου προς τα ανάντη για να συμπεριληφθεί και το τμήμα στο οποίο παρατηρήθηκαν τα πιο έντονα φαινόμενα διάβρωσης και στερεομεταφοράς (περιοχή Καντίνες). Σε αυτή την περίπτωση συνιστάται ο διαχωρισμός του υπολογιστικού πεδίου σε μικρότερες περιοχές με διαφορετική κοκκομετρική σύνθεση, ανάλογα με τα γεωλογικά δεδομένα.

Table of Contents

1. Introduction.....	1
1.1. General information about flash floods	1
1.2. The Mandra flash flood	2
1.3. Diploma thesis scope	3
1.4. Diploma thesis structure.....	4
2. Literature survey	5
2.1. Aim of the literature survey	5
2.2. Shallow water equations.....	5
2.3. Introduction to the sediment transport processes	6
2.4. Available sediment transport formulas	7
2.5. Mathematical models for flash flood simulations	10
2.6. Available programs for 2Dhydrodynamic models.....	10
2.7. Mesh generation and results visualization	11
2.8. The effect of solid materials in surface runoffs.....	12
3. Materials and methods	13
3.1. TELEMAC-MASCARET system	13
3.1.1. TELEMAC-2D software	14
3.1.2. SISYPHE module	16
4. Simulations of the benchmark case.....	21
4.1. Description	21
4.1.1. Selection of the benchmark case for the flash flood simulations.....	21
4.1.2. The Yen and Lee (1995) experiments.....	21
4.2. The benchmark model simulations.....	23
4.3. Previous numerical works	25
4.4. Results presentation	26
4.4.1. Run-1/non-uniform sediment simulations	26
4.4.2. Run-2/non-uniform sediment simulations	29
4.4.3. Run-3/non-uniform sediment simulations	32
4.4.4. Run-4/non-uniform sediment simulations	35
4.4.5. Run-5/non-uniform sediment simulations	38
4.4.6. Run-4/ uniform sediment simulations.....	41
4.5. Comparison between the results of the diploma thesis simulations and previous numerical works	45
4.6. Discussion of the results.....	46
5. The Mandra flash flood case study	47
5.1. Area of study	47
5.1.1. The city of Mandra	47
5.1.2. The hydrographic network of Mandra area	47
5.2. Characteristics of the flash flood event	48
5.3. In situ investigation in Mandra area	51
6. The Mandra flood integrative model	53
6.1. Input data into TELEMAC-2D	53
6.1.1. Numerical mesh	53

6.1.2. Technical works	55
6.1.3. Boundary conditions	55
6.2. Input data into SISYPHE.....	56
6.2.1. Boundary conditions	56
6.2.2. Definition of rigid areas	56
6.2.3. Limitations and assumptions	57
6.3. Results presentation	58
6.3.1. Geomorphological evolution on the upstream part of the s. Soures	58
6.3.2. Geomorphological evolution on the upstream part of the s. Agia Aikaterini	60
6.3.3. Geomorphological evolution of the cross-sectional profiles of Mandra streams	62
6.3.4. Integrative model predictions of the flooded area.....	63
6.4. Discussion of the results.....	64
6.5. Conclusions and suggestions for future work.....	64
7. Literature	65
APPENDIX.....	67

List of Figures

Figure 1.1. Total rainfall on 16/11/17 in Mandra.....	2
Figure 1.2. Intense runoff flow during the Mandra FF with apparent the stream bed erosion and the sediment/debris transport.....	3
Figure 2.1. Sketch concerning the non-conservative shallow water equations presenting the x and y axis as well as the total fluid column height η and the altitude h.....	5
Figure 2.2. Types of visualization in Blue Kenue.....	12
Figure 2.3. Intense sediment deposition that occurred during the August 2015 floods in parts of Switzerland.....	12
Figure 3.1. TELEMAT-MASCARET system modules and their scope.....	13
Figure 3.2. Aspects taken into account through SISYPHE correction of magnitude and direction of the bedload sediment transport.....	20
Figure 4.1. Hydrographs of the 5 experiments.....	21
Figure 4.2. Contours of bed deformation for the Run 1.....	22
Figure 4.3. The concept of hiding and exposure effect.....	24
Figure 4.4. Initial sediment size gradation curve.....	24
Figure 4.5. Filled contours of bed deformation for Cheng and Reid formulas compared to experimental data isolines.....	26
Figure 4.6. Filled contours of bed deformation for Meyer-Peter & Mueller and Einstein-Brown formulas compared to experimental data isolines.....	26
Figure 4.7. Filled contours of bed deformation for Hunzinger and Reid formulas compared to experimental data isolines.....	26
Figure 4.8. Comparison between sediment transport formulas predictions and the experimental data concerning the bed evolution in the cross-section experimentally defined as the area of maximum deposition (75° cross-section).....	27
Figure 4.9. Comparison between sediment transport formulas predictions and the experimental data concerning the bed evolution in the cross-section experimentally defined as the area of maximum deposition (165° cross-section).....	28
Figure 4.10. Filled contours of bed deformation for Cheng and Reid formulas compared to experimental data isolines.....	29
Figure 4.11. Filled contours of bed deformation for Meyer-Peter & Mueller and Einstein-Brown formulas compared to experimental data isolines.....	29
Figure 4.12. Filled contours of bed deformation for Hunzinger and Van Rijn formulas compared to experimental data isolines.....	29
Figure 4.13. Comparison between sediment transport formulas predictions and the experimental data concerning the bed evolution in the cross-section experimentally defined as the area of maximum deposition (75° cross-section).....	30
Figure 4.14. Comparison between sediment transport formulas predictions and the experimental data concerning the bed evolution in the cross-section experimentally defined as the area of maximum deposition (180° cross-section).....	31
Figure 4.15. Filled contours of bed deformation for Cheng and Reid formulas compared to experimental data isolines.....	32
Figure 4.16. Filled contours of bed deformation for Meyer-Peter & Mueller and Einstein-Brown formulas compared to experimental data isolines.....	32
Figure 4.17. Filled contours of bed deformation for Hunzinger and Van Rijn formulas compared to experimental data isolines.....	32
Figure 4.18. Comparison between sediment transport formulas predictions and the experimental data concerning the bed evolution in the cross-section experimentally defined as the area of maximum deposition (75° cross-section).....	33
Figure 4.19. Comparison between sediment transport formulas predictions and the experimental data concerning the bed evolution in the cross-section experimentally defined as the area of maximum deposition (180° cross-section).....	34
Figure 4.20. Filled contours of bed deformation for Cheng and Reid formulas compared to experimental data isolines.....	35
Figure 4.21. Filled contours of bed deformation for Meyer-Peter & Mueller and Einstein-Brown formulas compared to experimental data isolines.....	35

Figure 4.22. Filled contours of bed deformation for Hunzinger and Van Rijn formulas compared to experimental data isolines.....	35
Figure 4.23. Comparison between sediment transport formulas predictions and the experimental data concerning the bed evolution in the cross-section experimentally defined as the area of maximum deposition (90° cross-section).....	36
Figure 4.24. Comparison between sediment transport formulas predictions and the experimental data concerning the bed evolution in the cross-section experimentally defined as the area of maximum deposition (180° cross-section).....	37
Figure 4.25. Filled contours of bed deformation for Cheng and Reid formulas compared to experimental data isolines.....	38
Figure 4.26. Filled contours of bed deformation for Meyer-Peter & Mueller and Einstein-Brown formulas compared to experimental data isolines.....	38
Figure 4.27. Filled contours of bed deformation for Hunzinger and Van Rijn formulas compared to experimental data isolines.....	38
Figure 4.28. Comparison between sediment transport formulas predictions and the experimental data concerning the bed evolution in the cross-section experimentally defined as the area of maximum deposition (90° cross-section).....	39
Figure 4.29. Comparison between sediment transport formulas predictions and the experimental data concerning the bed evolution in the cross-section experimentally defined as the area of maximum deposition (180° cross-section).....	40
Figure 4.30. Filled contours of bed deformation for Ackers-White and Nielsen formulas compared to experimental data isolines.....	41
Figure 4.31. Filled contours of bed deformation for Cheng and Engelund-Hansen & Chollet-Cunge formulas compared to experimental data isolines.....	41
Figure 4.32. Filled contours of bed deformation for Frijlink and Einstein-Brown formulas compared to experimental data isolines.....	41
Figure 4.33.: Filled contours of bed deformation for Engelund-Hansen and Meyer-Peter & Mueller formulas compared with experimental data isolines.....	42
Figure 4.34. Filled contours of bed deformation for Karim-Kennedy and Van Rijn formulas compared with experimental data isolines.....	42
Figure 4.35.: Filled contours of bed deformation for Reid and Yang-Lim formulas compared to experimental data isolines.....	42
Figure 4.36. Comparison between sediment transport formulas predictions and the experimental data concerning the bed evolution in the cross-section experimentally defined as the area of maximum deposition (75° cross-section).....	43
Figure 4.37. Comparison between the sediment transport formulas predictions and the experimental data concerning bed evolution in the cross-section experimentally defined as the area of maximum scour (165° cross-section).....	44
Figure 4.38. Diploma thesis (Van Rijn) and Villaret et al. (2013) predictions with measurements in the cross-sections of maximum deposition (left) and scour (right).....	45
Figure 4.39. Diploma thesis and TELEMAC-MASCARET example simulations with Run-4 measurements in the cross-sections of maximum deposition (left) and scour (right).....	45
Figure 5.1. The Thriasian Plain and the Attica basin (source: Google Earth).....	47
Figure 5.2. The streams of Mandra and their technical works.....	48
Figure 5.3. The regulated part of the s. Soures after the flood (Stamou, 2018).....	48
Figure 5.4. The rainfall rate of the main storm events as recorded by the radar XPOL of the National Observatory of Athen (N.O.A.).....	49
Figure 5.5. The accumulated rainfall of the main storm events as recorded by the radar XPOL of the National Observatory of Athens (N.O.A.).....	49
Figure 5.6. Evolution of the rainfall events during November 15 th , 2017 as recorded by the Ymmitos radar of the Hellenic National Meteorological Service (H.N.M.S.).....	49
Figure 5.7. Mandra area before the November 15 th flash flood event.....	50
Figure 5.8. Mandra area after the November 15 th flash flood event.....	50
Figure 5.9. Maximum flooded area of Mandra at November 15 th	50
Figure 5.10. Map of Mandra area, highlighting 5 areas of interest.....	51
Figure 6.1. The finite element mesh of the geometry file used in Mandra model.....	53
Figure 6.2. The methodology.....	54

Figure 6.3. Upstream hydrographs.....	55
Figure 6.4. Mandra flood MM domain and the liquid boundaries.....	56
Figure 6.5. Non-erodable areas in Mandra model domain (blue). The area of Mandra city, the industrial zone and the inflow boundaries enclosed by black lines.....	57
Figure 6.6. Geomorphological evolution due to the flood flows on the upstream part of the s. Soures at 6 hours and 8 hours from the start of the simulation.....	58
Figure 6.7. Geomorphological evolution due to the flood flows on the upstream part of the s. Soures at 6 hours and 8 hours from the start of the simulation.....	59
Figure 6.8. Geomorphological evolution due to the flood flows on the upstream part of the s. Aikaterini at 2 hours and 4 hours from the start of the simulation.....	60
Figure 6.9. Geomorphological evolution due to the flood flows on the upstream part of the s. Aikaterini at 6 hours and 8 hours from the start of the simulation.....	61
Figure 6.10. Geomorphological evolution of the cross-sectional profiles of Mandra streams.....	62
Figure 6.11. The model predictions concerning the flooded area at 2 hours (left) and 4 hours (right) after the start of the simulation.....	63
Figure 6.12. The model predictions concerning the flooded area at 6 hours (left) and 8 hours (right) after the start of the simulation.....	63
Figure 6.13. Comparison between the model predictions of the maximum flooded area (3.5 hours after the start of the computation) and the in situ measurements (black line).....	63

List of Tables

Table 2.1. General parameters for sediment transport in riverine environments.....	7
Table 2.2. Comparison of the input data for different sediment transport formulas.....	9
Table 2.3. Data ranges for different calculation methods.....	9
Table 4.1. Characteristics of the 5 experiments.....	22
Table 4.2. Transverse variation at section of maximum deposition.....	23
Table 4.3. Transverse variation at section of maximum scour.....	23
Table 4.4. Sediment size classes used in the non-uniform sediment simulations.....	24
Table 6.1. Corresponding Corine codes to Manning coefficient values.....	53
Table 6.2. Manning Values for stream's bed.....	53
Table 6.3. Corresponding Corine codes to Manning coefficient values.....	54

1. Introduction

1.1. General information about flash floods

Natural disasters cause huge economic damages each year (Swiss Re, 2003). In many European countries floods are the major natural hazard (Cruz et al., 2006). Germany, Czech Republic and Russia in August 2002 were struck by the most devastating flood events recorded in European history (J. Linnerooth-Bayer & A. Amendola). Nevertheless, the effects of the recent major floods in European countries are comparable with the worldwide trend, where floods are attributed the greatest economic damages out of all natural events.

Flood events can be divided into several categories depending on the area they develop, the mechanism they are generated from and the effects they have on the natural and manmade environment. These categories according to the National Severe Storms Laboratory are the following: Coastal floods, which are caused by higher than average high tide alongside heavy rainfall and onshore winds. Storm surges, which are a rise in the water level in coastal areas, above the regular tide, caused by forces generated from a severe storm's wind, waves, and low atmospheric pressure. Pretty much all of the other cases can be grouped as inland floods. More specifically, a river flood is the rise of the river water level due to the excessive rain over the same area for extensive periods of time. Last but not least, there is the flash flood which is examined in the diploma thesis.

Flash Floods (FF) are defined (Grutfest & Huber, 1991) as strong and fast runoff flows that occur from a few minutes to several hours after the rainfall (NOAA, 2017). Apart from the extreme rainfall events they can be generated from hydraulic structure (dams, levees) failures. The magnitude of a FF depends mainly on the rainfall characteristics (intensity, duration, amount and time-space distribution) and the characteristics of the watershed such as area, length, slopes, type of soil, vegetation and land use. Georgakakos (1986a) described the FF generation mechanism in non-arid climates as follows: Firstly, areas adjacent to the stream channels become saturated. The water table rises due to the excess rainfall and the lower catchment slopes become saturated due to the outflow. The groundwater is also discharged near the river channel resulting in an increased groundwater contribution to the river hydrograph. The scale of the FF effects on economy and human lives though, suggests that their generating mechanism is still not sufficiently understood.

FF are one of the major natural hazards causing serious loss of life and economic damage (Eric Gaume et al., 2008). The average annual economic loss due to natural hazards is estimated at €40 billion worldwide (Munich Re, 2003) which can be compared to the total economic damages estimated at €1.2 billion for the Gard 2002 single flood event (Huet et al., 2003) and €3.3 billion in the case of Aude 1999 FF (Lefrou et al., 2000). The death toll caused by FF in European Mediterranean countries is striking, with notable examples the Barcelona flood in Spain in 1962 with over 400 deaths recorded (Lopez Bustos, 1964), the Piedmont region floods in Italy in 1968 and 1994 with 72 and 69 deaths respectively (Ferro, 2005; Guzzeti et al., 2005). A more recent FF event took place in Mandra, Greece (2017), resulting in the death of 23. These figures suggest that the mechanism of FF generation is still poorly understood.

Lately, several studies have implied that a correlation between extreme rainfall events (which generate FF) and global warming really exists due to the increased atmospheric water vapor and warmer air (IPCC, 1995). The expected consequence of this trend is the increased frequency of FF occurrence which will have disproportionately negative effects in arid and semi-arid regions like the ones in the Mediterranean basin, Greece (Alpert et al., 2002). In arid climates rain may also generate crusting of soils, which prevents the soil infiltration, thus enhancing the flood generating processes (C. G. Collier, 2007).

An important aspect of FF events is that they tend to be much more devastating in urban areas, compared to the ones occurring in rural areas, due to the high population density, and the impervious surfaces found in cities (Davis, 2001). Urban development is not always followed by the construction of hydraulic structures that support the new land use. When urbanized areas have insufficient flood defense infrastructure and also when urban expansion is not accompanied by appropriate measures to mitigate flood effects, the impacts of the floods are further intensified (Papathanasiou et al., 2012). Infrastructure is usually developed in order to cover specific needs that arise from the socioeconomic growth, thus it may have negative impact on the response of a catchment to potential flooding (C. Papathanasiou et al., 2015). This is the case for structures that either alternate the geomorphology of the basin or increase the impermeable areas.

1.2. The Mandra flash flood

The growth pattern of Mandra city implies that it is a typical example of urban/suburban sprawl. A sprawl can be defined as the expansion of a community without concern for its consequences, in short, unplanned, and incremental urban growth, which is regarded unsustainable (Batty et al., 1999). According to the National Statistical Service of Greece, Mandra's population has tripled in less than 60 years, which alongside the development of the industrial zone and the construction of the "Attiki Odos" motorway, changed dramatically the response of the catchment in rainfall.

Several rainfall events took place in Greece during 14-16 of November 2017 (Figure 1.1.). The area of Mandra was the one affected the most, after a devastating FF event that occurred at the first hours of November 15. The study of the meteorological and satellite data highlighted that a number of storm events on the southern slopes of Pateras mountain (1.131m) led to the disastrous events of November 15. The water was initially accumulated in soil and the several mountain streams were supplied by runoff and subsoil water, which contribute to the stream Agia Aikaterini and the stream Soures, which cross Mandra city. The flow rates were determined for a return period equal to T=50 years. One of the characteristics of the flood event was the heavy sediment transport due to the erosion of the alluvial plains found on the upstream part of the basin (E. Lekkas et al., 2017). The effects of the FF on the area were further enhanced due to the fact that the city has been developed in a perpendicular to the creeks pattern as has also been the case with the motorway system. The area has experienced many FF incidences of smaller magnitude, the most recent of which occurred at June 26 2018.

The conclusion of the Secretary General of Public Administration concerning the flood events of 2017 in Mandra highlighted that 39 buildings, both private and public, were illegally constructed in the Soures creek, a football field and bus depot included.

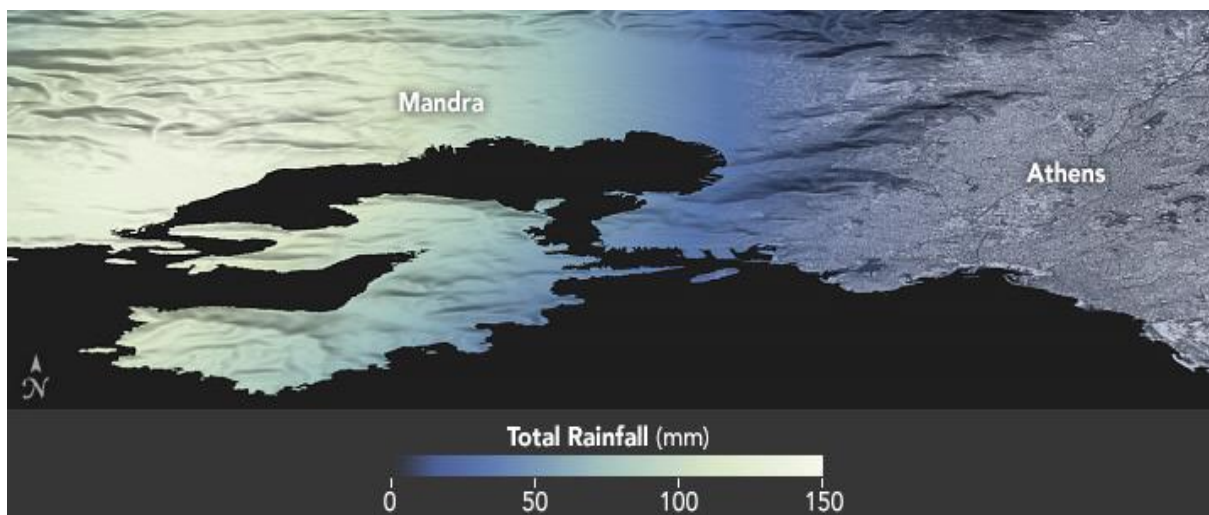


Figure 1.1. Total rainfall on 16/11/17 in Mandra (<https://earthobservatory.nasa.gov>).

1.3. Diploma thesis scope

FF events are associated with intense soil erosion processes that result in sediment and debris transport. These take place mainly within catchments in arid and semi-arid areas lacking vegetation. The solid materials transported by the fast flows of the FF induced surface runoff are expected to affect the hydrodynamic flow regime. Furthermore, the solid material effect on flood flows is expected to increase in future due to the risk of desertification that about the 35% of world land surface is facing according to UNEP. The last has also concluded that each year more than 20 million hectares worldwide are reduced to near or complete uselessness. Desertification is defined as land degradation in arid and semi-arid areas resulting mainly from anthropogenic activities (UNEP, 1991) and is expected to dramatically increase the rate of soil erosion in these areas.

Currently the effect of solid materials that are carried downstream and the riverbed morphological changes are not considered in the various models used for FF simulation. Mandra FF, studied in the diploma thesis, was characterized by heavy sediment transport and intense erosion (Figure 1.2), thus the solid materials' contribution to the flow regime cannot be neglected. The scope of this thesis is to answer the research question *"How can we model the effect of sediment in Mandra flood?"*.



Figure 1.2. Intense runoff flow during the Mandra FF with apparent the stream bed erosion and the sediment/debris transport (source: <https://edition.cnn.com>).

1.4. Diploma thesis structure

The diploma thesis consists of 7 Chapters and 1 APPENDIX.

The concept of FF and its effects on human lives and the economy on a worldwide scale are introduced in Chapter 1. The research question that this study aims to answer is posed and the thesis structure is presented.

Chapter 2 concerns the literature survey, its purpose and the reasons that led to the selection of the modelling system for the Mandra FF model (TELEMAC-MASCARET modeling system). The available sediment transport formulas are presented, as well as the mathematical models for flash flood simulations. An introduction to the pre-processing and post-processing tools has also been done in this chapter.

In Chapter 3 the materials and methods (TELEMAC-2D coupled with SISYPHE module) used in order to answer the research question, the available modules and the equations that describe the hydrodynamic and sediment transport processes are thoroughly discussed.

Chapter 4 is concerned with the benchmark case simulations. The criteria that led to the selection of the Yen and Lee (1995) experiments for the benchmark case model are presented. The results of models, utilizing several sediment transport formulas, are displayed and discussed.

In Chapter 5 the Mandra flash flood event is introduced. The information about the area of study is introduced, including the city of Mandra and the hydrographic network. The flash flood characteristics are shown, as well as the in situ investigations' purpose.

The hydrodynamic/sediment transport/morphological model of Mandra flash flood is thoroughly discussed in Chapter 6. The geometry including the numerical mesh, the surface roughness and the non-erodable areas are presented as well as the technical works, the boundary conditions, and the hydrographs used for the simulation are presented. The results concerning the hydrographs, the water depths, and the bottom evolution are displayed, compared with the results of the clear water model, and discussed.

The FORTRAN code concerning the sediment transport formulas used in the diploma thesis that are not included in SISYPHE module can be found in the APPENDIX.

2. Literature survey

2.1. Aim of the literature survey

The purpose of the literature survey is to select the mathematical model that will be used in the diploma thesis, as well as to select the benchmark case that will be used for model validation. Some criteria that the model has to meet are:

1. Reputation and credibility
2. Availability of the source code
3. The ability to use a variety of sediment transport formulas

In order to choose the model that better simulates the FF flow regime and the sediment transport processes the governing equations have to be expressed alongside the different mathematical models that are suited for FF simulation.

2.2. Shallow water equations

Floods are characterized by the unsteady flow regime and the extensive horizontal axis compared to the vertical one. For these reasons the shallow water equations (SWE) are ideal for flood modeling. Shallow water equations are a set of hyperbolic partial differential equations (PDE) that derive from depth-integrating the Navier-Stokes equations, also called Saint-Venant equations after Adhemar Jean Claude Barre de Saint-Venant. In the cases that horizontal length is much greater than the vertical one the vertical velocity of the fluid is very small, the vertical pressure gradients are nearly hydrostatic, and the horizontal velocity field is constant throughout the depth of the fluid. Vertically integration of horizontal velocity enables the removal of the vertical velocity from the equations. SWE are derived from the equations of mass conservation and conservation of linear momentum. The following set of equations is the so called conservative form of the SWE, where there is horizontal bed, no Coriolis forces as well as no frictional or viscous forces. The first equation is derived from mass conservation, the second two from momentum conservation:

$$\frac{\partial(\rho\eta)}{\partial t} + \frac{\partial(\rho\eta u)}{\partial x} + \frac{\partial(\rho\eta v)}{\partial y} = 0 \quad (2.1)$$

$$\frac{\partial(\rho\eta u)}{\partial t} + \frac{\partial}{\partial x}(\rho\eta u^2 + \frac{1}{2}\rho g\eta^2) + \frac{\partial(\rho\eta uv)}{\partial y} = 0 \quad (2.2)$$

$$\frac{\partial(\rho\eta v)}{\partial t} + \frac{\partial(\rho\eta uv)}{\partial x} + \frac{\partial}{\partial y}(\rho g\eta v^2 + \frac{1}{2}\rho g\eta^2) = 0 \quad (2.3)$$

where: η is the total fluid column height,
 u is the horizontal velocity component across the x axis,
 v is the horizontal velocity component across the y axis,
 g is the acceleration due to gravity,
and ρ is the fluid density.

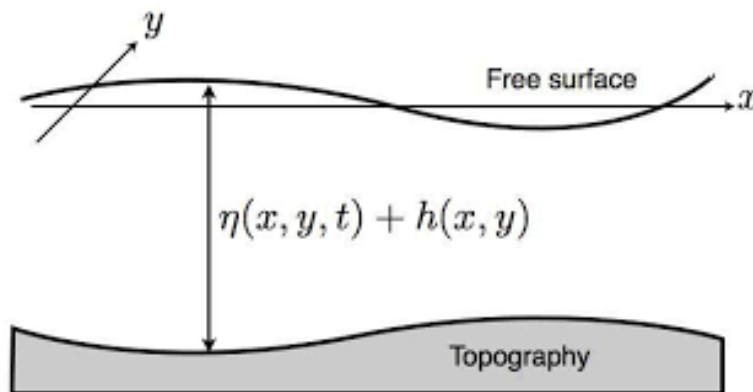


Figure 2.1. Sketch concerning the non-conservative shallow water equations presenting the x and y axis as well as the total fluid column height η and the altitude h .

Expanding the derivatives using the product rule, the non-conservative form of the SWE is derived (Figure 2.1.). Contrarily to the conservative form the non-conservative does not hold across a shock or hydraulic jump, due to the fact that velocities are not subject to a fundamental conservation equation. The non-conservative form takes into account the Coriolis force, frictional and viscous forces as presented in the following page:

$$\frac{\partial h}{\partial t} + \frac{\partial((H+h)u)}{\partial x} + \frac{\partial((H+h)v)}{\partial y} = 0 \quad (2.4)$$

$$\frac{\partial u}{\partial t} + u \frac{\partial u}{\partial x} + v \frac{\partial u}{\partial y} - fv = -g \frac{\partial h}{\partial x} - bu + v \left(\frac{\partial^2 u}{\partial x^2} + \frac{\partial^2 v}{\partial^2 y} \right) \quad (2.5)$$

$$\frac{\partial v}{\partial t} + u \frac{\partial v}{\partial x} + v \frac{\partial v}{\partial y} - fu = -g \frac{\partial h}{\partial y} - bv + v \left(\frac{\partial^2 v}{\partial x^2} + \frac{\partial^2 v}{\partial^2 y} \right) \quad (2.6)$$

where: u is the horizontal velocity component across the x axis,
 v is the horizontal velocity component across the y axis,
 g is the acceleration due to gravity,
 h is the height deviation of the horizontal pressure surface from its mean height,
 H is the mean height of the horizontal pressure surface,
 g is the acceleration due to gravity,
 f is the Coriolis coefficient,
 b is the viscous drag coefficient,
and ν is the kinematic viscosity

In cases where the components of the horizontal velocity, u and v , are relatively small the following set of equations can be obtained:

$$\frac{\partial h}{\partial t} + H \left(\frac{\partial u}{\partial x} + \frac{\partial v}{\partial y} \right) = 0 \quad (2.7)$$

$$\frac{\partial u}{\partial t} - fv = -g \frac{\partial h}{\partial x} - bu \quad (2.8)$$

$$\frac{\partial v}{\partial t} + fu = -g \frac{\partial h}{\partial y} - bv \quad (2.9)$$

2.3. Introduction to the sediment transport processes

Sediment transport is the displacement of soil particles that get entrained due to the movement of fluid and are susceptible to gravitational forces. Sediment transport takes place in natural systems where the particles are clastic (sand, gravel or boulder), mud or clay. The fluid motion that causes the sediment transport can be air, water, ice or a combination of them. These processes occur in rivers, lakes, seas, glaciers or terrestrial surfaces under the influence of wind. There are cases of sediment transport due to gravity only that occur on slopping surfaces, as hill slopes, scraps, cliffs and the continental shelf.

One of the mechanisms of soil erosion and sediment transport is the runoff flows of rain water on earth's surface that takes place in riverbeds and floodplains. The main sources of sediment in natural streams are erosion by overland flow, stream-channel erosion, bank cutting and supply from small erosion channels formed in unconsolidated soil (F. Englund and E. Hansen, 1967).

A big part of the particles that get entained by the runoff flows takes place in alluvial plains. An alluvial plain can be defined as a relatively flat landform created by the deposition of sediment over a long period of time. The streams in which the moving sediment and the sediment in the underlying bed is of the same quality are characterized as alluvial. However, most natural streams carry a certain amount of very fine particles, the so-called wash or suspended load that is not represented in the bed. The knowledge of bed material composition does not permit any prediction of wash load transportation.

2.4. Available sediment transport formulas

Over the years several sediment transport formulas have been developed in order to predict the sediment transport rate. Most of these predict the bedload or the total sediment flux, which includes both the bedload and the suspended or wash load. The contribution of the second to the sediment transport processes is minimal, thus it is usually not taken into account. The general parameters used in the sediment transport formulas are presented in the table below (Table 2.1.), in which ρ_s is the sediment density, ρ_w is the water density, g is the gravitational acceleration, D_{50} the sediment size that 50% is finer, τ_b is the bottom shear stress and ν the kinematic viscosity.

Table 2.1. General parameters for sediment transport in riverine environments.

General parameters	
Relative density	$\Delta = \frac{\rho_s - \rho_w}{\rho_w}$
Dimensionless grain size	$D_* = \left(\frac{g\Delta}{\nu}\right)^{1/3} D_{50}$
Critical Shields parameter Shields curve approximation – Van Rijn (1993)	$\theta_{cr} = \begin{cases} 0.24D_*^{-1}, & 1 \leq D_* \leq 4 \\ 0.14D_*^{-0.64}, & 4 < D_* \leq 10 \\ 0.04D_*^{-0.1}, & 4 < D_* \leq 20 \\ 0.013D_*^{0.29}, & 20 < D_* \leq 150 \\ 0.055, & D_* > 150 \end{cases}$
Soulsby (1997)	$\theta_{cr} = \frac{0.3}{1 + 1.2D_*} + 0.55[1 - \exp(-0.02D_*)]$
Skin friction	$\mu = \frac{C'_F}{C_F}$, where $C'_F = 2\left[\frac{k}{\log\left(\frac{12h}{k_s}\right)}\right]^2$, $k=0.40$ (von Karman)
Non cohesive sediment settling velocity	$W_s = \begin{cases} \frac{(s-1)gD_{50}^2}{18\nu}, & D_{50} \leq 10^{-4}m, \\ \frac{10\nu}{D_{50}} \left[\sqrt{\left(1 + 0.01 \frac{(s-1)gD_{50}^3}{\nu} - 1\right)}, & 10^{-4} < D_{50} \leq 10^{-3}m \\ 1.1\sqrt{(s-1)gD_{50}}, & D_{50} > 10^{-3}m \end{cases}$
Soulsby (1997)	$W_s = \frac{\nu}{D_{50}} [(10.36^2 + 1.049D_*^3)^{1/2} - 10.36]$
Shields parameter	$\theta = \frac{\tau_b}{(\rho_s - \rho_w)gD_{50}}$
Shear velocity	$U_* = \sqrt{\frac{\tau_b}{\rho_w}}$

The sediment transport formulas predict the sediment transport rate Q_b in m^2/s and then the SISYPHE module solves the conservative law equation for sediment mass, the so called Exner equation, in order to predict the bed evolution:

$$(1 - \lambda) \frac{\partial z_b}{\partial t} + (1 - \lambda) \frac{\partial z_b}{\partial t} + \nabla Q_b = 0 \quad (2.10)$$

in which Q_b is the vector of volumetric transport rate per unit width without pores, with components Q_{bx} , Q_{by} in the x and y direction respectively, z_b is the bottom elevation and λ the bed porosity.

The dimensionless current-induced sediment transport rate Φ_b is expressed by the equation:

$$\Phi_b = \frac{Q_b}{\sqrt{g(s-1)d^3}} \quad (2.11)$$

which in many formulas is used to calculate the sediment transport rate.

Some of the widely used sediment transport formulas are presented below:

- Asida-Michiue (1974) Bedload Transport Formula

$$Q_b = \alpha \sqrt{(s-1)gD_{50}} \theta^m \left(1 - \xi \frac{\theta_{cr}}{\theta}\right)^p \left(1 - \sqrt{\xi \frac{\theta_{cr}}{\theta}}\right)^p, \text{ where: } \xi \text{ is the hiding factor and:}$$

$$\begin{aligned} \alpha &= 17.0 \\ m &= 1.5 \\ p &= 1.0 \\ q &= 1.0 \end{aligned}$$

- Schoklich(1962) Bedload Transport Formula

$$q_{cr} = 0.21J^{-1.12} \sqrt{gD_{16}^3}, \text{ where } J \text{ is the energy slope}$$

$$q = H\sqrt{U^2 + V^2} \text{ is the scalar flowrate}$$

$$Q_b = \begin{cases} 0, & \text{if } q \leq q_{cr} \\ \frac{2.5}{s} J^{\frac{3}{2}} (q - q_{cr}), & \text{if } q > q_{cr} \end{cases}$$

- Rottner (1959) Bed Load Transport Formula

$$Q_b = \sqrt{(s-1)gD_{50}^3 \left\{ \frac{\sqrt{U^2 + V^2}}{(s-1)gD_{50}} [0.0667 \left(\frac{D_{50}}{H}\right)^{2/3} - 0.14] - 0.778 \left(\frac{D_{50}}{H}\right) \right\}}$$

- Nielsen (1992) Bedload Transport Formula

$$Q_b = \sqrt{(s-1)gD_{50}^3} = \left(\frac{12\tau_b}{\rho_w(s-1)gD_{50}} - 0.05 \right) \sqrt{\frac{\tau_b}{\rho_w(s-1)gD_{50}}}$$

$$\text{The formula is valid for: } \begin{cases} 1.25 < s < 4.22 \\ 0.00069m < D_{50} < 0.0287m \end{cases}$$

- Meyer-Peter & Muller (1947) Bedload Transport Formula

$$\Phi_b = \begin{cases} 0, & \text{if } \theta < \theta_{cr} \\ a_{mpm}(\theta - \theta_{cr})^{3/2}, & \text{if } \theta > \theta_{cr} \end{cases}$$

$$a_{mpm} = 8.0 \text{ (default),}$$

$$Q_b = \Phi_b \sqrt{g(s-1)D_{50}^3}$$

- Van Rijn (1993) Bedload Transport Formula

$$\Phi_b = \begin{cases} 0, & \text{if } \theta < \theta_{cr} \\ 0.053D_*^{-0.3} \left(\frac{\theta - \theta_{cr}}{\theta_{cr}}\right)^{2.1}, & \text{if } \theta > \theta_{cr} \end{cases}$$

$$Q_b = \Phi_b \sqrt{g(s-1)D_{50}^3}$$

- Cheng (2002) Bedload Transport Formula

$$\Phi_b = 13.0\theta^{1.5} \exp\left(-\frac{0.05}{\theta^{1.5}}\right)$$

$$Q_b = \Phi_b \sqrt{g(s-1)D_{50}^3}$$

- Karim-Kennedy (1983) Total Sediment Transport Formula

$$Q_t = k_1 \left[\frac{\sqrt{U^2 + V^2}}{\sqrt{g(s-1)D_{50}}} \right]^{2.97} \left(\frac{U_*}{W_s} \right)^{1.47} \sqrt{g(s-1)D_{50}^3}, \text{ in which } k_1 = 0.00139$$

- Engelund-Hansen Total Sediment Transport Formula

$$Q_b = 0.1 \sqrt{(s-1)gD_{50}^3} \left(\frac{\tau_b}{(\rho_s - \rho_w)gD_{50}} \right)^5 / C_F, \text{ where } C_F \text{ is the quadratic friction coefficient.}$$

- Frijlink Bedload Formula

The ripple factor is given by the equation $\mu = \frac{18 \log(\frac{12H}{D_{90}})}{18 \log(\frac{12H}{\delta})}$, where H is the local depth.

$$Q_b = D_{50} \mu U^* \exp\left(\frac{-0.27 D_{50} (s-1) \rho_w g}{\mu \tau_b}\right), \text{ where } B=5.0 \text{ (dimensionless coefficient).}$$

- Ackers-White (1973) Total Load Transport Formula

Ackers and White advice the use of D_{35} , thus the D_{50} should be substituted with D_{35} .

$$\text{If } 1 \leq D_* \leq 60: \begin{cases} n = 1 - 0.5 \log(D_*) \\ A = \frac{0.23}{\sqrt{D_*}} + 0.14 \\ m = \frac{9.66}{D_*} + 1.34 \\ \log(C) = 2.86 \log(D_*) - [\log(D_*)]^2 - 3.53 \end{cases}$$

$$\text{If } D_* > 60: \begin{cases} n = 0 \\ A = 0.17 \\ m = 1.50 \\ C = 0.025 \end{cases}$$

$$F_{gr} = \frac{U_*^n}{\sqrt{g D_{50} (s-1)} \sqrt{32 \log(\frac{10H}{D_{50}})}} \left[\frac{\sqrt{U^2 + V^2}}{\sqrt{U^2 + V^2}} \right]^{1-n}$$

$$Q_t = \frac{G_{gr} D_{50} \sqrt{U^2 + V^2}}{(\frac{V^*}{\sqrt{U^2 + V^2}})^n}, \text{ where } G_{gr} = \begin{cases} 0, & \text{if } F_{gr} \leq A \\ C \left(\frac{F_{gr}}{A} - 1\right)^m & \end{cases}$$

The following tables present the results of Karamisheva et al. (2006) study concerning the review of 9 widely used sediment transport formulas. The first table (Table 2.2.) presents the types of data needed in each model and more specifically: Depth (d), Slope (S), particle diameter (D), Viscosity (v), mean velocity (V), shear velocity (U^*) and fall velocity (w).

Table 2.2. Comparison of the input data for different sediment transport formulas (Karamisheva et al., 2006).

Sediment transport formula	d	S	D	v	V	U^*	w
Meyer-Peter & Muller	Yes	Yes	Yes	-	Yes	-	-
Schoklitch	-	Yes	Yes	-	Yes	-	-
Engelund-Hansen	Yes	Yes	Yes	-	Yes	Yes	-
Ackers-White	Yes	Yes	Yes	Yes	Yes	Yes	-
Yang	Yes	Yes	Yes	Yes	Yes	Yes	Yes
Karim-Kennedy	Yes	Yes	Yes	-	Yes	Yes	Yes
Van Rijn	Yes	Yes	Yes	Yes	Yes	Yes	-
Molinas-Wu	Yes	-	Yes	-	Yes	-	Yes
Yang-Lim	Yes	Yes	Yes	Yes	Yes	Yes	Yes

Table 2.3. Data ranges for different calculation methods (Karamisheva et al., 2006).

Sediment transport formulas	Depth (m)	Slope	D (mm)	V (m/s)
Meyer-Peter & Muller	0.01-1.20	0.0004-0.02	0.4-29.0	0.36-2.90
Scholkitch	0.01-0.22	0.00012-0.055	0.3-4.9	0.24-1.40
Engelund-Hansen	0.06-0.31	0.000055-0.019	0.19-0.93	0.19-1.90
Ackers-White	0.18-11.5	0.000022-0.0015	0.04-4.0	0.33-0.87
Yang	0.01-15.0	0.000043-0.028	0.15-1.7	0.24-1.95
Karim-Kennedy	0.03-5.20	0.00015-0.024	0.14-28.65	0.31-2.84
Van Rijn	0.10-16.0	NA	0.19-3.6	0.34-1.55
Molinas-Wu	1.50-62.2	0.000002-0.0025	0.02-2.6	0.2-2.42
Yang-lim	0.01-16.5	0.0003-0.013	0.02-57.0	NA

2.5. Mathematical models for flash flood simulations

Mathematical models (MMs) are the basic tool for FF simulations. They are used for risk assessment of both the current situation and feasible future scenarios but generally have a multipurpose role (van Duivedijk, 2005). They examine the effectiveness of flood defense structures, they are used to evaluate flood damages and for the flood risk maps design. They are also used to evaluate the effects that flood has on buildings, the infrastructure and changes in land use. Last but not least they are useful for the development of Early Warning Systems (EWS), thus contributing to the public safety. MMs for the FF simulation can be stochastic, based on flood frequency analysis, and deterministic which are based on the physical properties of the elements that affect FF (Mambretti et al., 2008).

Deterministic MMs are commonly flood routing MMs that estimate the evolution of a given inflow FF hydrograph, which is the flowrate (Q) as a function of time (t), along the stream, river or flood plain. In 1D hydrodynamic models a set of 2 equations, the continuity and the momentum conservation along x axis, are solved in order to calculate 2 variables of the flow, which are the average velocity (U) in the main direction and the water elevation (H). Flood routing models can be hydrologic or hydrodynamic.

Hydrologic models solve the equation of mass conservation and an empirical equation between flow and storage to determine the outflow hydrograph at the downstream liquid boundary. They are much simpler than the hydrodynamic models; however they should not be applied in cases of rapidly rising inflow hydrographs, such as the case of FF, due to the fact that they neglect backwater effects. Hydrodynamic models, on the other, hand are best suited in these cases, because through solving the 1D or 2D Navier Stokes equations, they calculate the Q , U and H values along the watercourse.

Nowadays, 1D and 2D hydrodynamic models are mostly used for flood risk assessment (Kvočka et al., 2017), even though most of the modeling systems also offer a 3D version. It is of great importance to find an eligible compromise between accuracy and the requirements of the model implication (Diallo, 2010). The choice of the model dimension depends mainly on the domain scale (Huybrechts et al., 2010). Considered once a compromise, 2D models are widely applied to medium scale domains (Mohamed Gharbi et al., 2018), contrarily to the 1D which are used for large domains and 3D applied to small domains.

2.6. Available programs for 2D hydrodynamic models

Several hydrodynamic models are available in the literature for flood modeling, the most popular of which are presented in the following paragraphs.

TELEMAC-MASCARET is owned by the Laboratoire National d'Hydraulique et Environnement (LNHE), part of the R&D group of Electricite de France. The program can be used for a wide variety of applications concerning free-surface flows as flooding, waves generated by dam break, sediment transport and deposition and wind generated waves. It consists of 7 modules, each one being an integrated suite of solvers, focused in different applications. The program can be downloaded via the TELEMA-MASCARET website. Tools for data pre-processing as well as post-processing like results presentation have also been developed and are available for free. An important feature of the program is the open source code that enables the user to make changes.

CCHE2D-Flow is an integrated software package developed at the National Center for Computational Hydroscience and Engineering, the University of Mississippi. It is a numerical model for 2D simulation and analysis of the free surface flows in rivers, lakes, estuaries, and coasts including floods and dam break flows. The processes of sediment transport, morphologic change, pollutant transport and water quality can also be studied using specific modules of the software.

HEC-RAS is probably the most widely used modelling system for simulations concerning water flow in riverbeds or through open channels. The computer program was developed by the US Department of Defense, Army Corps of Engineers in order to manage the rivers, harbors and other public infrastructure under their jurisdiction. The Hydrologic Engineering Center (HEC) in Davis, California developed the River Analysis System (RAS) as a tool for hydraulic engineers who work in channel flow analysis and floodplain determination. It offers numerous data entry capabilities, numerous components for data analysis, data storage and management features, as well as several options for graphing and reporting. Prior to Version 5.0 the program was one dimensional, thus it was unable to model the hydraulic effect of cross section shape changes, bends and other two or three dimensional aspects of the flow. The release of Version 5.0 not only enabled 2D modeling but also the sediment transport study. The basic computational procedure for steady flow is the solution of the 1D energy equations. For unsteady flow, HEC-RAS solves the full, dynamic, 1D Saint Venant Equation using an implicit, finite difference method. The program can be downloaded for free from HEC website.

MIKE FLOOD is also a program that can be considered as candidate for the case study. It is developed by DHI and it is practically a toolbox for flood modelers, which includes numerous 1D and 2D specialized engines, through dynamically coupling 1D (Mike 11 and Mouse) and 2D (MIKE21) modeling techniques. It can be expanded with a range of modules and methods including a flexible mesh overland flow solver, MIKE URBAN, rainfall-runoff modeling and dynamic operation of structures. For these reasons it can be used in many different cases as river and floodplain modeling, flooding in urban environment, streets, drainage networks, coastal areas, dams, levee and dike breaches or any combination of the aforementioned cases. It is widely used worldwide and although it is commercial software, it can be downloaded as a 30 days trial for free.

2.7. Mesh generation and results visualization

Blue Kenue is a widely used application for data pre-processing and post-processing procedures based on EnSim technology that provides tools for computation parameters like mesh generator and geometry, boundary conditions, liquid boundaries, initial conditions and several parameters. The EnSim Simulation Environment was developed at the Canadian Hydraulics Centre (CHC) in order to meet the needs of environmental prediction. The EnSim Core includes a variety of applications like Blue Kenue, Green Kenue, AnemoScope and ECDataExplorer. Blue Kenue was used for mesh editing and mesh generation in the diploma thesis, thus a short presentation of these procedures takes place in the following paragraphs.

Blue Kenue is used for the 2D Triangular Meshes. The T3 Channel Mesher is used to produce triangular meshes of unbranched channels which are then incorporated in the main mesh produced by the T3 Mesh Generator. Each bank of the channel is defined with a set of 2 open lines. Then a value for the "CrossChannelNodeCount" is given, which represents the number of nodes that span the channel, including the edge nodes, with minimum value 2. After a value for the "AlongChannelInterval" is given, which represents the space between the edge nodes. The sub-meshes generated with the T3 Channel Mesher are encompassed in the main mesh produced by the T3 Mesh Generator.

The sub-meshes generated with the T3 Channel Mesher are encompassed in the main mesh produced by the T3 Mesh Generator. The "Outline", the closed line that defines the limit of the computational domain, as well as the "Soft Lines" are first resampled according to the supplied "Density" objects. Next the nodes from "Hard Points", "Hard Lines" and the outline of "Submeshes" are added. Starting from the node with the highest density the algorithm surrounds each node with new ones at a distance determined by the given density. Each node created by the algorithm is inserted in the sorted nod list, with each node being surrounded by 6 others.

As mentioned in the first paragraph Blue Kenue is used except from mesh generation for visualization purposes also. Visualization is provided by 1D, 2D, 3D (Figure 2.2) and Spherical views that can be recorded as digital movies or saved as images for technical reports or presentations. Views and data are geo-referenced and coordinate conversion is supported.

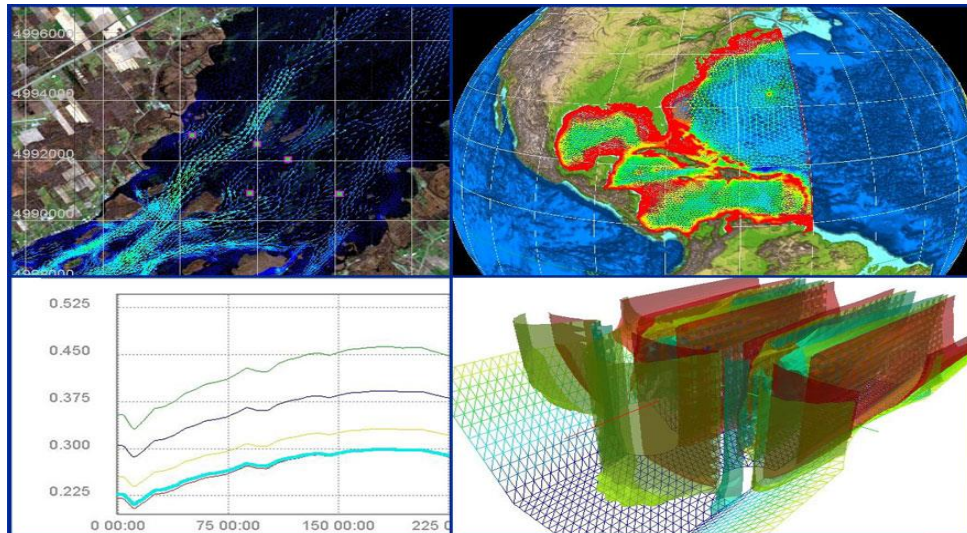


Figure 2.2. Types of visualization in Blue Kenue (source: www.nrc-cnrc.gc.ca).

2.8. The effect of solid materials in surface runoffs

Several studies have been conducted recently in order to investigate the effect of sediment transport and more importantly the FF induced geomorphological changes on the evolution on the flood phenomenon itself. Guan et al. (2015) and Guan et al (2016) came to the conclusion that geomorphological changes increase the flood peak, fact that was confirmed with experiments and MM simulations. Carr et al. (2015) and Tu et al. (2017) analyzed the effect of the morphological changes on the flood magnitude simulating MM.

Rickenmann et al. (2015) studied the contribution of sediment-related processes to the overall damage caused by the flood events caused the rainstorms of 20 to 22 August 2005 in the northern Alps and Prealps, Switzerland. The floods resulted in elevated discharges and flooding in many headwater catchments and mountain rivers. In steeper parts of the areas of study, geomorphic processes were responsible for flow overtopping and sediment deposition (Figure 2.3), both in and outside of the channel network. The study reached to the conclusion that due to the decreasing channel gradient, there was a tendency for bed aggradation, and generally less bedload per unit water discharge.



Figure 2.3. Intense sediment deposition that occurred during the August 2005 floods in parts of Switzerland (source: wileyonlinelibrary.com/journal/espl).

3. Materials and methods

3.1. TELEMAC-MASCARET system

TELEMAC-MASCARET system was selected for the study since it meets the following criteria:

1. The program can be downloaded for free from the system’s website
2. It contains a 2D hydrodynamic module which can be used for flood modeling
3. It also contains a state of the art sediment transport (SISYPHE) module that can be coupled with the hydrodynamic model (TELEMAC-2D).
4. The program’s source code is also accessible in FORTRAN language enabling programming by the user, thus further expanding its versatility.

TELEMAC-MASCARET system is a suit of finite element computer program that can be used for a wide variety of applications concerning free-surface flows. These include flooding, waves generated by dam break, sediment transport and deposition and wind generated waves. It consists of 7 modules (Figure 3.1.), each one being an integrated suite of solvers, which are:

- SISYPHE is the sediment transport and bed evolution module used for complex morphodynamic processes in rivers, lakes, estuaries and shores.
- NESTOR utilizes the data from dredging operations in river beds to model the resulting changes in the bottom level.
- MASCARET 1 is the 1D hydrodynamic module for free surface flow applications as flood propagation, wave resulting from dam break, regulation of managed rivers, flow in torrents, canals wetting, sediment transport and water quality.
- ARTEMIS module is used for wave propagation towards coast or into harbors in a relatively small area or larger domains in cases of long wave simulation.
- TELEMAC-2D is the module used to simulate free surface flows in two dimensions of horizontal space, where vertical speed can be neglected.
- TELEMAC-3D utilizes the same horizontally unstructured mesh to solve the three-dimensional equations as the free surface flow equations and the transport-diffusion equations of intrinsic quantities (temperature, salinity, concentration).

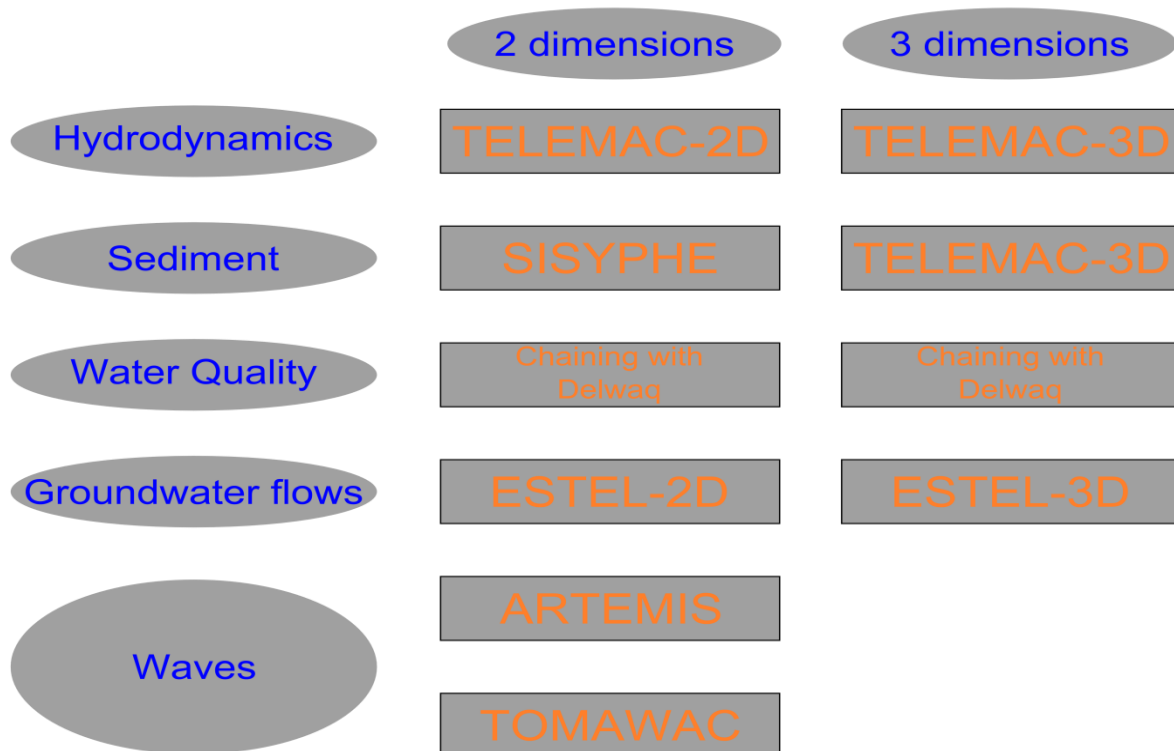


Figure 3.1. TELEMAC-MASCARET system modules and their scope (source: <https://sites.google.com/a/aquacloud.net/15he08/>).

3.1.1. TELEMAC-2D software

The TELEMAC-2D code solves the free surface flow equations with the depth averaged horizontal velocity, neglecting the vertical velocity, known as shallow water equations (described in 2.4.). The software can be used for a wide variety of applications concerning maritime and river hydraulics, like the sizing of port structures and the study of the effects of levees on river flow respectively. Some special applications include the study of thermal plumes, dam breaks, transport of decaying or conservative tracers. The following phenomena are incorporated in the suite of solvers or in one of the coupled modules:

- Propagation of long waves
- Bottom friction
- Coriolis force
- Meteorological phenomena like atmospheric pressure, rain, evaporation and wind
- Turbulence
- Supercritical and subcritical flows
- Horizontal temperature and salinity density gradients
- Cartesian or spherical coordinates
- Land surfaces for flood or shore erosion modeling
- Entrainment and diffusion of a tracer by currents
- Particle tracking and computation of Lagrangian drifts
- Treatment of singularities like levees and culverts
- Levee breaching
- Drag forces generated by vertical structures
- Porosity in solid boundaries
- Wave-induced currents (when coupled with Artemis and Tomawac modules)
- Sediment transport and bed evolution (when couple with Sisyphe module)
- Water quality control (when coupled with water quality tools)

The versatility of the TELEMAC-2D software can be further expanded with the programming of specific functions of the simulation file. This can be done through modification of certain subroutines named "user subroutines".

There are several files that are used as input for the simulation, some mandatory and others optional that are used for specific applications and/or coupling Telemac-2D with other available modules. The input files used by TELEMAC- 2D are the following:

1. The steering file contains the configuration of the computation and is created by a text editor or by the FUDAA-PREPRO software. It can be described as the software' s control panel, where the user can select the keywords for the computational procedure and assign specific values to the model parameters. A common practice for Telemac-Mascaret users is to utilize the existing archive of examples and modify the one that better fits their model. If a keyword is not contained in the file, TELEMAC-2D assigns automatically the default value defined in the dictionary file of the corresponding FORTRAN subroutine. In case that a default value is not defined in the dictionary file, the computation will stop with an error message. A utility called DAMOCLES is used by the software in order to read the dictionary and steering files. The steering file is the first one to be read during the computational procedure. When the steering file is being created, it is necessary to comply with the rules of syntax used in DAMOCLES.

2. The geometry file is a binary file that contains all the information concerning the computational mesh, more specifically the number of mesh points, the number of elements, the number of nodes per element, arrays X and Y containing the coordinates of all the nodes and array IKLE containing the connectivity table. The file can also contain topography information and/or friction at each mesh point. TELEMAC-2D stores the information on the geometry at the start of the results file. Because of this, the computation results file can be used as a geometry file if a new simulation is to be run on the same mesh.

3. The boundary condition file is generated automatically by the BlueKenue or other mesh generator and it can be modified with a standard text editor. Each line of the file is dedicated to one point on the mesh boundary. The numbering used for points on the boundary is that of the file lines. The contour of the domain is described trigonometrically, starting from the bottom left-hand corner and then the islands in a clockwise direction.
4. In case that an initial state of the computation is needed for the model, Telemac-2D enables the use of a previous computation file.
5. The bottom topography file which contains the elevation of the bottom. The bottom information is already available in the geometry file, thus this file is no longer useful.
6. The reference file, which contains the reference results and is used in the frame of a validation procedure.
7. The liquid boundaries file enables the user to specify values for time dependent boundary conditions necessary for unsteady flow simulations.
8. The FORTRAN file, which contains all the subroutines modified by the user and those that have been specifically developed for the computation. This file is compiled and linked so as to generate the executable program for the simulation. Since version 5.0 of the software this file has become optional.
9. The friction data file, which contains information concerning bottom friction
10. The stage-discharge curves file, where the characteristics are prescribed according to specific elevation/flowrate laws. It is a text file that enables the user to configure the evolution of the prescribed value on specific open boundaries.
11. The source file enables the prescription of the values for the time dependent conditions.
12. The sections input file is a text file that enables the user to configure the control sections used during the simulation.
13. The oil spill steering file, which contains all the parameters necessary to the simulation of an oil spill event.
14. The tidal model file, which contains data used for the tide simulation.
15. The ASCII tidal database file.
16. The binary database 1 and 2 files.
17. The weirs file which contains the parameters related to weirs.
18. The culvert data file.
19. The tubes or bridges data file.
20. The breaches data files, containing the characteristics of breaches initiation and growth.
21. The drogues file, which contains the parameters of drogues creation and release.
22. The zones file which contains the description of the friction or other zones.
23. The water quality steering file which contains the parameters used by the water quality module of TELEMAC-2D, which is independent of the water quality handled by DELWAQ.
24. Water quality dictionary which contains the key-words dedicated exclusively to the water quality module.

The output files are the following:

1. The results file, containing graphical results. It is usually in Selafin Format and it contains the information of mesh geometry, the names of the stored variables and the evolution of their values with the time for each time step.
2. The listing printout, which is the "log file" of the computation. If necessary, the user can get additional information by activating the "debugger" keyword, thus the sequence of calls of the subroutines will be presented in the user screen.
3. The section output file, which contains the results of the control section computation.

Telemac2d code solves the following partial differential equations:

$$\frac{\partial h}{\partial t} + u \nabla (h) + h \operatorname{div}(u) = S_h \quad \text{Continuity} \quad (3.1)$$

$$\frac{\partial u}{\partial t} + u \nabla (u) = -g \frac{\partial Z}{\partial x} + S_x + \frac{1}{h} \operatorname{div}(h v_t \nabla u) \quad \text{momentum along x} \quad (3.2)$$

$$\frac{\partial v}{\partial t} + u \nabla (v) = -g \frac{\partial Z}{\partial y} + S_y + \frac{1}{h} \operatorname{div}(h v_t \nabla v) \quad \text{momentum along y} \quad (3.3)$$

$$\frac{\partial T}{\partial t} + u \nabla (T) = S_T + \frac{1}{h} \operatorname{div}(h v_t \nabla T) \quad \text{tracer conservation} \quad (3.4)$$

in which:

- h (m) depth of water
- u, v (m/s) velocity components
- t (m/l or °C) passive (non-buoyant) tracer
- g (m/s²) gravity acceleration
- v_t, v_T (m²/s) momentum and tracer diffusion coefficients
- Z (m) free surface elevation
- t (s) time
- x, y (m) horizontal space coordinates
- S_h (m/s) source or sink of fluid
- S_T (m/s) source or sink of tracer
- H, u and T are the unknowns

3.1.2. SISYPHE module

SISYPHE is the sediment transport and bed evolution module of the TELEMAC-MASCARET SYSTEM. It can be used for complex morphodynamic processes in cases like coasts, rivers and estuaries, for a variety of sediment size classes. In the module sediment transport processes are grouped as bedload, suspended or total load and can be predicted with several formulas from the available library. It can be applied for non-cohesive sediments that are uniform or non-uniform, cohesive sediments or even to sand-silt-clay mixtures. Vertical stratification of sediments can be considered via a multi-layered model. For currents only, as is the case of the flash flood study, the module can be coupled to the depth-averaged shallow water module TELEMAC-2D, or in cases that the vertical component of the speed cannot be neglected TELEMAC-3D. To account for the effect of waves or combined waves and currents SISYPHE can be internally coupled to TOMAWAK. The effect of the secondary currents is also incorporated in SISYPHE module as well as the effect of bed slope associated with the influence of gravity.

Morphological models can be run fully coupled or decoupled depending on the rate of evolution processes. In the case of rapid sediment flow, as the case of FF, a fully coupled approach should be followed. On the other hand when the sediment transport processes evolve in a much larger scale than the hydrodynamic ones, the decoupled approach should be followed. Hydrodynamic solution is used to solve the hydrodynamic continuity and momentum equations on a short time, during which the bottom is frozen and the discretized equation is solved separately (Figure 3.1.). In SISYPHE, there are 2 sediment transport modes according to the transport mechanisms, the bed load and the suspended load: $q_t = q_b + q_s$, where q_b is the total sediment transport, q_b is the bed load, and q_s is the suspended transport.

For the calculation of the suspended sediment transport rate, Sisyphé uses the finite element method to numerically solve the equation presented above. For the bed evolution, Sisyphé solves the Exner equation given by:

$$(1 - p) \frac{\partial Z_b}{\partial t} + \frac{\partial(\delta_c c_b)}{\partial t} + \frac{\partial(qt, x)}{\partial x} + \frac{\partial(qt, y)}{\partial y} + n_e - n_d = 0 \quad (3.5)$$

in which:

- Z_b the bed elevation
- p the bed porosity
- c_b sediment concentration in the bed load layer

The vertical flow of sediment, between the bedload and the suspended layer, is taken into consideration in both the development funds equation as well as the trans-diffusion equation. Several empirical equations have been proposed, they introduce the equilibrium concentration, which represents the concentration at the interface when saturation is reached (Celik and Rodi, 1988). The erosion and deposition are given by: $n_d = V_s c_{ref}$ and $n_e = V_s c_{eq}$ respectively, where c_{ref} the reference concentration and V_s the settling velocity.

Simulations with non-uniform sediment can also be done through the following steps:

- i. the bedload transport rate is computed separately for each class using the one of the available sediment transport formulas in the module's library
- ii. the Exner equation is solved for each class of sediment
- iii. the bed evolution is calculated for each sediment class and then the total bed evolution is calculated

In cases of non-uniform bedload sediment transport moving sediment particles collide and interact as well as they tend to experience hiding and exposure effects, since fine particles are more likely to be hidden and more coarse particles are more exposed to the flow.

The module can incorporate cohesive sediment transport formulas for simulations concerning sediments where silt and clay particles prevail. Generally fine particles display cohesive properties but the definition of what size a fine particle is differs in many countries (63 μ m in the Netherlands, 75 μ m in USA according to Winterwerp and Van Kesteren). Due to the cohesive properties of the fine particles macro-flocs larger than 100 μ m can be formed. In Sisyphé cohesive sediments are accounted by solving the 2D advection-diffusion equation.

Sediments in nature rarely are fine or coarse only, in most cases they are a mixture of both, including gravel, sand, silt, clay and organic material. These complex scenarios can be modeled by a combination of cohesive and non-cohesive sediments. More specifically the sediment mixture can be modeled by a two class bed material, mud and sand. The mud fraction is the slower settling element and the sand fraction the fast settling one.

In order to run a morphodynamic simulation the following set of files is demanded:

1. The steering file which contains the necessary information for running a simulation, including the values of parameters that are different from the default values:
 - i) Input and output files.
 - ii) Physical parameters like particle diameter and settling velocity.
 - iii) Main sediment transport processes as the transport and settling mechanisms.
 - iv) Additional sediment transport processes (secondary currents, the slope effect etc.).
 - v) Numerical options and parameters as the selected numerical scheme and the solvers.
2. The geometry file.
3. The boundary condition file.
4. Any additional or optional input files as the FORTRAN file and the reference file.

SISYPHE solves the conservative law equation for sediment mass or Exner equation in order to calculate the bedload transport flux:

$$(1 - \lambda) \frac{\partial z_b}{\partial t} + \nabla Q_b = 0 \quad (3.6)$$

in which Q_b is the vector of volumetric transport rate per unit width without pores, with components Q_{bx} , Q_{by} in the x and y direction respectively, z_b is the bottom elevation and λ the bed porosity. The bedload transport vector can be decomposed into x and y direction components as: $Q_b = (Q_{bx}, Q_{by}) = (Q_b \cos \alpha, Q_b \sin \alpha)$ in which Q_b is the bedload transport rate per unit width, computed as a function of the equilibrium sediment load closure and α is the angle between the sediment transport vector and the downstream.

The dimensionless current-induced sediment transport rate Φ_b is expressed by:

$$\Phi_b = \frac{Q_b}{\sqrt{g(s-1)d^3}} \quad (3.7)$$

in which s is the ratio ρ_s/ρ , ρ_s is the sediment density, ρ is the water density, d the sand grain diameter and g the gravity acceleration constant.

The available formulas in SISYPHE for non-cohesive uniform sediment transport are presented below. The number shown in brackets corresponds to the one the user has to prescribe in the SISYPHE "cas" file in order to call the specific formula:

- Meyer-Peter & Muller (1) – bedload transport formula
- Einstein- Brown (2) – bedload transport formula
- Engelund-Hansen + Cholley and Cunge (3) – total sediment transport formula
- Engelund-Hansen (30) – total sediment transport formula
- Van-Rijn (7) – bedload transport formula

Suspended sediment transport is predicted by solving the equation:

$$\frac{\partial hC}{\partial t} + \frac{\partial hUC}{\partial x} + \frac{\partial hVC}{\partial y} = \frac{\partial}{\partial x} \left(h \varepsilon_s \frac{\partial C}{\partial x} \right) + \frac{\partial}{\partial y} \left(h \varepsilon_s \frac{\partial C}{\partial y} \right) + E - D \quad (3.8)$$

where $C = C(x, y, t)$ is the depth-averaged concentration expressed in volume percentage, U and V are the depth-averaged components of the velocity in the x and y directions, respectively, ε_s is the turbulent diffusivity of the sediment, often related to the eddy viscosity $\varepsilon_s = \nu_t / \sigma_c$, with σ_c the Schmidt number. In SISYPHE, $\sigma_c = 1.0$.

In SISYPHE it is assumed a Rouse profile for the vertical concentration distribution, which is theoretically valid in uniform steady flow conditions:

$$C(z) = C_{Zref} \left(\frac{z-h}{z} \frac{\alpha}{\alpha-h} \right)^R \quad (3.9)$$

where R is the Rouse number, with k the von Karman constant ($k=0.4$), u_* the friction velocity corresponding to the total bed shear stress, and α the reference elevation above the bed elevation. The distance α , defined variously by different authors.

By depth-integration of the Rouse profile, the following relation can be established between the depth-averaged concentration and the reference concentration:

$$C_{zref} = FC \quad (3.10)$$

$$F^{-1} = \left(\frac{Z_{ref}}{h} \right)^R \int_{Z_{ref}/h}^1 \left(\frac{1-u}{u} \right)^R du \quad (3.11)$$

In SISYPHE, the following expression is used to compute F :

$$F^{-1} = \begin{cases} \frac{1}{(1-Z)} B^R (1 - B^{(1-R)}), & \text{if } R \neq 1 \\ -\text{B} \log B, & \text{if } R = 1 \end{cases} \quad (3.12)$$

with $B = Z_{ref}/h$.

By considering suspended sediment transport, the bed evolution is computed by:

$$(1 - \lambda) \frac{\partial Z_\beta}{\partial t} = D - E \quad (3.13)$$

with λ the bed porosity, and z_b the bed level.

The available formulas in SISYPHE for suspended sediment transport are presented below:

- Zyserman and Fresdoe
- Bijker
- Van Rijn
- Sousby & Van Rijn

In the case of non-uniform sediment transport, moving particles collide and interact. Bed sediment particles experience the hiding and exposure effects, because fine particles are more likely to be hidden and coarse particles have more chance to be exposed to flow. For suspended sediment transport, if the sediment concentration is low, interactions among the moving sediment particles are usually negligible, so that each size class of the moving sediment mixture can be assumed to have the same transport behavior as uniform sediment.

Each sediment class can be transported by suspended-load or bedload. Suspended load mass is exchanged vertically between the water column and the uppermost bed layer. Bedload mass is exchanged horizontally between the top layer of the bed.

In SISYPHE the following steps are performed to account for non-uniform bedload transport: (i) the sediment transport rate is computed separately for each class using the classical formulas, corrected for sand grading effects such as hiding and/or exposure; (ii) the Exner equation is then solved for each class of sediment and (iii) the individual bed evolution due to each class of bed material is then added to give the total evolution due to bedload. Similarly, the suspended transport equation is solved for each class of sediment and the resulting bed evolution for each class is then added to give the total evolution due to the suspended load.

In the following it is assumed a non-uniform sediment mixture divided into N size classes. For bedload sediment transport processes, the evolution of bed topography is governed by the continuity equation, written in Cartesian coordinates for each grain size fraction as:

$$(1 - \lambda) \left(\frac{\partial Z_b}{\partial t} \right)_k + \frac{\partial Q_{bxk}}{\partial x} + \frac{\partial Q_{byk}}{\partial y} = 0 \quad (3.14)$$

where Q_{bxk} , Q_{byk} (m^2/s) are the components of transport rates of the k^{th} size class of bedload; $(\partial Z_b / \partial t)_k$ (m/s) is the rate of change in the bed elevation due to size class k ; and λ is the bed porosity.

For suspended sediment transport processes, the advection-diffusion equation is applied to determine the transport of each size class of suspended load:

$$\frac{\partial}{\partial t} (hC_k) + \frac{\partial (hUC_k)}{\partial x} + \frac{\partial (hVC_k)}{\partial y} = \frac{\partial}{\partial x} (h\varepsilon_s \frac{\partial C_k}{\partial x}) + \frac{\partial}{\partial y} (h \frac{\partial C_k}{\partial y}) + \omega_{sk} (C_{eqk} - C_{Zrefk}) \quad (3.14)$$

where the subscript k indicates the sediment size class index; C_{Zrefk} and C_{eqk} are the actual and near-bed equilibrium concentrations of the k^{th} size class of suspended load, respectively; and ω_{sk} (m/s) is the settling velocity of the k^{th} size class.

There are case studies that modification of the magnitude and the direction of the bedload sediment transport should be done. Three aspects, which can be taken into consideration through different methods in SISYPHE, are presented in the following bullets (Figure 3.2.):

- a. The effect of the local bed slope
- b. Secondary flow effects on the direction of the bed shear stress, also referred as to helical flows in the literature
- c. The bed shear stress partitioning into components affected by skin friction and drag force from bedforms

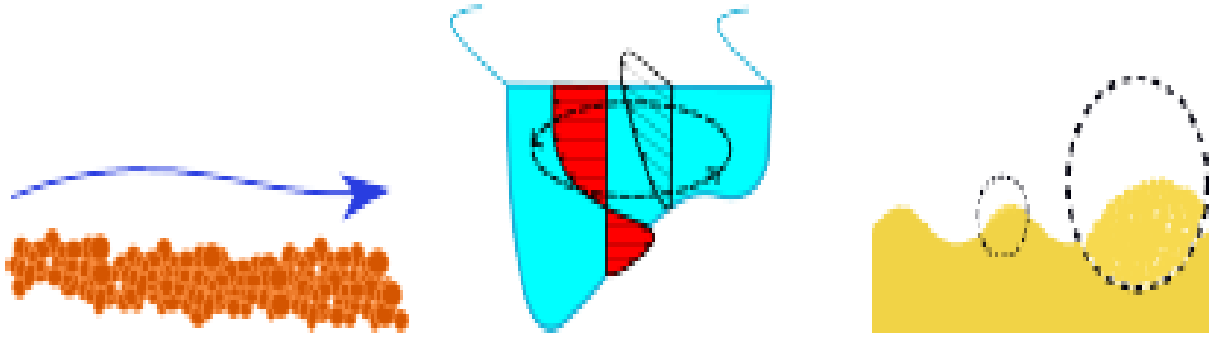


Figure 3.2. Aspects taken into account through SISYPHE correction of magnitude and direction of the bedload sediment transport :the effect of the local bed slope (a), secondary flow effects on the direction of the bed shear stress (b) and the bed shear stress partitioning into componets affected by skin friction and drag force from bedforms.

The angle α is the angle between the sediment transport direction and the x-axis direction will deviate from that of the shear stress by combined action of a transverse slope and secondary currents. In the Cartesian coordinate system, the relation of van Bendegon is:

$$\tan\alpha = \frac{\sin\delta - \frac{1}{f(\theta)} \frac{\partial Z_b}{\partial y}}{\cos\delta - \frac{1}{f(\theta)} \frac{\partial Z_b}{\partial x}} \quad (3.15)$$

Above the term $\frac{\partial Z_b}{\partial x}$ and $\frac{\partial Z_b}{\partial y}$ represent respectively the transverse and longitudinal slopes, Z_b the bottom position and δ the angle between the sediment transport vector and the flow direction, modified by spiral flow. The sediment shape function $f(\theta)$ is a function weight-shear stress or Shields parameter θ . It can be computed according to:

$$\text{Koch and Flokstra:} \quad f(\theta) = \frac{4}{6\theta} \quad (3.16)$$

$$\text{Talmon et al.:} \quad f(\theta) = \frac{1}{\beta_2 \sqrt{\theta}} \quad (3.17)$$

where β_2 is an empirical coefficient. The default value is $\beta_2=0.85$, but an optional value of 1.6 was suggested for the simulation of dunes and bars in a laboratory channel.

The module offers the choice of correction of the magnitude of sediment transport to the user through selecting 1 of the 2 available methods. Koch and Flokstra proposed the following equation based on the modification of the bed load transport rate by a factor that acts as a diffusion term in the bed evolution equation:

$$Q_b^* = Q_b \left(1 + \beta \frac{\partial Z_b}{\partial x}\right) \quad (3.18)$$

where β is an empirical factor accounting for the streamwise bed slope effect (1.3 by default). Soulsby proposed a correction based on the modification of the critical Shields parameter and is therefore only valid for the threshold bedload formulas:

$$\frac{\theta_{\beta cr}}{\theta_{cr}} = \frac{\cos\psi \sin\chi + \sqrt{\cos^2\chi \tan^2\varphi - \sin^2\psi \sin^2\chi}}{\tan\varphi} \quad (3.19)$$

where $\theta_{\beta cr}$ is the critical Shields number for a sloping bed, θ_{cr} is the critical Shields number for a flat, horizontal bed, φ is the angle of repose of the sediment, χ is the angle with the horizontal, and ψ is the angle between the flow and the bed slope directions.

4. Simulation of the benchmark case

4.1. Description

4.1.1. Selection of the benchmark case for the flash flood simulations

Some key aspects of a suited benchmark case for the FF model calibration, concerning the experiment geometry, flow regime and sediment transport processes are respectively:

1. Sloping alluvial channel bend
2. Unsteady flow regime
3. Non-uniform sediment

These features are selected in order to better emulate the FF mechanisms. A benchmark case that meets these criteria is the Yen and Lee experiment (Yen & Lee, 1995) that was selected for model validation in the diploma thesis. The experiment investigated the bed topography and transverse sediment sorting in an alluvial channel under unsteady flow. The mechanisms concerning sediment transport in channel bends, which are common in river topography, are much more complex than in straight channels. More specifically this complexity is defined by the transverse sediment transport due to the transversal flow occurring in the bend area and the deposition of highly non-uniform sediment not only in the longitudinal but also the transverse direction as well as the unsteadiness of the flow.

4.1.2. The Yen and Lee (1995) experiments

Five case studies were conducted in a laboratory 180° channel bend with $r_c=4\text{m}$, width $B=1\text{m}$, and a slope of $S=0.002$. The bend is connected with a stilling basin, an upstream straight reach of 11.5m, a downstream straight reach of the same length, and a sediment settling tank. The water depth was controlled by a weir at the downstream end, which was placed in order to achieve a uniform flow along the bend. Each cross section of the bend is identified by its respective angular position. In the upstream straight reach, it is identified by the distance from the beginning of the bend (negative), and in the downstream one by the distance from the end of the bend (positive), respectively. Layer of sand around 20 cm thick, with $d_o=1.0\text{mm}$ and $\sigma_o=2.5$, was placed on the bed before each run of the experiment. Sand was first sieved into eight sizes, and then laid on the channel.

The base flow was set at $0.02\text{m}^3/\text{s}$ which corresponds to the water depth of 5.44 cm, and the sand mass median diameter $d_{50}=1.0\text{mm}$. The maximum peak discharge was selected in order to avoid the undesirable cross wave phenomenon at the downstream part of the bend (Figure 4.1, Table 4.1). The peak of each hydrograph was set to the first third of its duration.

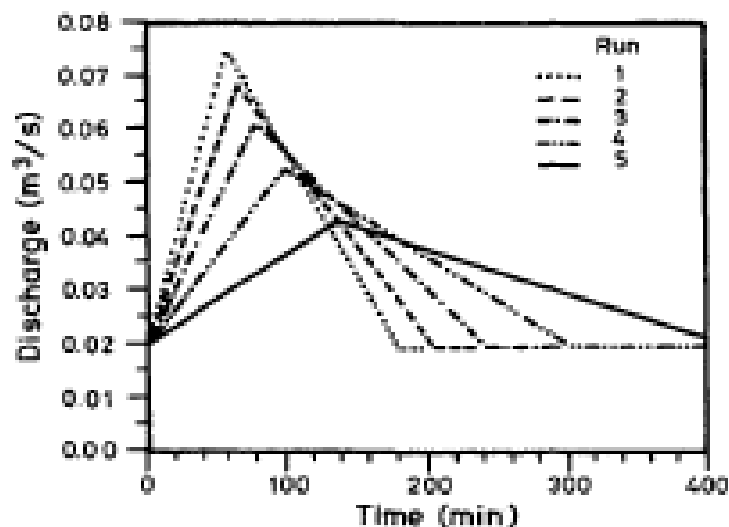


Figure 4.1. Hydrographs of the 5 experiments.

Table 4.1. Characteristics of the 5 experiments (source: Yen & Lee, 1995).

Run	Q_p (m ³ /s)	h_p (m)	T_d (min)
1	0.0750	0.129	180
2	0.0685	0.121	204
3	0.0613	0.113	240
4	0.0530	0.103	300
5	0.0436	0.091	420

Measurements of water levels were taken by a gauge point at the upstream end as well as the measurements of the bed elevation at the peak and the end of the hydrograph for each one of the flow scenarios. After each experiment the flow was stopped and the water slowly drained. The settling tank was lifted in order for the sediment to be weighted and 6 measurements were done in each cross section. The sampling technique that was used was introduced by Little and Mayer (1972) and Yen and Lin (1990). Melted wax was poured into rectangular sections (15 cm by 20 cm) of settled sediment. Then the solidified wax sheet with sediment adhered to it was carefully removed and placed in hot water to separate the sediment particles from the wax. The sediment was then dried, weighted, and sieved.

The results of the 5 runs were presented as isolines (Figure 4.2) of a product of $\Delta Z_b/h_o$, where ΔZ_b the bed deformation and h_o the initial water depth.

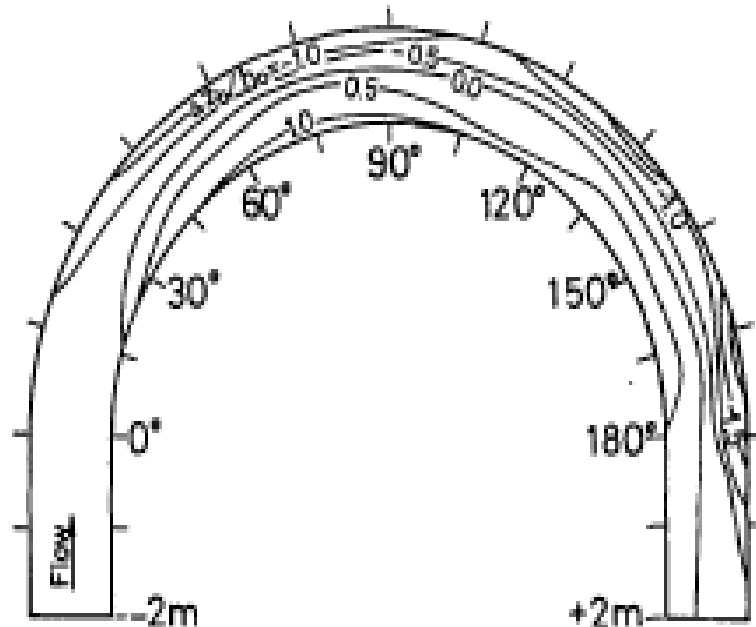


Figure 4.2. Contours of bed deformation for the Run 1 (source: Yen & Lee, 1995).

Contours were presented for all 5 runs, which enable a good understanding of the bed evolution across the channel. The bed evolution data was also thoroughly presented in the cross-sections where the maximum deposition and scour took place (Table 4.2 and Table 4.3). The sediment deposition and scour were measured at distances from the center of the semicircular bend as a product of r/r_c , where r is the radial coordinate of the channel bend and r_c the radius of curvature along the central line in bend. The maximum deposition ($\Delta Z_b/h_o=1.13$) occurred in the inner bank at section 75° for Run 1, which was the experiment during which the maximum scour also took place near the outer bank at section 165°.

Contours of d/d_o were also presented, thus enabling the observation of the longitudinal and transverse variation of the grain size. The experimental results revealed that the maximum variation of d/d_o occurred near the 90° section for all the flow scenarios which was 3.60 in the case of Run 1 and the minimum 0.63 also in the Run 1.

Table 4.2. Transverse variation at section of maximum deposition (Yen & Lee, 1995).

Run	Section	r/r _c										
		0.900	0.913	0.925	0.950	0.975	1.000	1.025	1.050	1.075	1.088	1.100
1	75°	1.13	1.03	0.99	0.86	0.75	0.55	0.30	-0.50	-1.25	-1.47	-1.54
2	75°	0.92	0.81	0.70	0.57	0.35	0.03	-0.11	-0.33	-0.79	-0.88	-1.00
3	75°	0.88	0.81	0.74	0.53	0.30	-0.06	-0.18	-0.24	-0.47	-0.57	-0.65
4	90°	0.81	0.74	0.65	0.33	0.17	-0.07	-0.11	-0.29	-0.33	-0.44	-0.58
5	90°	0.75	0.72	0.63	0.29	-0.02	-0.07	-0.07	-0.13	-0.42	-0.42	-0.40

Table 4.3. Transverse variation at section of maximum scour (source: Yen & Lee, 1995).

Run	r/r _c										
	0.900	0.913	0.925	0.950	0.975	1.000	1.025	1.050	1.075	1.088	1.100
1	0.86	0.80	0.73	0.53	0.37	0.29	0.06	-0.66	-1.34	-1.77	-2.06
2	0.83	0.66	0.61	0.51	0.28	0.16	-0.03	-0.35	-1.04	-1.43	-1.62
3	0.82	0.69	0.62	0.40	0.28	0.07	-0.21	-0.66	-0.96	-1.39	-1.55
4	0.52	0.40	0.36	0.13	0.04	-0.07	-0.14	-0.19	-0.33	-0.60	-0.67
5	0.32	0.18	0.08	-0.03	-0.09	-0.08	-0.07	-0.18	-0.24	-0.35	-0.42

4.2. The benchmark model simulations

Several models of the Yen and Lee (1995) experiments were used, in the context of the diploma thesis, based on the model released with the v7p3r0 version of TELEMAC-MASCARET SYSTEM. Many simulations of the 5 Runs were conducted and the results of 42 of them are presented in the following pages as filled contours and cross-sectional graphs. 12 of them concern the uniform simulations of the Run-4 and the rest the non-uniform simulations of the 5 Runs. The goal of these simulations was to investigate:

1. The better suited bedload sediment transport formula for the model
2. The contribution of sediment transport processes in the hydrodynamic characteristics of the flow
3. The selection of a multigrain or a uniform sediment approach for the model.

Two dimensional hydrodynamic models might be suited for flood simulations but lack certain aspects essential to simulate the secondary currents occurring in meandering channels. Recirculating cells in the transverse direction are responsible for the occurrence of meandering, which is an important process in river morphology (Abad et al., 2008). Consequently when coupled with 2D flow models, the effect of secondary currents on the direction and magnitude of the sediment transport rate needs to be parameterized (C. Villaret et al., 2013). The effect of bed effects on bed morphology were simulated by calibrating the PRODUCTION COEFFICIENT FOR SECONDARY CURRENTS in the TELEMAC-2D ".cas" file and the PARAMETER FOR DEVIATION in the Talmon et al. formulation in the SISYPHE ".cas" file. These parameters, A and β_2 , can be calibrated by trial and error. A. Mendoza et al. (2016) suggested the values of 12 and 1.6 for A and β_2 respectively for meandering channel simulations. These values were also used for the diploma thesis simulations, since they produced the most accurate results. Other cases of lower A parameter and higher β_2 value were found to give favorable results in some experiment simulations (low flowrate, high duration) but generally lacked the consistency of the predictions of A. Mendoza et al. (2016) calibration.

An essential part of the benchmark case study was to investigate the efficiency of several STF in conditions that share similar characteristics with FF. SISYPHE module includes some of the most used sediment transport formulas, more specifically: Meyer-Peter & Mueller, Einstein-Brown, Engelund-Hansen & Cholley-Cunge, Engelund-Hansen, Van Rijn and Hunziker (developed only for non-uniform sediment simulations). This catalogue was further expanded in the context of the diploma thesis and Karim Kennedy, Cheng, Reid, Yang Lim, Ackers White and Frijlink formulas were also included. This was possible due to the flexibility of the open source system that enables the user to use other sediment transport formulas. Simulations of 12 models using different formulas were first conducted using single grain sediment and then the 6 that performed better were used for the multigrain simulations.

Simulations were conducted both with the mass median diameter of 1mm and the grain-size distribution curve proposed by M. Bui & P. Rutschmann (2009) (Table 4.4, Figure 4.4). The exact sediment gradation is not given by Yen and Lee (1995), only the mass median diameter and the distribution of the sediment is provided. Different approaches exist in the literature, of which the M. Bui & P. Rutschmann (2009) was considered the one that better fits the benchmark case, since it consists of 8 fractions with grain sizes described in the experiments. The results of the uniform and non-uniform sediment simulations can be compared in order to determine the contribution of the hiding and exposure effect (Figure 4.3).

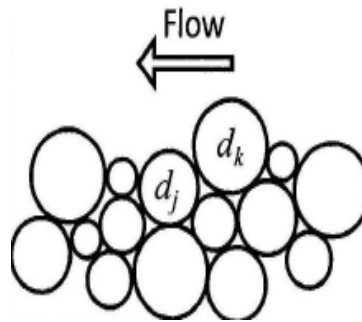


Figure 4.3. The concept of hiding and exposure effect (source: SISYPHE manual).

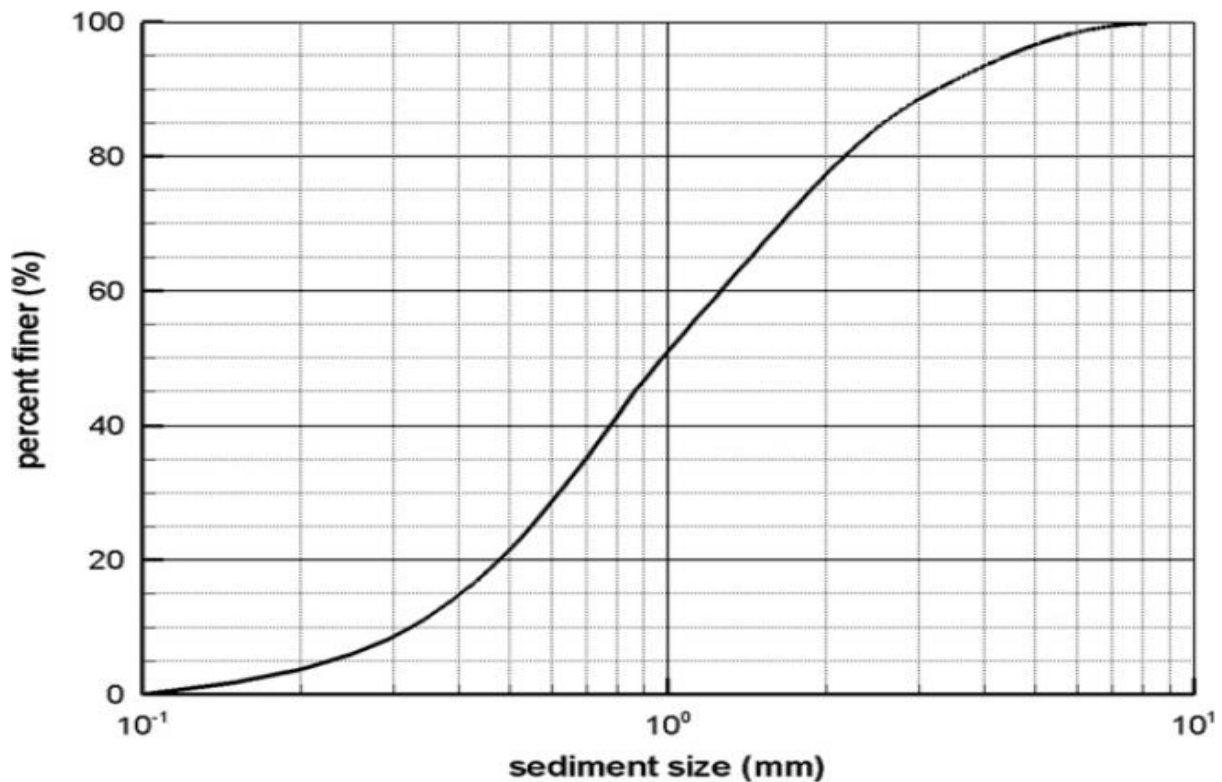


Figure 4.4. Initial sediment size gradation curve (M. Bui & P. Rutschmann, 2010).

Table 4.4. Sediment size classes used in the non-uniform sediment simulations.

Size class	1	2	3	4	5	6	7	8
Grain size (mm)	8.52	4.76	3.36	2.00	1.19	0.84	0.42	0.25
Fraction (%)	5.0	5.0	14.0	18.0	18.0	25.0	10.0	5.0

A critical Shields parameter of 0.047 was selected for the model. A friction coefficient of 0.0035m was used to simulate the flat bed conditions. A Talmon et al. approach was used for the correction of the direction of bedload transport rate and Koch and Flokstra approach for the correction of the intensity of bedload transport rate.

4.3. Previous numerical works

C. Villaret et al. (2013) studied the flow and sediment transport in a curved channel through a TELEMAC-2D/SISYPHE model simulation of Yen & Lee (1995) Run-4 experiment, emphasizing in the effects of the secondary currents on the direction and magnitude of the sediment transport. The sediment was assumed uniform in order to focus in the calibration of the secondary current approach. The bedload formula of Meyer-Peter & Mueller was applied with a critical Shields parameter of 0.033, corresponding to the mean grain size. The bed roughness was taken 3 times the mean diameter ($k_s=0.003m$), which corresponds to the flat bed conditions. For the sloping bed effect, the approach of Koch and Flokstra (1981) for magnitude and Talmon (1992) for the direction was used. The parameter in the secondary current parameterization was set to $\alpha'=1$, because no bed forms occurred in the experiment. The model results were considered satisfactory according to the authors.

M. Bui & P. Rutschmann (2010) used the computer code FAST3D to simulate the Yen & Lee experiments. The code calculates the flow field by solving the full Reynolds-averaged Navier-Stokes equations with $k-\epsilon$ turbulence model. The bed load transport was simulated with a non-equilibrium adaptation length, which characterizes the distance for sediment to adjust from a non-equilibrium state to an equilibrium state. Based on the stochastic bed-load description of Einstein 1950; Tsubaki and Saito (1967) were the first to investigate the non-equilibrium concept to sediment transport used in the model. The governing equations are solved numerically with a finite volume method on an adaptive, non-staggered grid. The authors concluded that the non-equilibrium approach could not produce good results for the case with strong unsteadiness characteristics. The adaptation-length formula proposed by Phillips and Sutherland gave the best results.

The model found in the "examples" file of v7p3r0 used the bedload formula of Engelund-Hansen & Cholley-Cunge and a 5 class sediment approach. A critical Shields parameter value of 0.047 was selected for all sediment classes and the bed roughness was taken 0.0035m, which corresponds to the flat bed conditions. For the sloping bed effect, the approach of Koch and Flokstra (1981) for magnitude and Soulby for the direction was used. The parameter in the secondary current parameterization was set to $\alpha'=1$, because no bed forms occurred in the experiment. The effect of the secondary currents was not taken into account in the hydrodynamic model. The β_2 parameter for direction correction was selected 0.85 and the friction angle of the sediment 35° .

Xiao et al. (2012) studied the formation of meandering channel by a 2D numerical simulation of a 2D depth-averaged model for hydrodynamic, sediment transport and bed evolution model developed by Wang et al. (2010). This model was further expanded in order to incorporate the secondary current effects that characterize the Yen & Lee (1995) experiments. The hydrodynamic model is solved in the orthogonal curvilinear grid system by using the Beam and Warming alternating-direction implicit scheme. The influence of the secondary flow on sediment transport was taken into account with Koch and Flokstra (1981). A six class sediment simulation was conducted and the bed armoring was also taken into account. The results were considered very satisfactory.

J. Abad et al. (2007) presented a 2D depth-averaged hydrodynamic, sediment transport and bed morphology model named STREMR HySeD. The depth-averaged sediment equations are derived from the 3D dilute, multiphase, flow equations and are incorporated into the hydrodynamic model STREMR. The hydrodynamic model includes a two equation turbulence model and a correction for the mean flow due to secondary flows. A Manning coefficient of 0.028 was used and the porosity was set to 0.4. The bedload formula used in the model is Meyer-Peter & Mueller (1948). Bernard (1993) implemented a correction for secondary flows that allows the STREMR to shift the maximum core of the velocity to the outer bank. According to the authors the numerical results were found to be encouraging.

4.4. Results presentation

4.4.1. Run-1/non-uniform sediment simulations

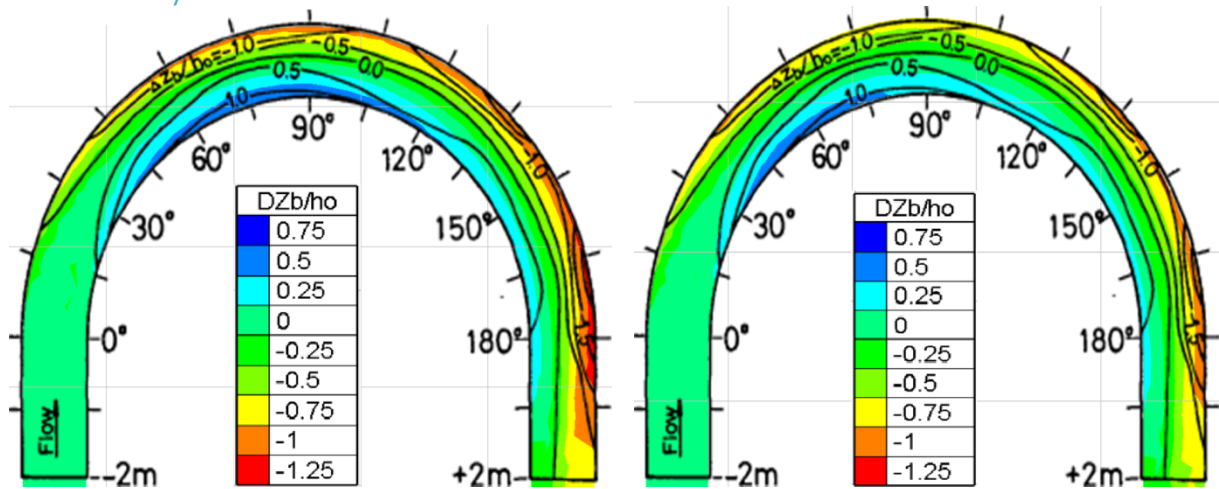


Figure 4.5. Filled contours of bed deformation for Cheng and Reid formulas compared to experimental data isolines.

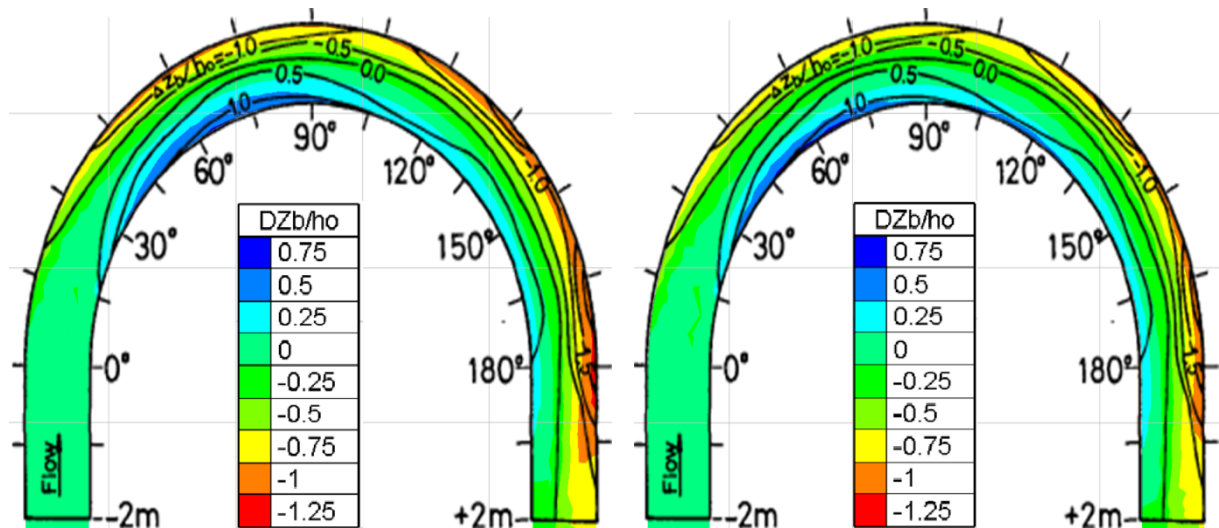


Figure 4.6. Filled contours of bed deformation for Meyer-Peter & Mueller and Einstein-Brown formulas compared to experimental data isolines.

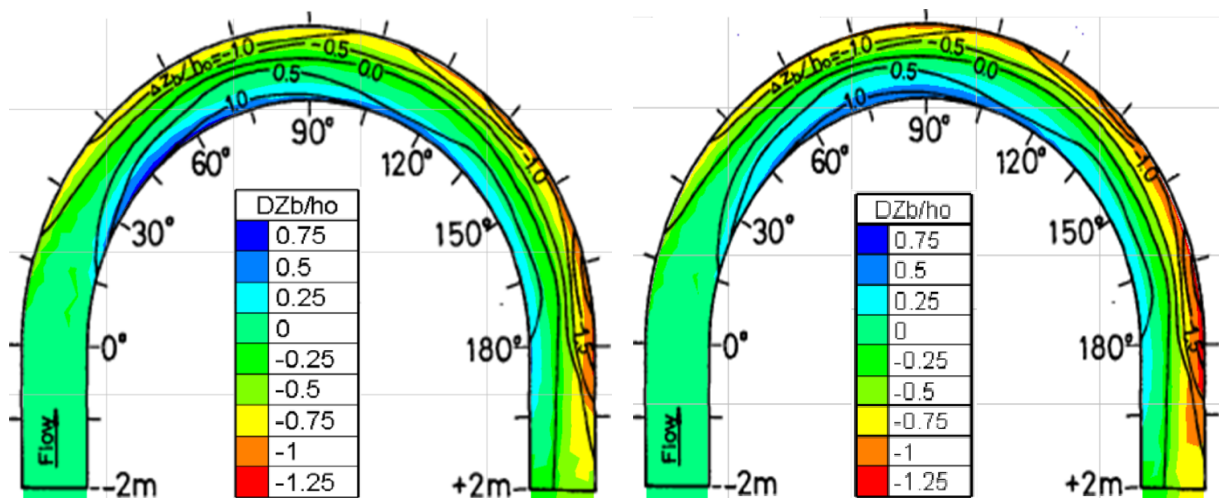


Figure 4.7. Filled contours of bed deformation for Hunzinger and Van Rijn formulas compared to experimental data isolines.

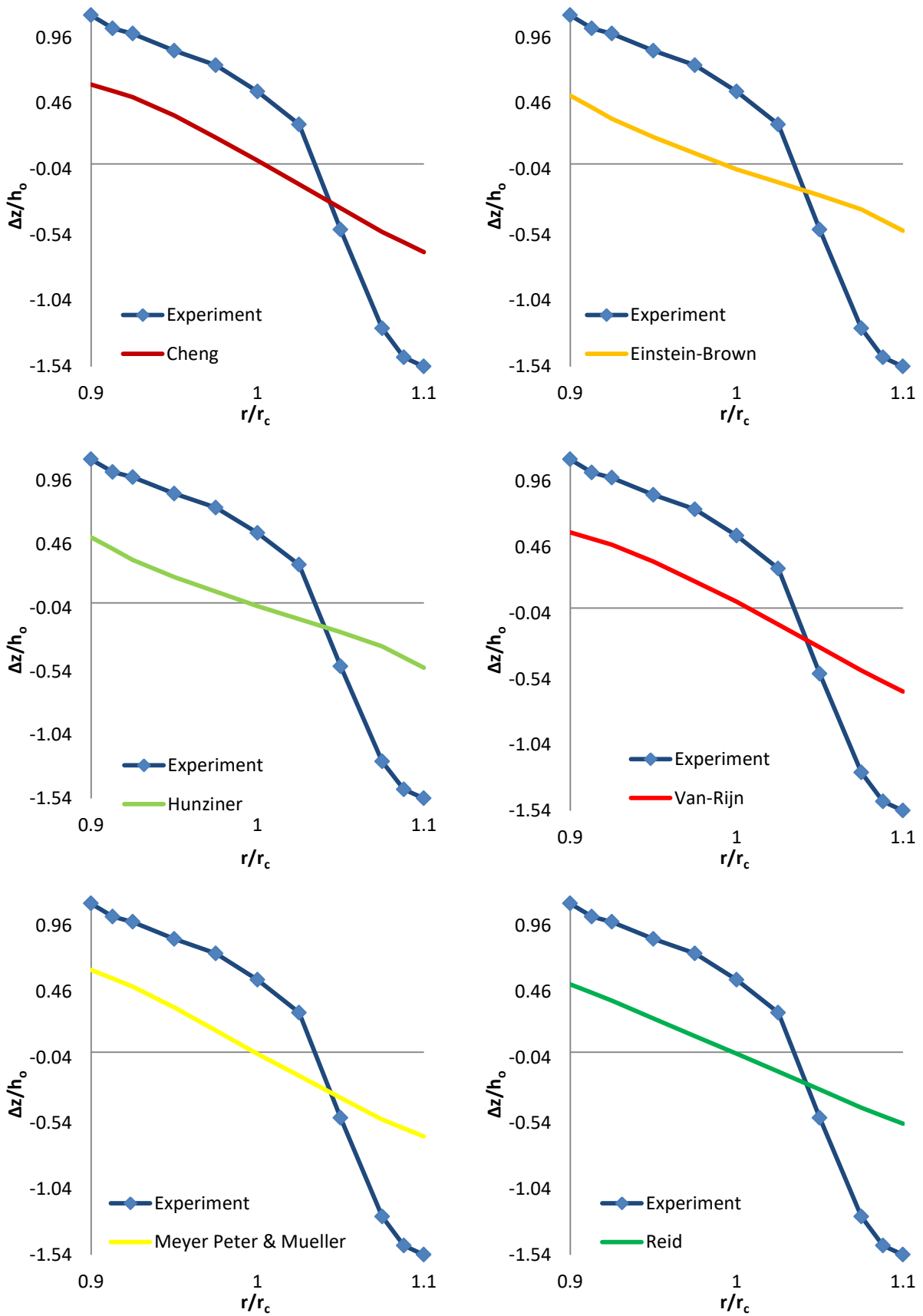


Figure 4.8. Comparison between sediment transport formulas predictions and the experimental data concerning the bed evolution in the cross-section experimentally defined as the area of maximum deposition (75° cross-section).

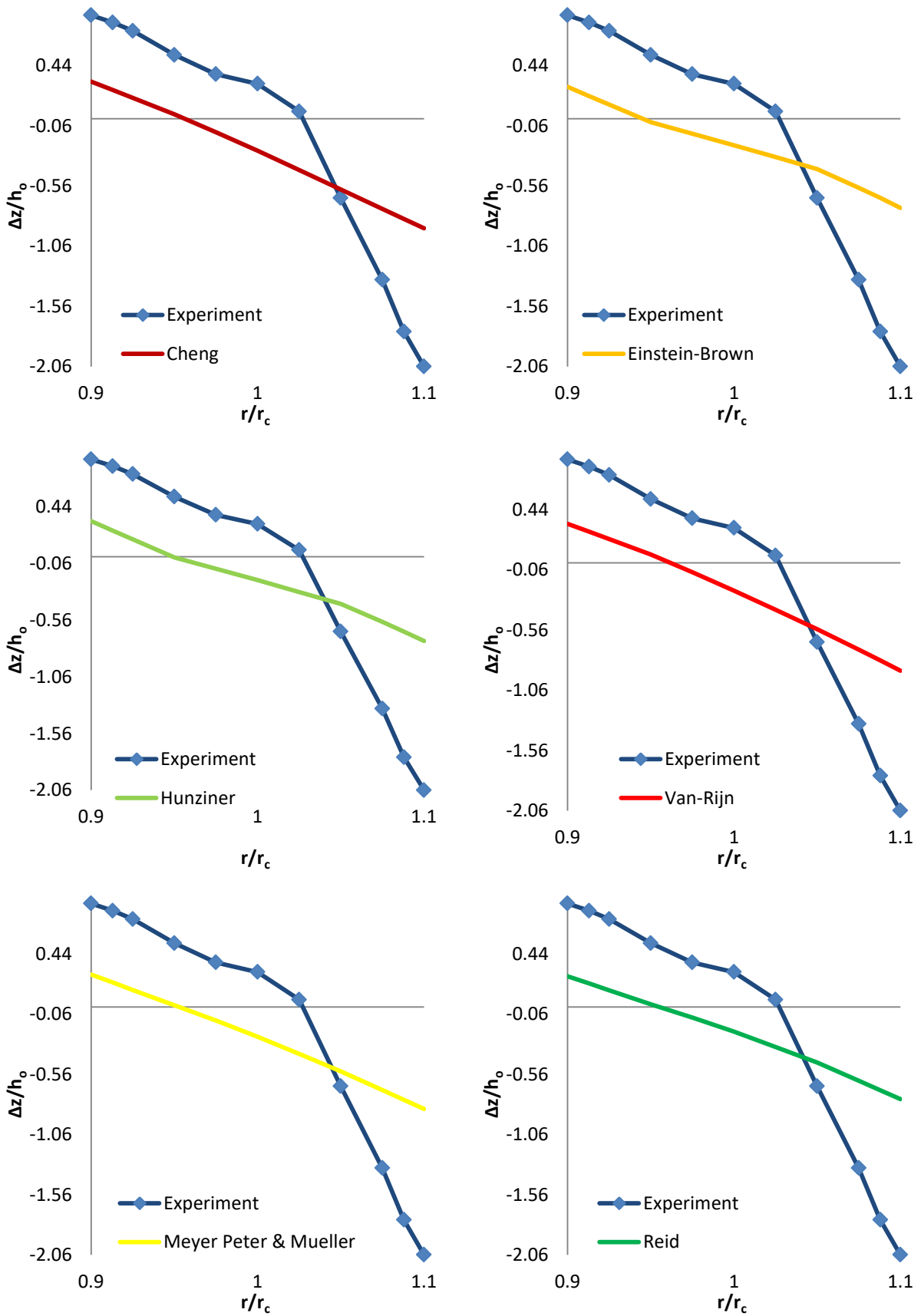


Figure 4.9. Comparison between sediment transport formulas predictions and the experimental data concerning the bed evolution in the cross-section experimentally defined as the area of maximum deposition (165° cross-section).

4.4.2. Run-2/non-uniform sediment simulations

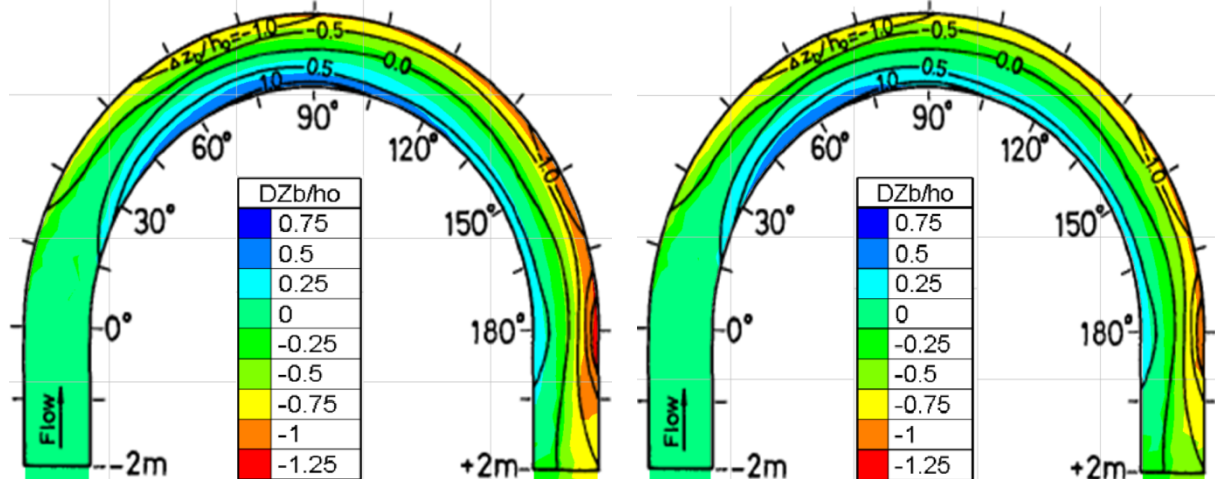


Figure 4.10. Filled contours of bed deformation for Cheng and Reid formulas compared to experimental data isolines.

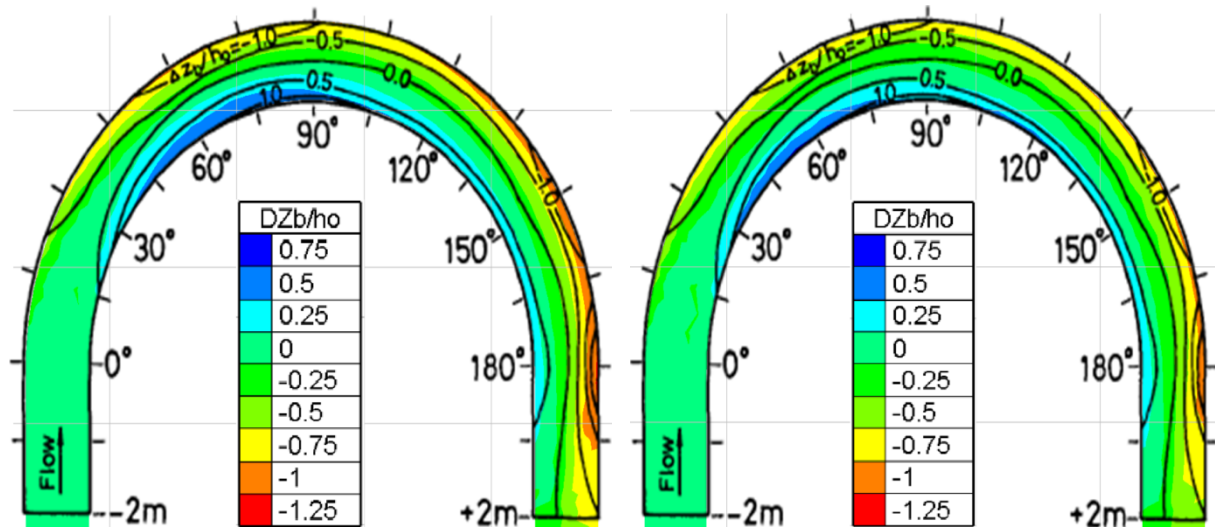


Figure 4.11. Filled contours of bed deformation for Meyer-Peter & Mueller and Einstein-Brown formulas compared to experimental data isolines.

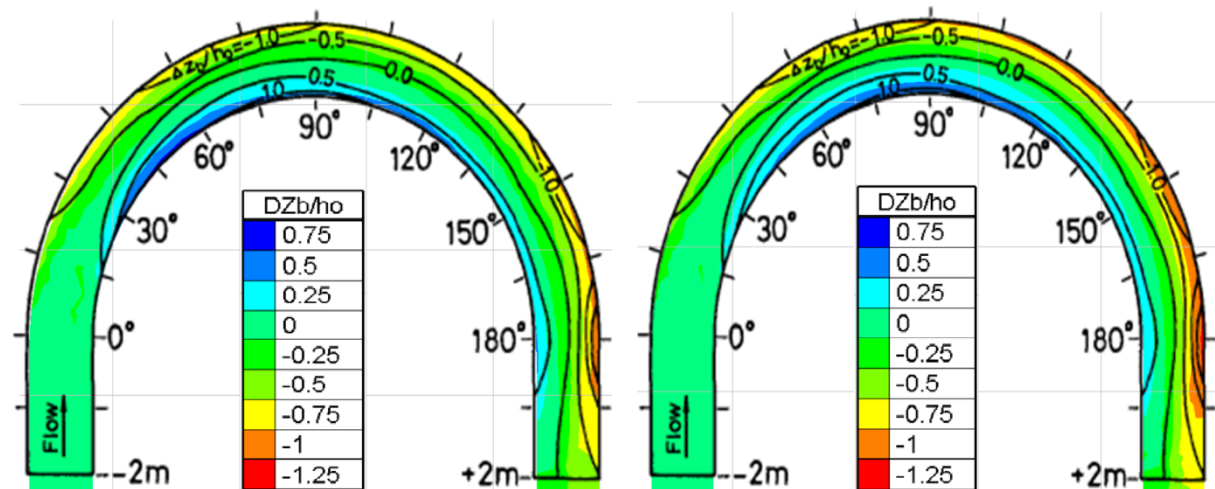


Figure 4.12. Filled contours of bed deformation for Hunzinger and Van Rijn formulas compared to experimental data isolines.

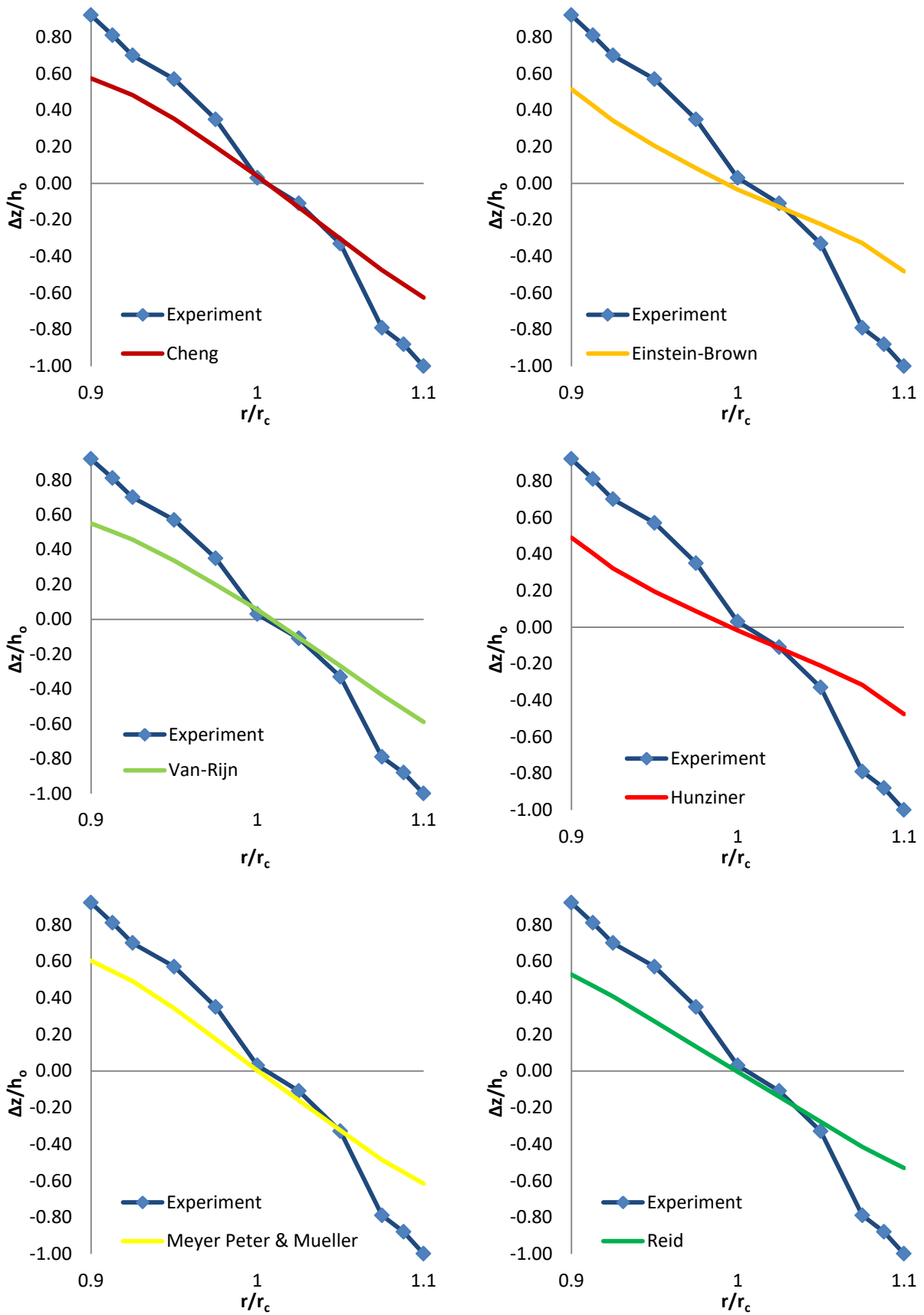


Figure 4.13. Comparison between sediment transport formulas predictions and the experimental data concerning the bed evolution in the cross-section experimentally defined as the area of maximum deposition (75° cross-section).

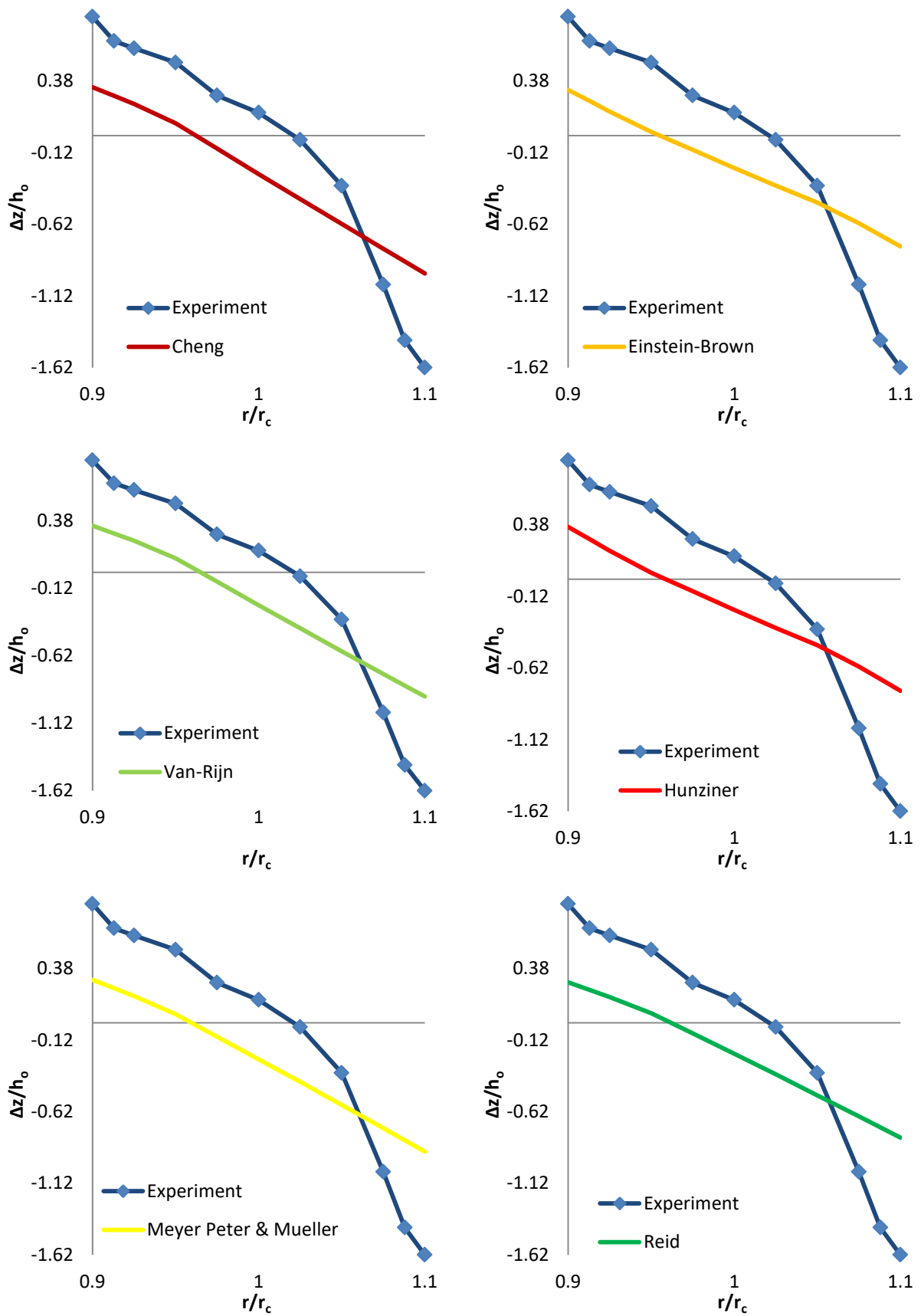


Figure 4.14. Comparison between sediment transport formulas predictions and the experimental data concerning the bed evolution in the cross-section experimentally defined as the area of maximum deposition (180° cross-section).

4.4.3. Run-3/non-uniform sediment simulations

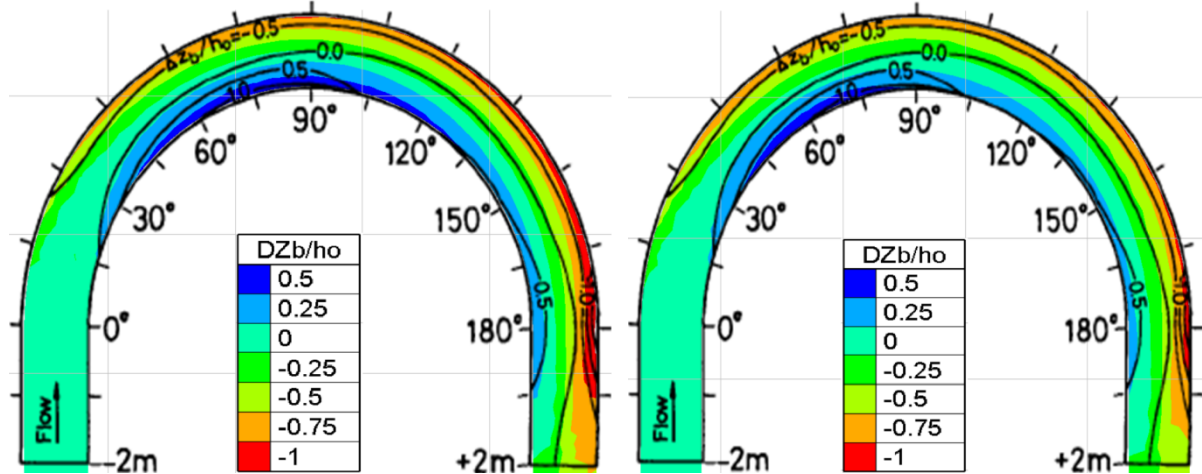


Figure 4.15. Filled contours of bed deformation for Cheng and Reid formulas compared to experimental data isolines.

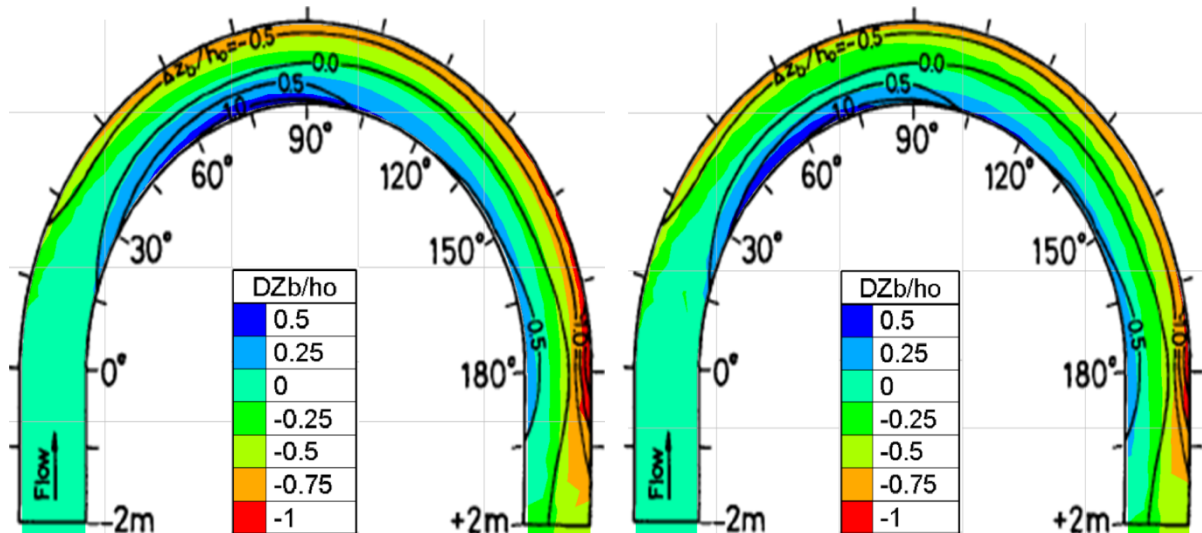


Figure 4.16. Filled contours of bed deformation for Meyer-Peter & Mueller and Einstein-Brown formulas compared to experimental data isolines.



Figure 4.17. Filled contours of bed deformation for Hunzinger and Van Rijn formulas compared to experimental data isolines.

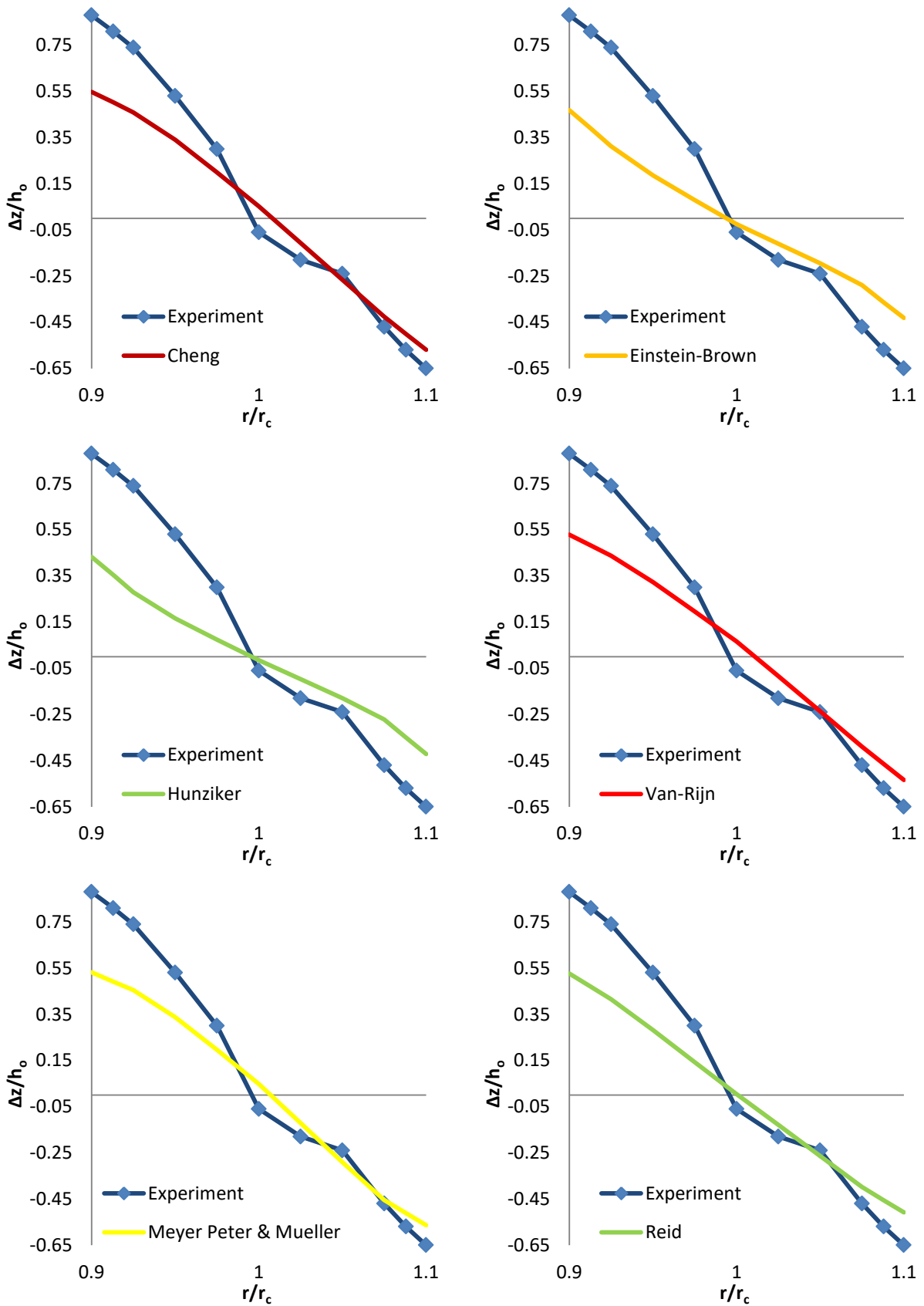


Figure 4.18. Comparison between sediment transport formulas predictions and the experimental data concerning the bed evolution in the cross-section experimentally defined as the area of maximum deposition (75° cross-section).

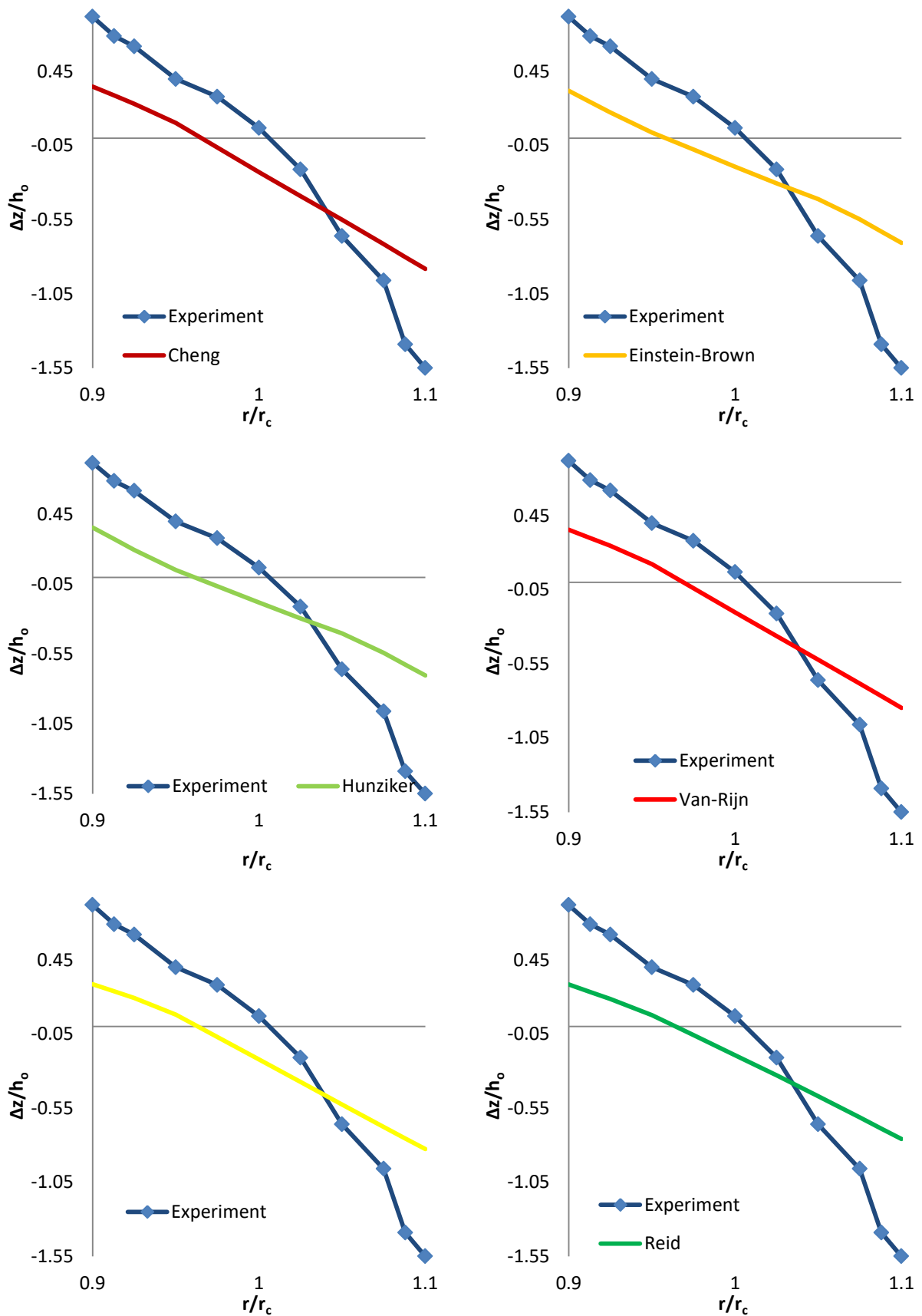


Figure 4.19. Comparison between sediment transport formulas predictions and the experimental data concerning the bed evolution in the cross-section experimentally defined as the area of maximum deposition (180° cross-section).

4.4.4. Run-4/non-uniform sediment simulations

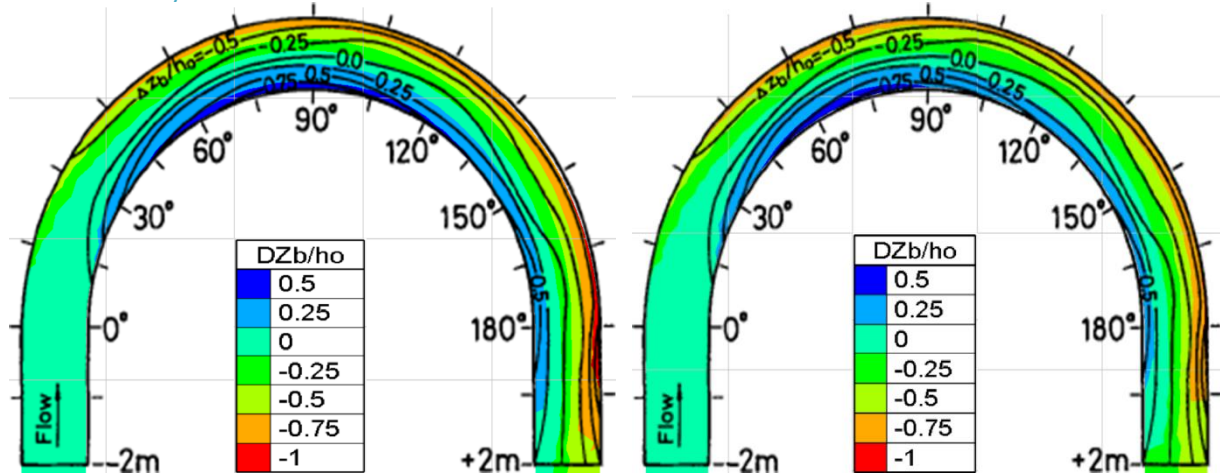


Figure 4.20. Filled contours of bed deformation for Cheng and Reid formulas compared to experimental data isolines.

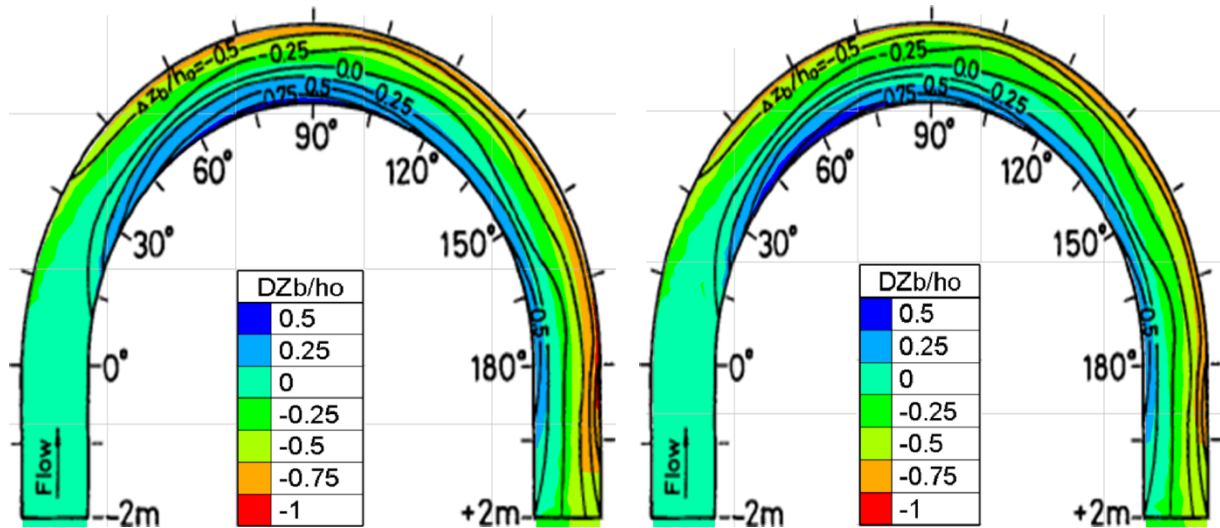


Figure 4.21. Filled contours of bed deformation for Meyer-Peter & Mueller and Einstein-Brown formulas compared to experimental data isolines.

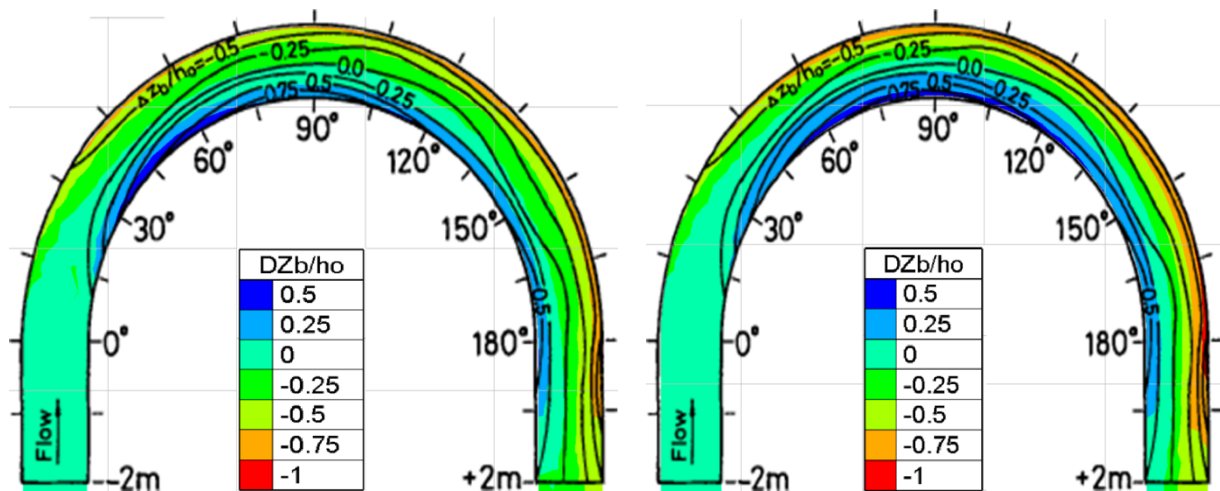


Figure 4.22. Filled contours of bed deformation for Hunzinger and Van Rijn formulas compared to experimental data isolines.

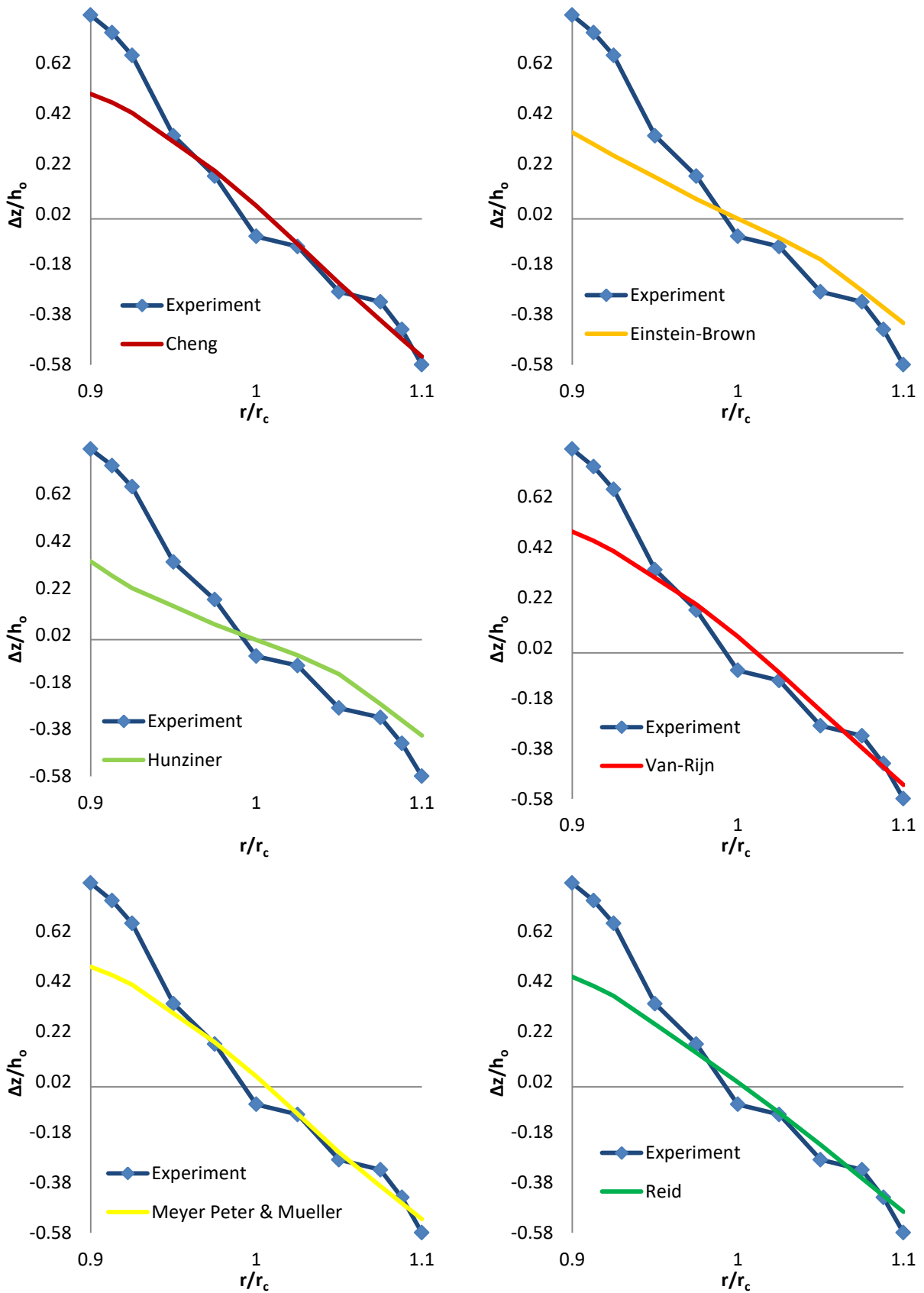


Figure 4.23. Comparison between sediment transport formulas predictions and the experimental data concerning the bed evolution in the cross-section experimentally defined as the area of maximum deposition (90° cross-section).

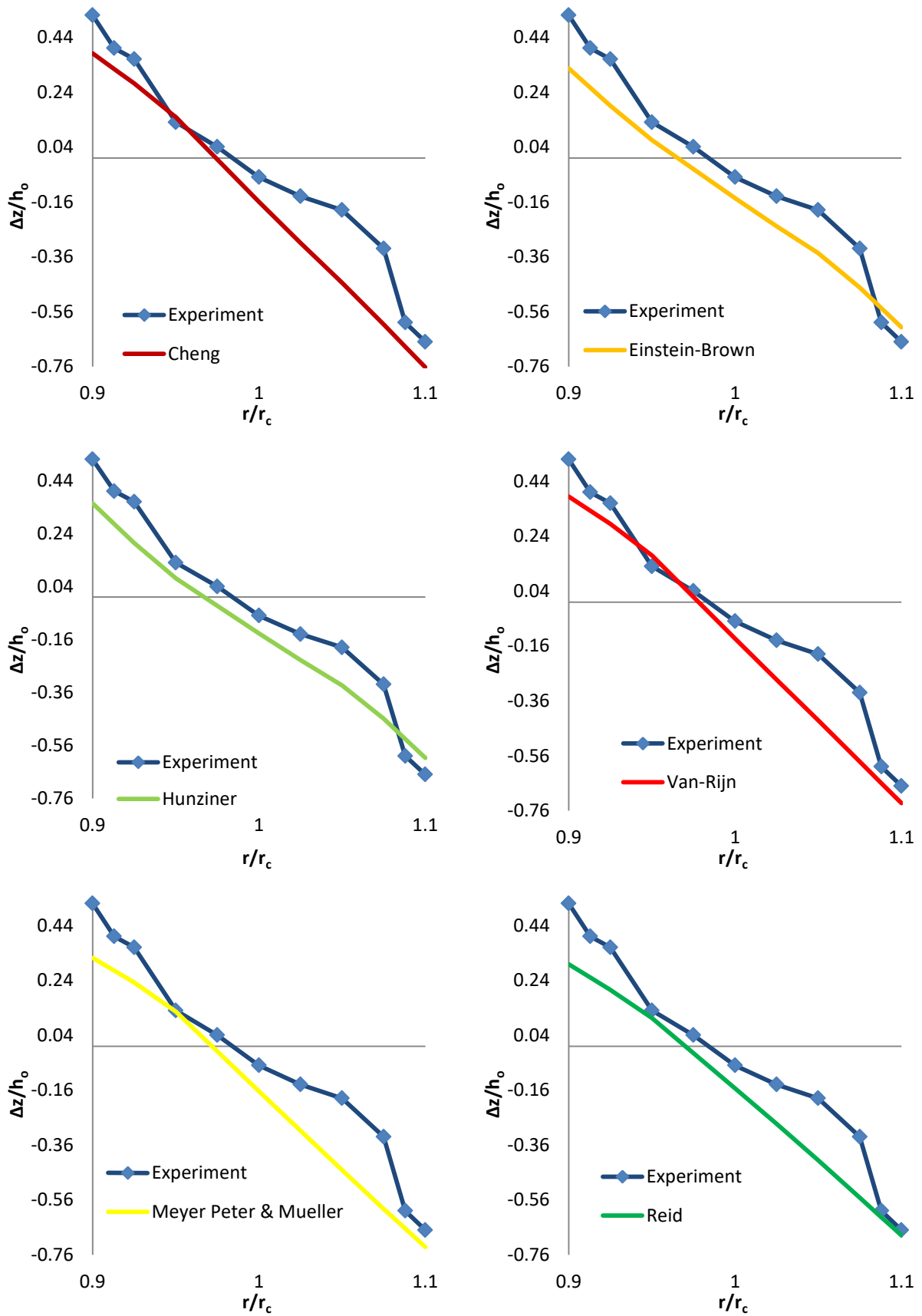


Figure 4.24. Comparison between sediment transport formulas predictions and the experimental data concerning the bed evolution in the cross-section experimentally defined as the area of maximum deposition (180° cross-section).

4.4.5. Run-5/non-uniform sediment simulations

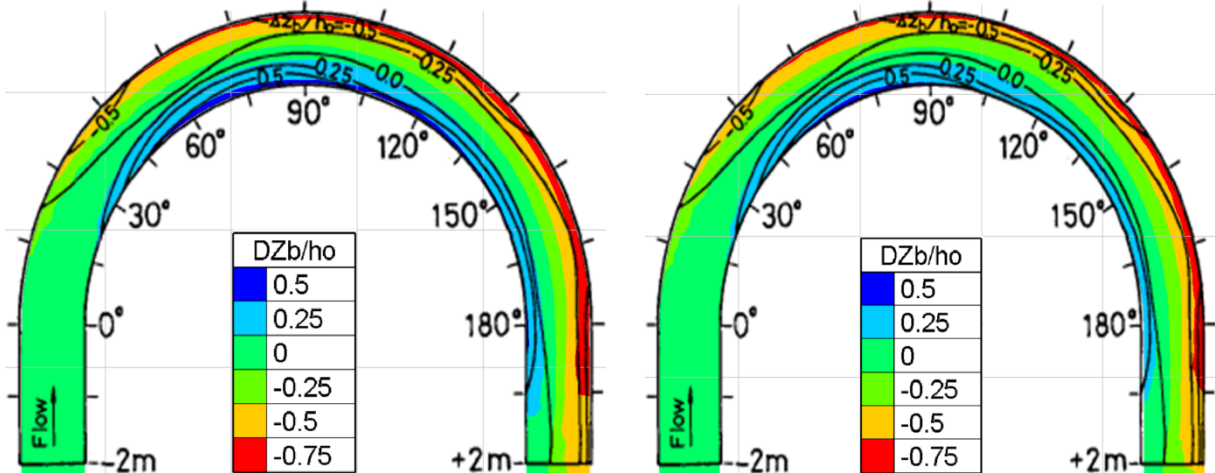


Figure 4.25. Filled contours of bed deformation for Cheng and Reid formulas compared to experimental data isolines.

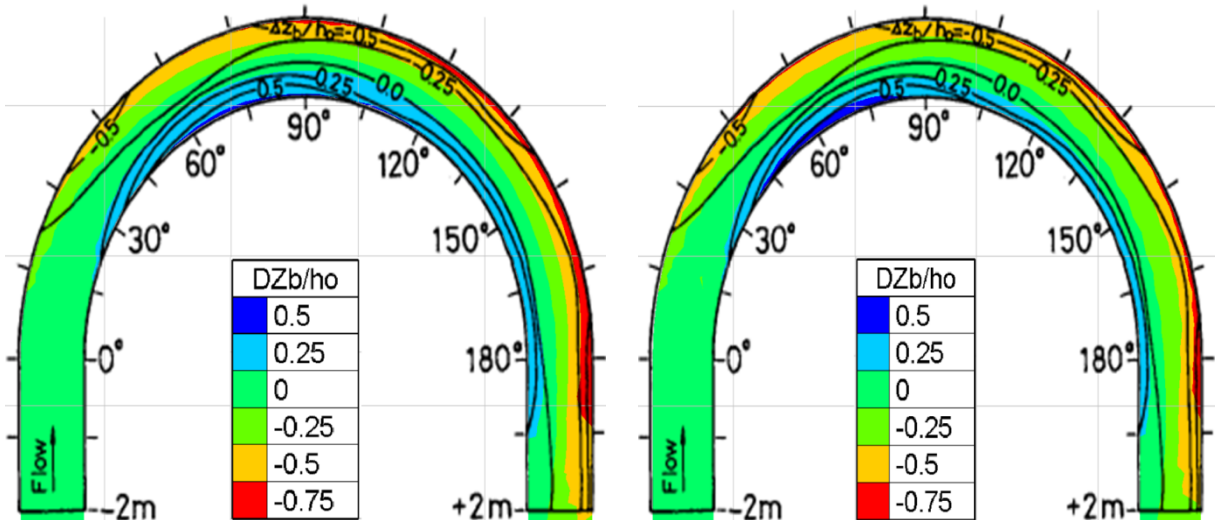


Figure 4.26. Filled contours of bed deformation for Meyer-Peter & Mueller and Einstein-Brown formulas compared to experimental data isolines.

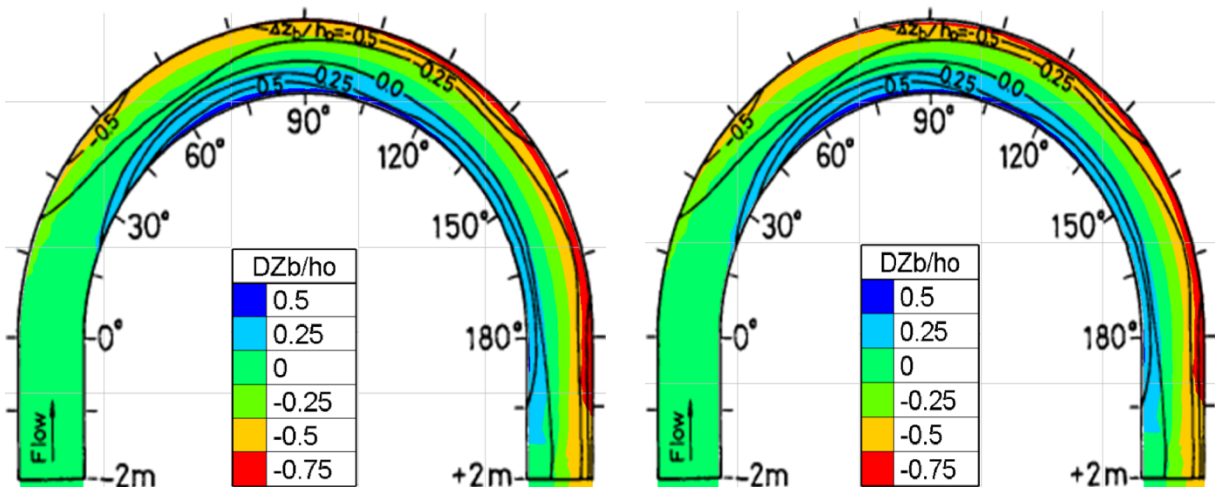


Figure 4.27. Filled contours of bed deformation for Hunzinger and Van Rijn formulas compared to experimental data isolines.

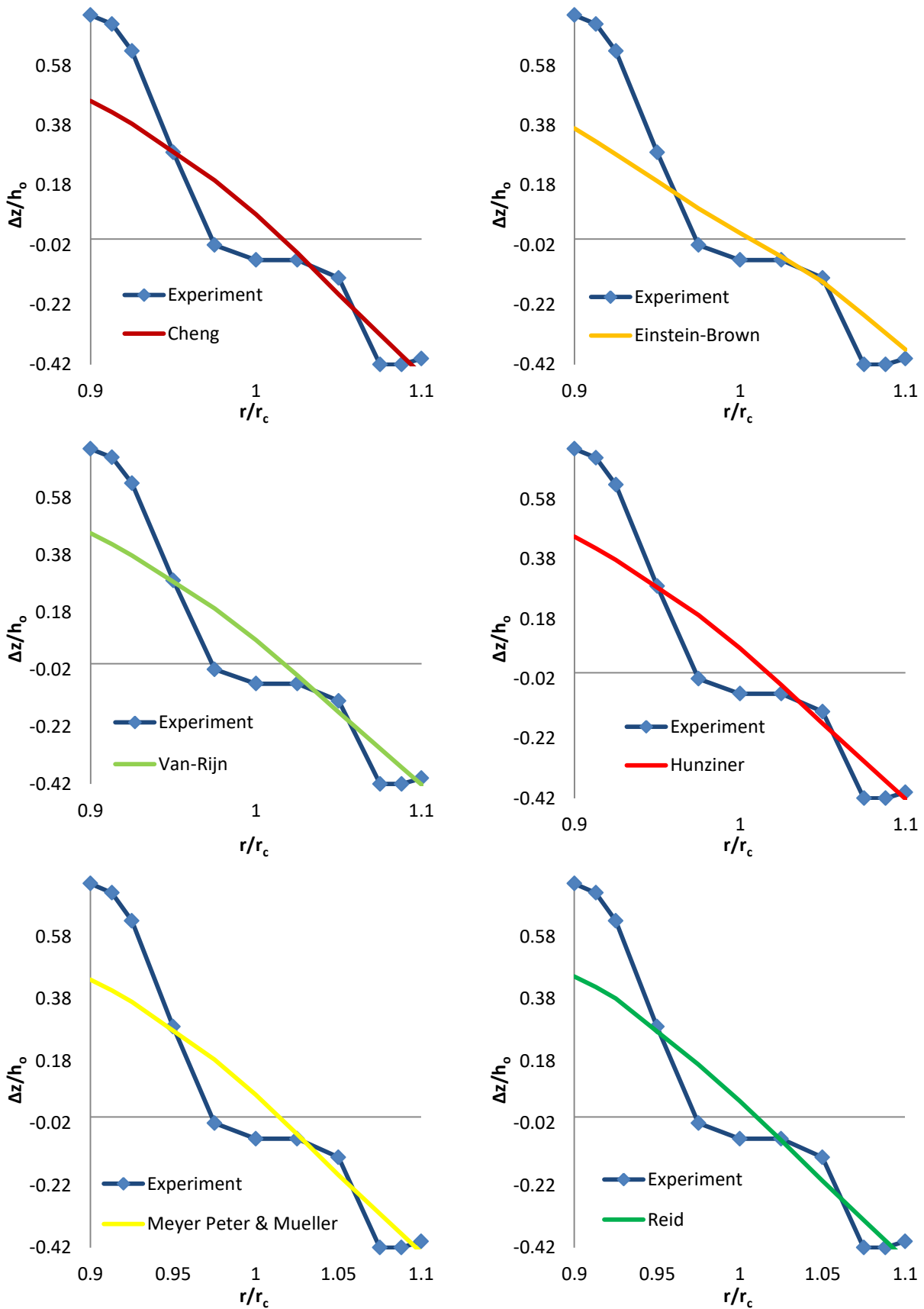


Figure 4.28. Comparison between sediment transport formulas predictions and the experimental data concerning the bed evolution in the cross-section experimentally defined as the area of maximum deposition (90° cross-section).

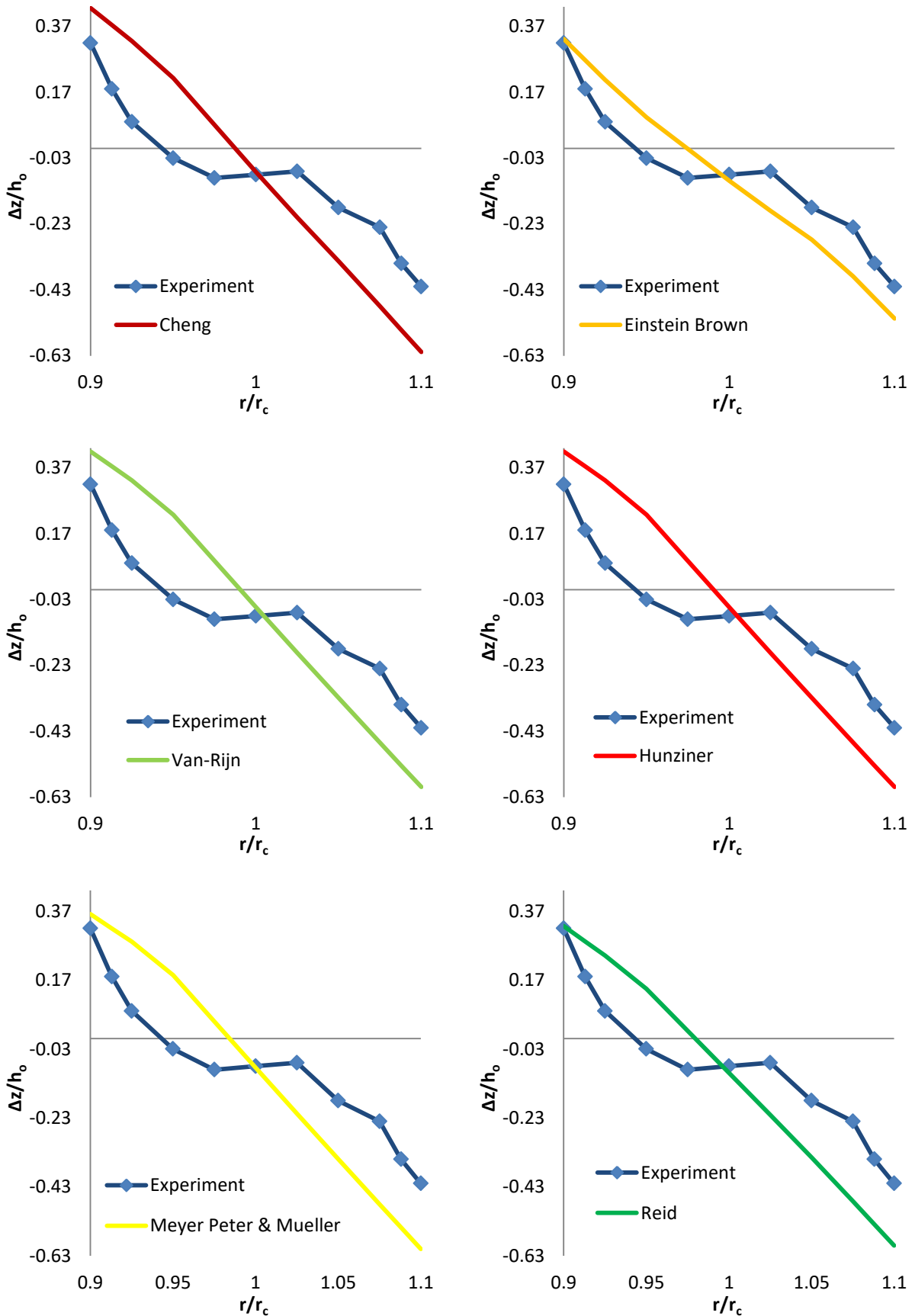


Figure 4.29. Comparison between sediment transport formulas predictions and the experimental data concerning the bed evolution in the cross-section experimentally defined as the area of maximum deposition (180° cross-section).

4.4.6. Run-4/ uniform sediment simulations

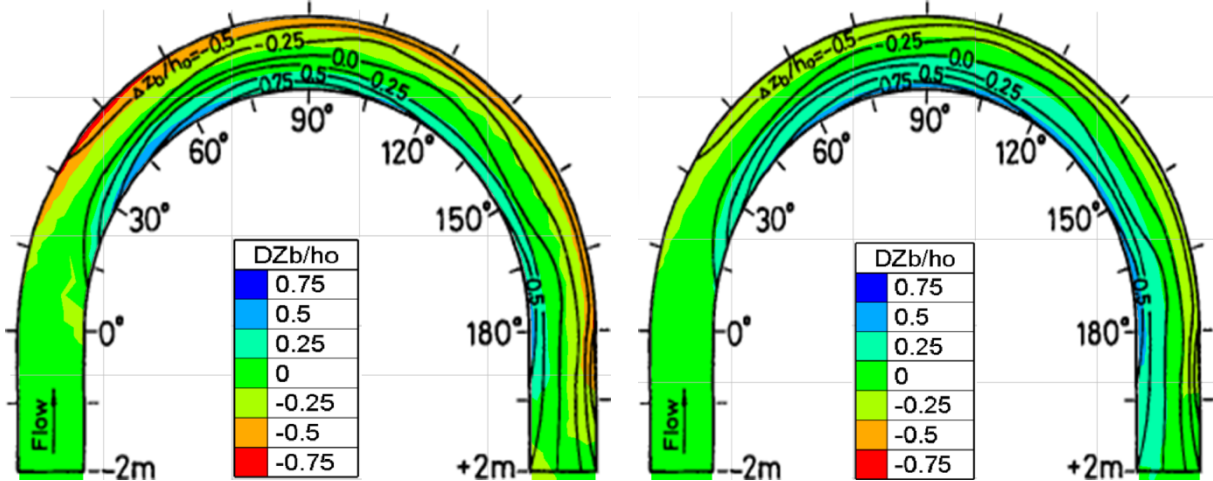


Figure 4.30. Filled contours of bed deformation for Ackers-White and Nielsen formulas compared to experimental data isolines.

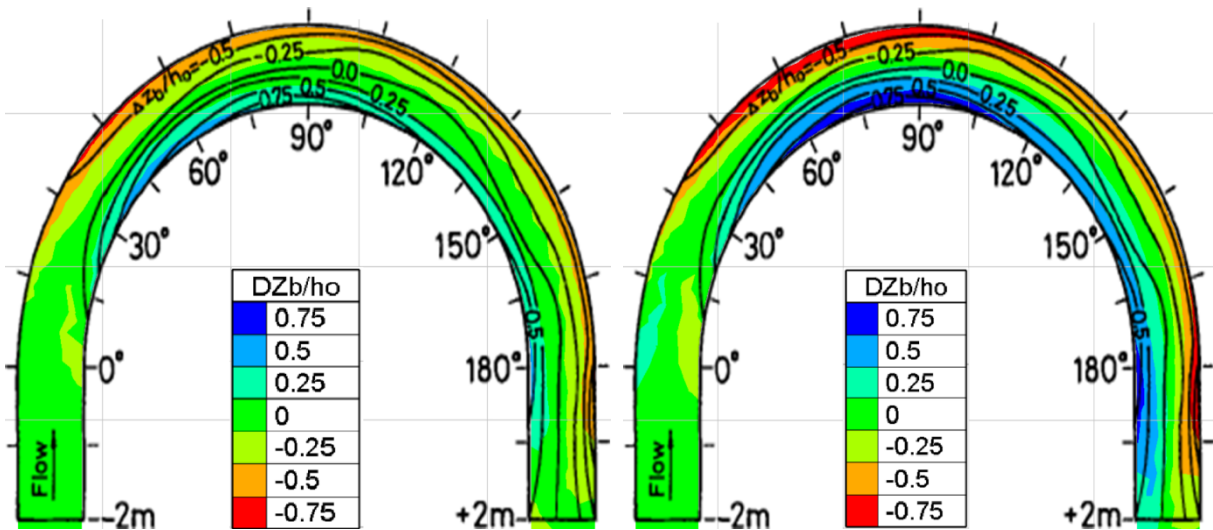


Figure 4.31. Filled contours of bed deformation for Cheng and Engelund-Hansen & Chollet-Cunge formulas compared to experimental data isolines.

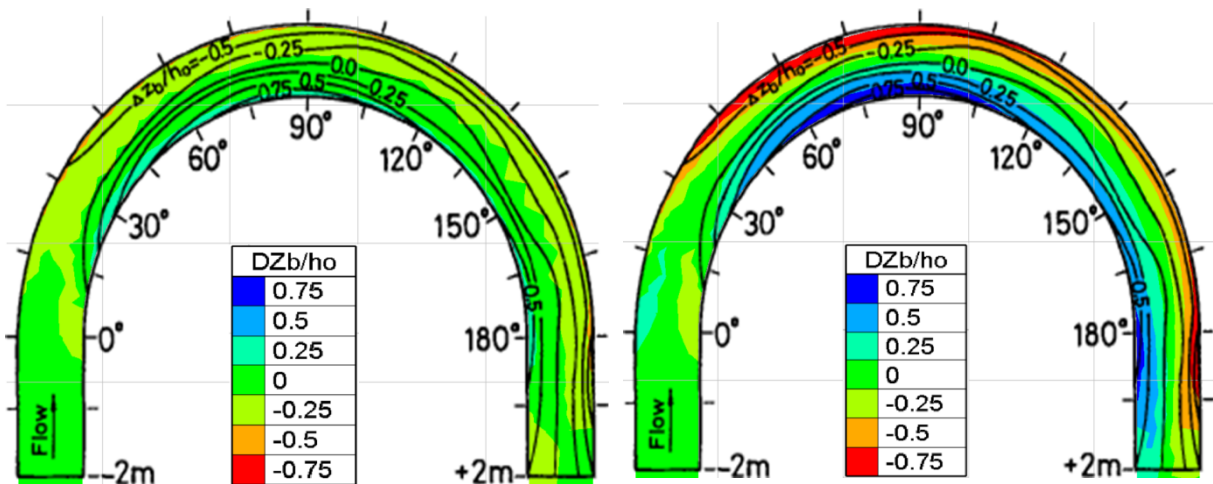


Figure 4.32. Filled contours of bed deformation for Frijlink and Einstein-Brown formulas compared to experimental data isolines.



Figure 4.33. Filled contours of bed deformation for Engelund-Hansen and Meyer-Peter & Mueller formulas compared with experimental data isolines.

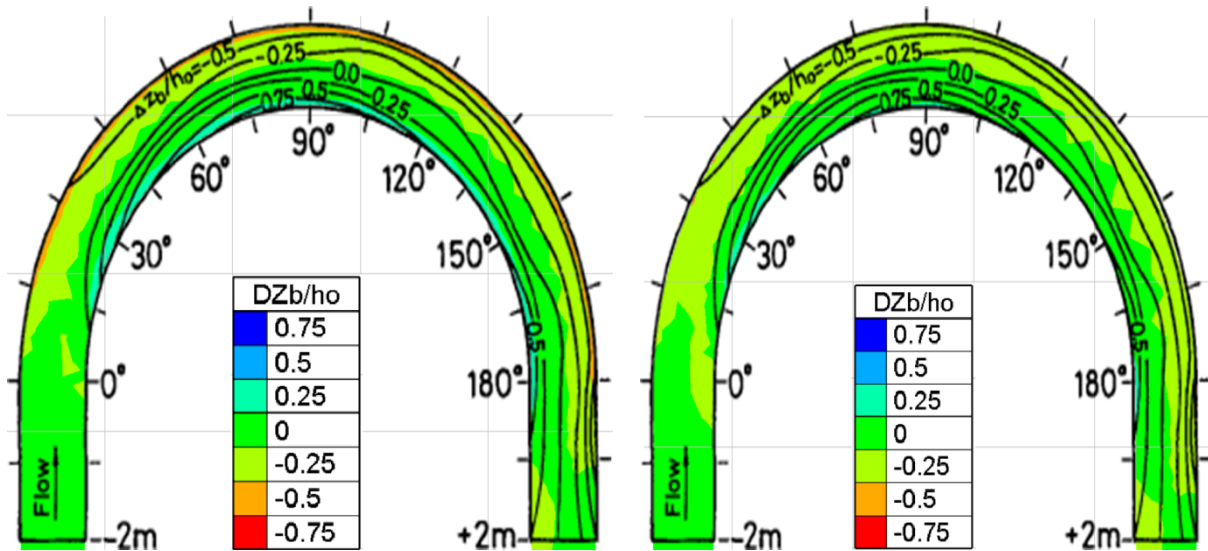


Figure 4.34. Filled contours of bed deformation for Karim-Kennedy and Van Rijn formulas compared with experimental data isolines.



Figure 4.35. Filled contours of bed deformation for Reid and Yang-Lim formulas compared to experimental data isolines.

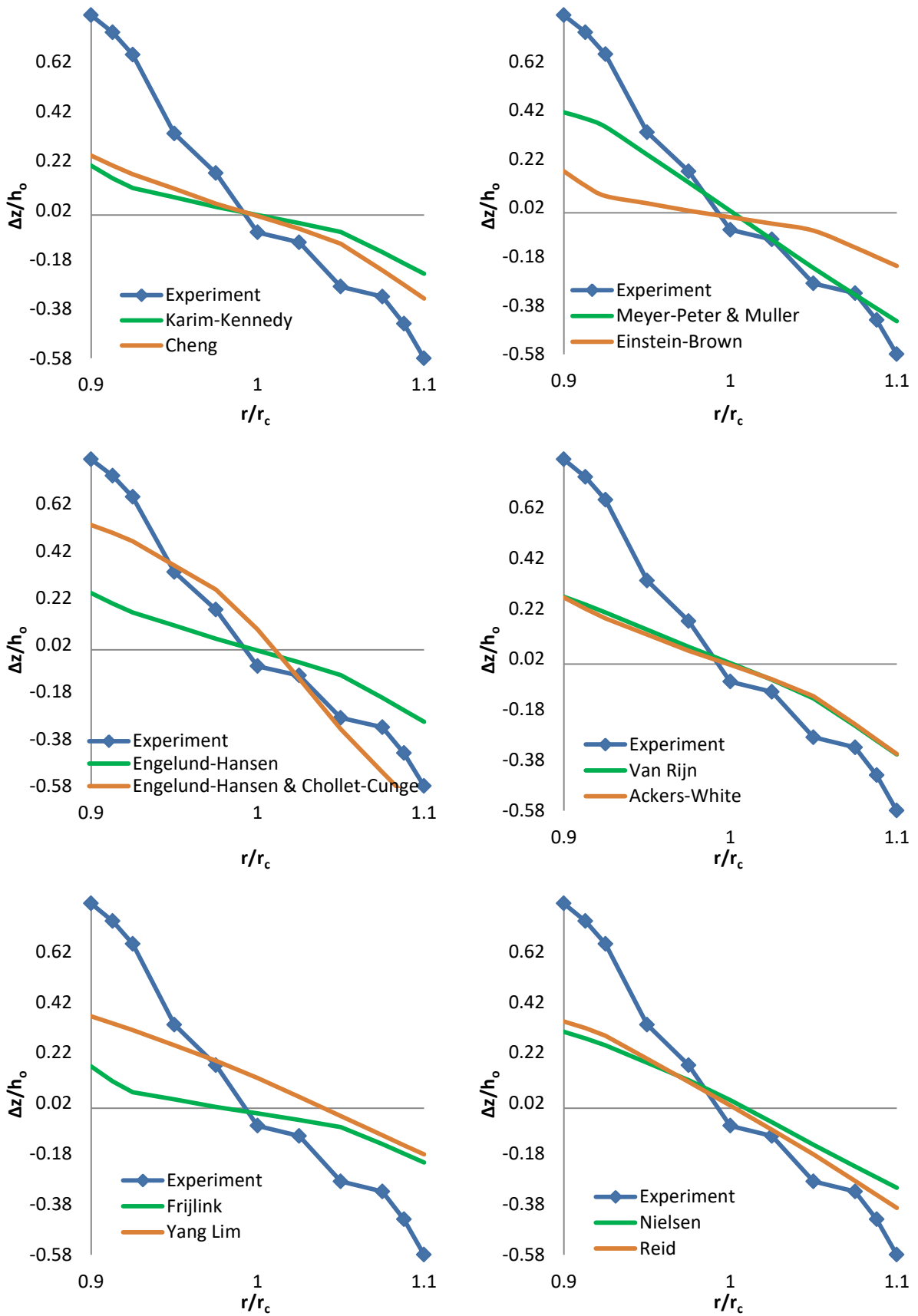


Figure 4.36. Comparison between sediment transport formulas predictions and the experimental data concerning the bed evolution in the cross-section experimentally defined as the area of maximum deposition (90° cross-section).

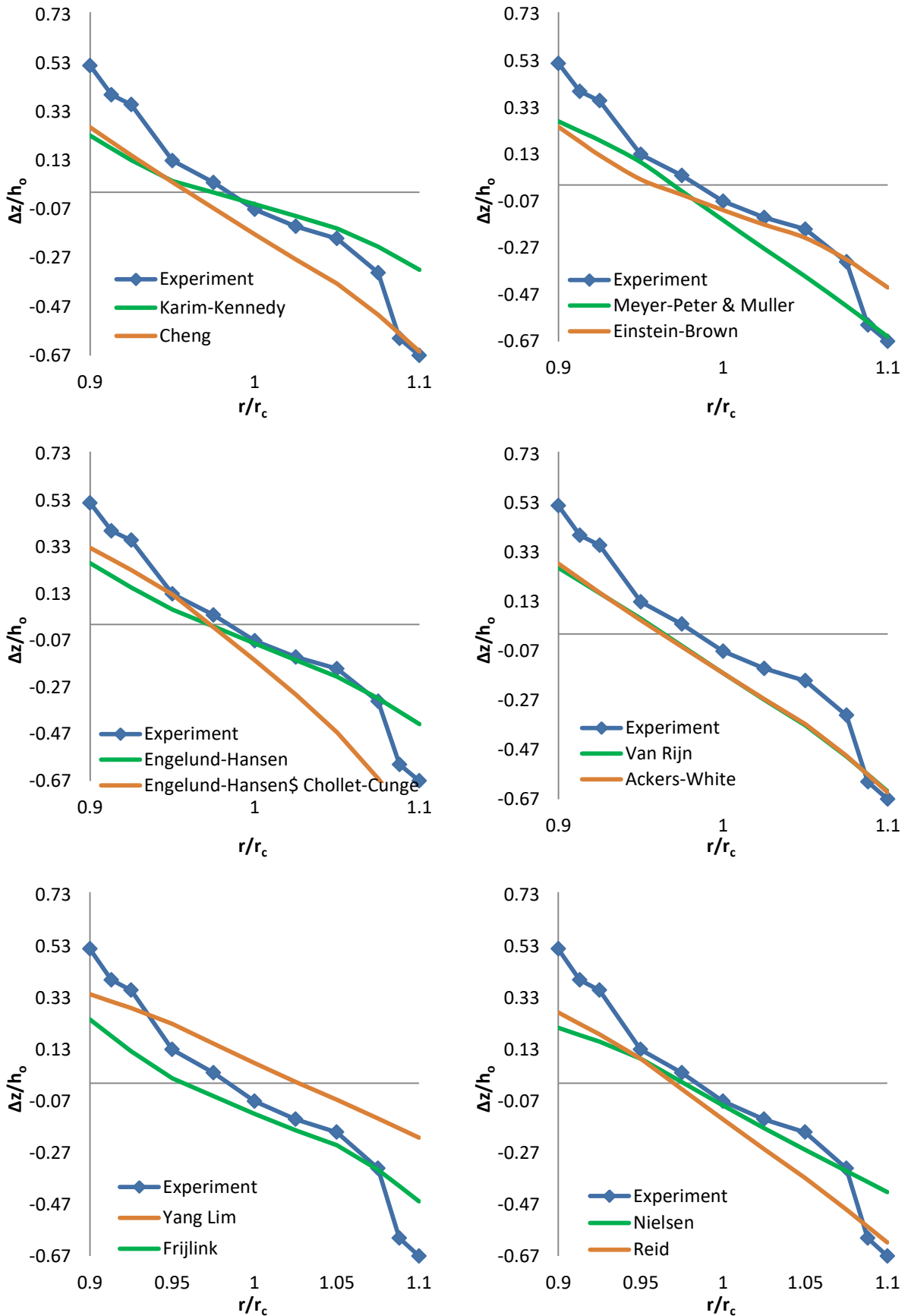


Figure 4.37. Comparison between the sediment transport formulas predictions and the experimental data concerning bed evolution in the cross-section experimentally defined as the area of maximum scour (180° cross-section).

4.5. Comparison between the results of the diploma thesis and previous models

The results of the diploma thesis simulations were, in general, in good agreement with the measurements. In this section the predictions of the Van Rijn model are compared with the results of 2 others, found in the literature. This model was simulated with the 8-class sediment proposed by M. Bui & P. Rutschmann (2009) and calibrated according to A. Mendoza et al. (2017) for meandering rivers and channel bends.

In the case of maximum deposition Villaret et al. (2013) predicted a final bed elevation closer to the measurements in the inner bank compared to the aforementioned diploma thesis model results (Figure 4.38). Contrarily to that the approximation of the outer bank section was better in the case of the diploma thesis model. The last also calculated a final bed elevation closer to the measured one (Figure 4.38). It should though be stated that Villaret et al. (2013) used a uniform sediment approach, which in the current study was found to give worst results compared to the non-uniform one.

The model results were also compared with the ones of the model found in the SISYPHE examples file. This model was simulated with a 5-class sediment and was calibrated with a 0.85 value for slope effect parameter of deviation. It also incorporated the Soulsby formula for bedload transport rate correction with a 35° friction angle of sediment parameter. Its results are not as good as the ones of the diploma thesis model simulation as shown in Figure 4.39.

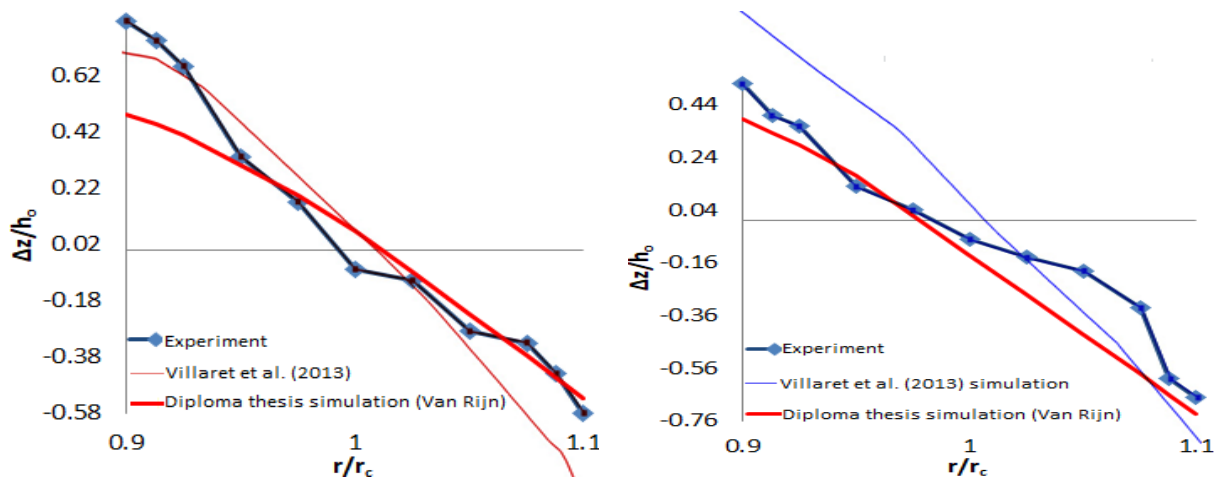


Figure 4.38. Diploma thesis (Van Rijn) and Villaret et al. (2013) predictions with measurements in the cross-sections of maximum deposition (left) and scour (right).

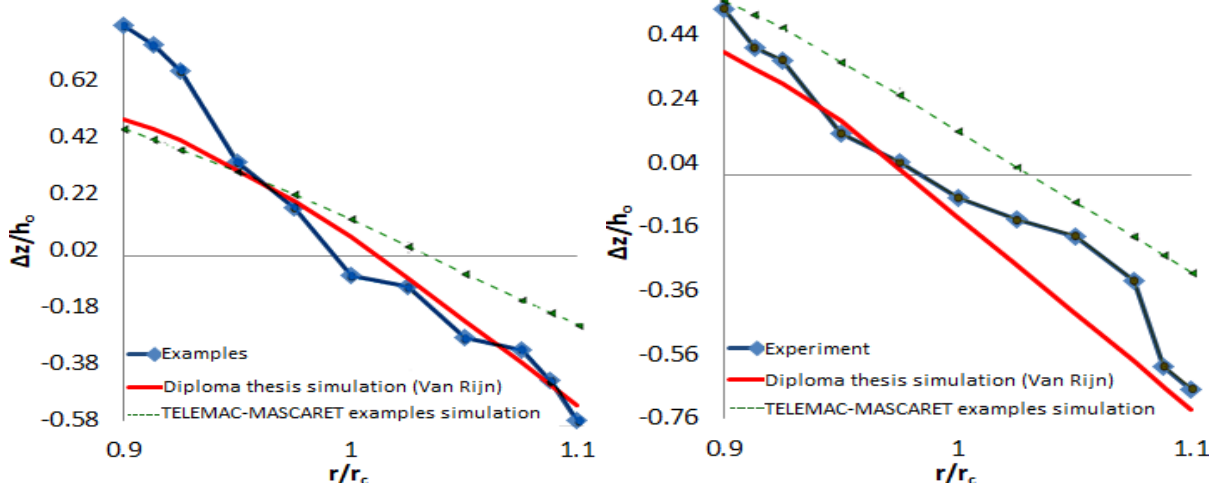


Figure 4.39. Diploma thesis and TELEMAT-MASCARET example simulations with Run-4 measurements in the cross-sections of maximum deposition (left) and scour (right).

4.6. Discussion of the results

The “Yen and Lee, 1995” experiments were conducted in order to investigate the correlation between different unsteady flow scenarios and the corresponding bed evolution, which is a fundamental problem in the riverine morphology studies. The alluvial river bed and the non-uniform sediment are also characteristics shared with most of the flood events that take place on riverbeds and floodplains. The results of the benchmark case simulations can be summed up to the following:

1. Overall, the sediment transport formulas (STF) predictions were found to be in good agreement with the measurements.
2. The areas of maximum scour and deposition, calculated by the models, are consistent with the respective areas resulting from the experiments.
3. The model predictions concerning the non-uniform sediment scenario were found to be a good approximation of the experimental results, contrarily to the uniform ones.
4. The results of the simulations utilizing the grain-size distribution curve proposed by M. Bui & P. Rutschmann (2009), used in the non-uniform sediment simulations, were in good agreement with the measured final riverbed elevations.
5. Out of the 12 STF incorporated in the models, used for the uniform sediment simulations, Engelund-Hansen & Cholley-Cunge’s results were the closest to the experimental results.
6. Different STF made good predictions of the final bed elevation in the uniform and the non-uniform approaches. Six of them were in good agreement with the measurements in the non-uniform sediment simulations, but 4 stood out as the best: Cheng, Meyer-Peter & Mueller, Van Rijn and Hunzinger formulas.
7. Results of the non-uniform simulations concerning Run-3, Run-4 and Run-5 were a good approximation of the measurements, contrarily to the Run-2 and especially the Run-1 case. The discordance in these 2 cases was interpreted as a result of secondary effect underestimation.
8. The approach of A. Mendoza et al. (2017) for meandering rivers and channel bends was used for model calibration, resulting in very good predictions compared to other relevant model results.
9. The contribution of suspended to the total sediment transport was negligible.
10. The effect of the sediment transport and riverbed evolution processes on the hydrodynamic flow regime was found to be minimal.

5. The Mandra flood case study

5.1. Area of study

5.1.1. The city of Mandra

The city of Mandra is situated in the Thriasian Plain (Figure 5.1.), West Attica, which is surrounded by Mountain Parnitha to the north, Mount Egaleo to the east, Mount Pateras to the west and the Bay of Eleusina to the south. It is the seat of the Mandra-Eidyllia municipality, which has an area of 426197 km² and 17885 citizens according to the General Population Census of 2011. According to the same study, 12792 of them live in Mandra municipal unit, which has an area of 205770 km². The municipal unit includes also the villages of Nea Zoi (518), Agios Sotiras (488), Diodia (116), Pournari (92) and several other settlements. Mandra is located 2km west of Magoula, 5 km northwest of Elefsina and 22 km northwest of Athens city center. Due to its strategic location it hosts an industrial zone which mainly serves as a logistics center, as well as the largest quarry in South East Europe.

The Greek National Road 3 crosses the eastern part of the city and ascends the Pateras mountain towards Thiva city. It is a single carriageway road that connects the suburbs of Athens with Bitola city in F.Y.R.O.M.. It served as the main route until the 60's, when it was replaced by A1 Motorway. The part of the road that runs alongside Soures creek suffered heavy damages during the flash flood of 15/11/17.



Figure 5.1. The Thriasian Plain and the Attica basin (source: Google Earth).

5.1.2. The hydrographic network of Mandra area

Mandra town lays within a catchment basin of roughly 75 km², which includes several converging creeks with steep slopes that form the two main streams (s.) crossing the town of Mandra that are s. Soures and s. Agia Aikaterini, whose catchment area is equal to 23.0 and 22.0 km², respectively. These streams (Figure 5.2.) are characterized by significant morphological changes due to the intensive construction activities in the greater area that resulted in a dramatic decrease of their available cross-sectional areas and the occurrence of floods even at low flow rates. The need to face the frequent flood problems in Mandra resulted in the beginning of the final study of the storm water works in July 2012; its environmental terms were approved in July 2014 and the boundaries of the two streams were specified in January 2016. The main components of these structural works (Figure 5.3.) are:

1. the regulation of s. Soures (length=L=1.74 km, flow rate=Q=91-125 m³/s and cross-sectional area=A=24.0-34.4 m²)
2. the partial diversion of the s. Agia Aikaterini (L=1.52 km, Q=47 m³/s and A=12.5-24.0 m²) to s. Soures. Downstream of its diversion location, the s. Agia Aikaterini flows through Mandra city via an existing, enclosed rectangular conduit (L=2.27 km, Q=10 m³/s and A=3.4 m²) until it meets s. Soures. Then, the latter ends up at the beginning of the existing, regulated part of the s. Soures that consists of a twin channel (4.0X3.0 m²).



Figure 5.2. The streams of Mandra and their technical works (Stamou, 2018).



Figure 5.3. The regulated part of the s. Soures after the flood (Stamou, 2018).

5.2. Characteristics of the flash flood event

Starting from the evening of 14 November 2017 up to 20:00 there was a rainfall event of minor scale at the northwestern part of Mandra area as well as the northern part of Nea Peramos and the eastern slopes of Mount Pateras. During night though, several storm events took place in the same area, which lasted about 8 hours.

The accumulated rainfall of the core event surpassed the 200 mm within 6 hours, most of which occurred between 5:00 and 8:00 a.m. (3-6 UTC) of November 15 2017, as shown in Figure 5.4. and Figure 5.5., according to National Observatory of Athens (N.O.A.). The data collected by the radar of Mount Ymmitos of the National Meteorological Association revealed that between the evening of 14 and 15 of November was about 80 mm.

According to Mandra residents the fast flood flows reached the northernmost buildings of the city at around 6:00 a.m. The flow was characterized by heavy sediment and debris transport, which is can be highlighted through the comparison between Figures 5.7. and 5.8.. The estimated maximum flooded area is also presented in Figure 5.9.

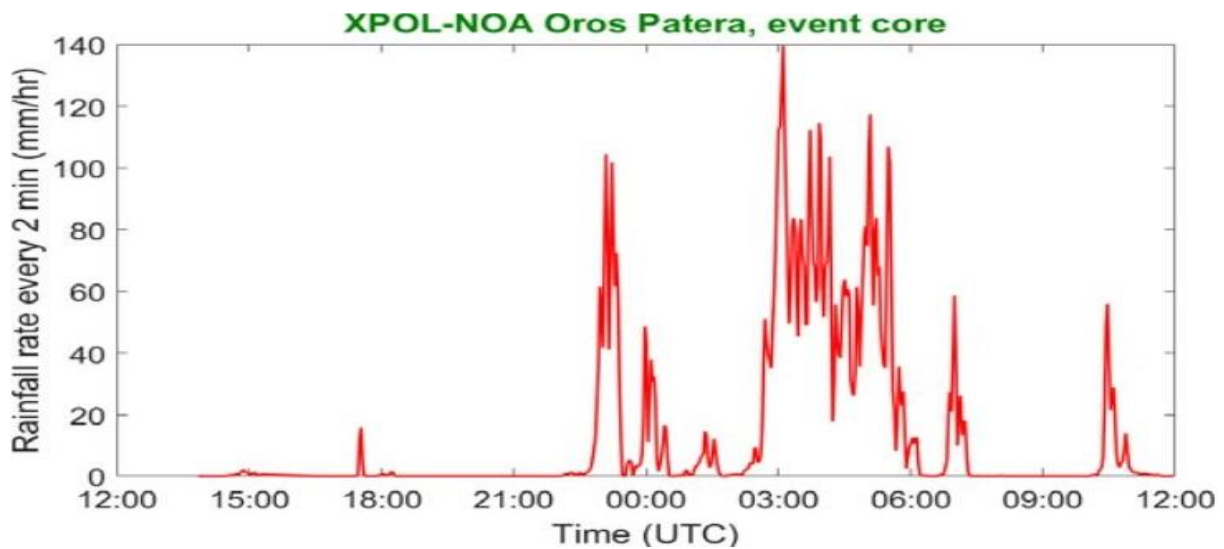


Figure 5.4. The rainfall rate of the main storm events as recorded by the radar XPOL of the National Observatory of Athen (N.O.A.).

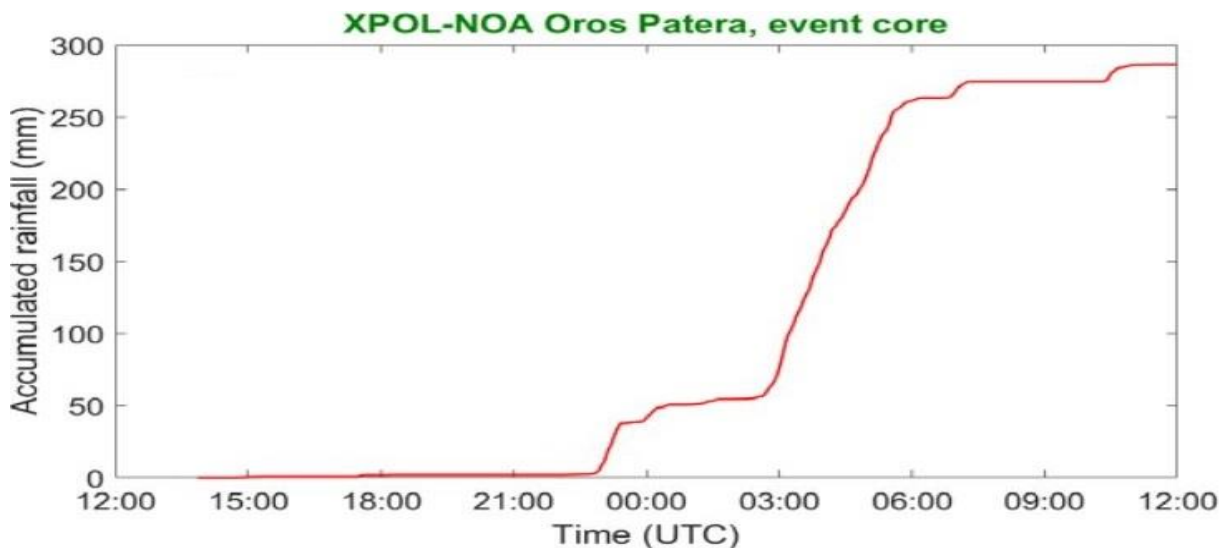


Figure 5.5. The accumulated rainfall of the main storm events as recorded by the radar XPOL of the National Observatory of Athens (N.O.A.).

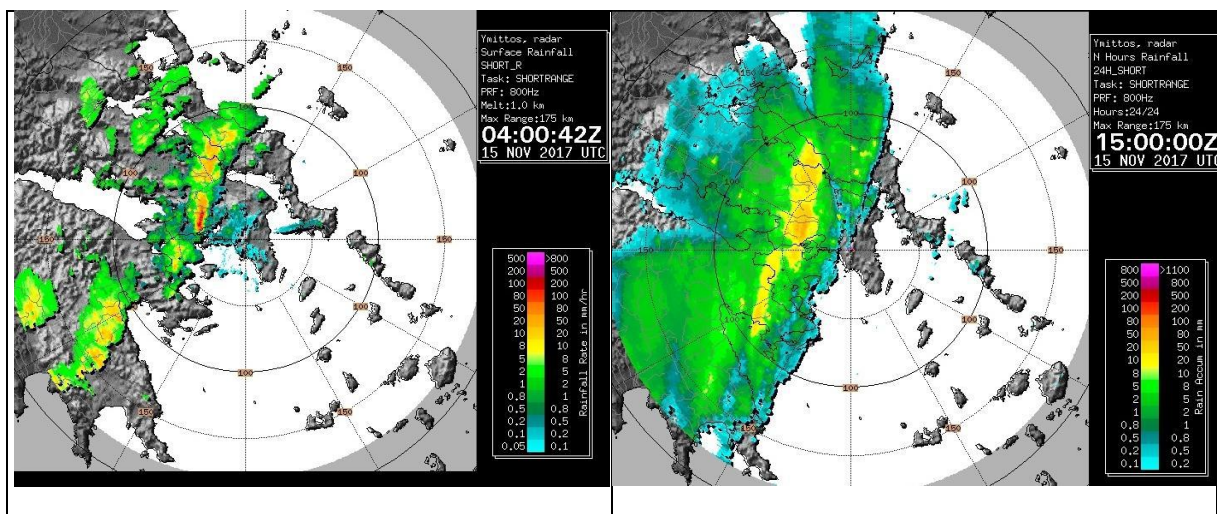


Figure 5.6. Evolution of the rainfall events during November 15th, 2017 as recorded by the Ymittos radar of the Hellenic National Meteorological Service (H.N.M.S.).



Figure 5.7. Mandra area before the November 15th flash flood event (Google Earth).



Figure 5.8. Mandra area after the November 15th flash flood event (Google Earth).



Figure 5.9. Maximum flooded area of Mandra at November 15th (E. Lekkas et al, 2017).

5.3. In situ investigation in Mandra area

The research team involved in the study of Mandra flash flood, consisting of undergraduate and graduate students of School of Civil Engineering of N.T.U.A. with Professor Stamou as coordinator, visited the area of interest 4 times during the fall of 2018. The first 2 times were dedicated in the data collection concerning the area topography (Figure 5.10) and the dimensions of the hydraulic structures related to the flood transition process, as well as resident interviews about the evolution of the flood event. The 3rd and 4th visits were devoted to the distribution of the questionnaires to Mandra citizens in order to collect data with the ultimate goal to propose the development of an Early Warning System. The data needed for the model as well as the area and methods used were firstly specified.

The maximum level that flood flows reached was recorded in several positions, which were used for hydrodynamic model calibration. The high concentration of these flows in sediment and more specifically clay enabled the data collection months after the flood event, since the mud stains were still visible on the city walls, indicating the maximum water level. Branches and garbage entrapped on trees and fences also helped to identify the maximum water level in certain areas. A tape measure and a laser distance meter were used for measuring both the maximum flood flows level and the dimensions of the hydraulic structures that were included in the model. These are mainly the culverts of the s. Soures and the s. Agia Aikaterini and the subterranean rectangular part of s. Soures that ends to s. Sarantapotamos. The information that the residents gave about the time-space evolution of the flood event was also used for the hydrodynamic model validation.



Figure 5.10. Map of Mandra area (based on Google Earth), highlighting 5 areas of interest. Presented clockwise: the culverts of National Road 3 in “Kantines” area, its damages due to the FF event, the estuary of the regulated part of the s. Soures in the s. Sarantapotamos, the part of the s. Soures crossing the industrial zone in a twin channel, and the s. Agia Aikaterini upstream of Mandra city.

6. The Mandra flood integrative model

6.1. Input data into TELEMAC-2D

6.1.1. Numerical mesh

The triangular mesh of Mandra in TELEMAC-2D that is shown in Figure 6.1 consists of 85753 nodes and 167051 triangular elements; it was produced with the Blue Kenue™ software. Blue Kenue offers two options for meshing areas: the T3 Channel Mesher and the T3 Mesh Generator. Initially, the high resolution (5.0 m x 5.0 m x 1.0 m) Raster DEM obtained by the National Cadastre & Mapping Agency S.A. (NCMA SA) was imported into ArcGIS to produce the Mandra.xyz file. Then, the NCMA SA map of the greater area was imported into ArcGIS to draw the banks of the streams and to develop the corresponding Stream.xyz file and the shape file (.shp) for the line boundaries (banks) of the two streams. The meshing of the streams was performed with the T3 Channel Mesher using 4 cross channel nodes, two of which were located at the banks and interval along the channel equal to 2.0 m. The mesh of the rest floodplain was constructed with resolution (edge length) equal to 30.0 m and edge growth ratio equal to 1.5. Elevations were sampled from Mandra.xyz using inverse distance weighted interpolation (Sephard, 1968). Land cover roughness was estimated based on the CORINE Land Cover (CLC12_GR) inventory in Greece of the year 2012 that includes 45 land cover classes. In the area of Mandra excluding the streams, 8 land cover classes were used (Table 6.1) with the corresponding codes, Manning values and references. The CLC12_GR.shp file was imported into ArcGIS together with Mandra.xyz to produce the file of the codes (code.xyz) that are translated into Manning values (Mandra_n.xyz) via a MATLAB program. In the streams we have constructed a xyz file (Stream_n.xyz) for the values n of Manning coefficient based on the characteristics of the various segments of the streams (Table 6.2). Manning values were sampled from Mandra_n.xyz and Stream_n.xyz using nearest neighbor values interpolation.

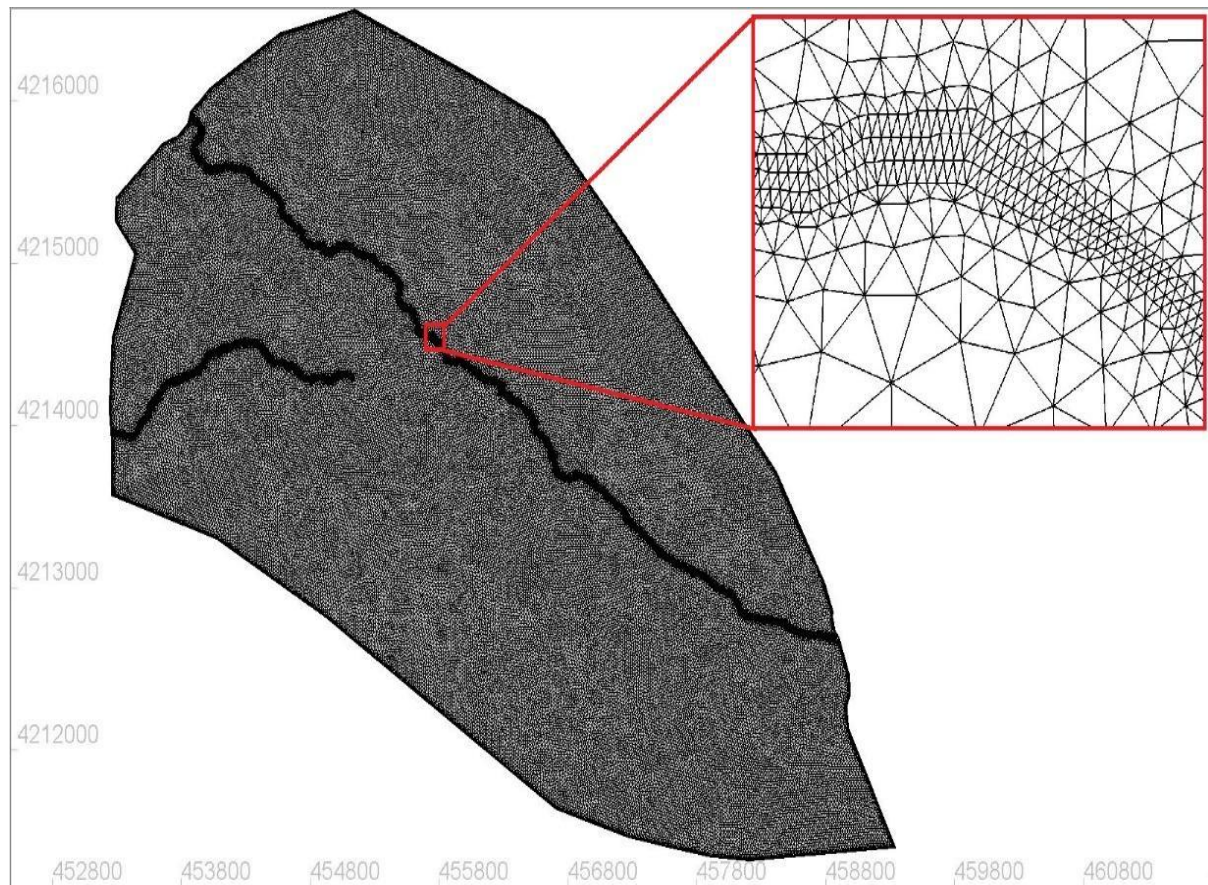


Figure 6.1. The finite element mesh of the geometry file used in Mandra model.

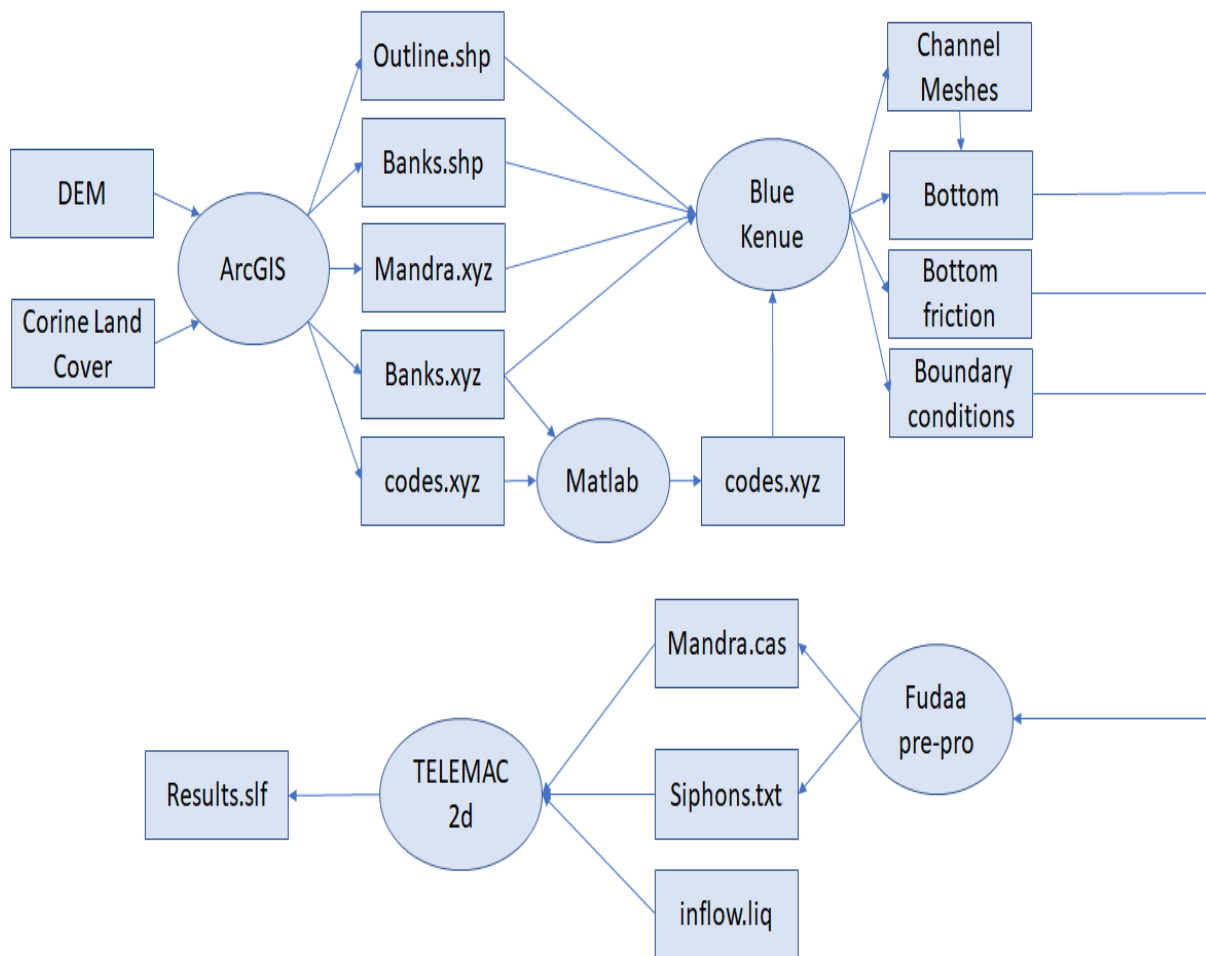


Figure 6.2. The methodology.

Table 6.1. Corresponding Corine codes to Manning coefficient values.

CODE	LAND COVER USE	Range of values based on literature	n
112	Discontinuous urban fabric	0.060-0.115	0.100
121	Industrial or commercial units	0.115-0.230	0.200
122	Roads, rail networks and associated land	0.013-0.038	0.020
223	Olive groves	0.043-0.050	0.045
243	Land principally occupied by agriculture, with significant areas of natural vegetation	0.058-0.100	0.060
313	Mixed forest	0.100-0.230	0.140
323	Sclerophyllous vegetation	0.072-0.125	0.100
333	Sparsely vegetated areas	0.050-0.070	0.070

Table 6.2. Manning Values for stream's bed.

STREAMS	DESCRIPTION	Range of values based on literature	n
Agia Aikaterini	sluggish reaches, weedy, deep pools	0.050-0.080	0.065
Soures (unconstructed)	sluggish reaches, weedy, deep pools	0.050-0.080	0.065
Soures (constructed)	Concrete float finished	0.013-0.016	0.016

1.1.1. Technical works

There are 16 technical works in the s. Soures and 2 in the s. Agia Aikaterini, that their dimensions are shown in Table 6.3.

Table 6.3. Corresponding Corine codes to Manning coefficient values.

No (-)	Technical work	Upstream Location (m)	Width or Diameter (m)	Height (m)	Length (m)
TW1	Twin-pipe	3890	2x4.0	1.35	25.0
TW2	Culvert	3740	3.0	1.5	35.0
TW3	Culvert	2013	2.0	1.0	27.0
TW4	Twin-channel	1202	2x4.0	1.25	61.0
TW5	Twin-pipe	1010	2x0.8		38.0
TW6	Culvert	760	3.5	2.0	15.0
TW7	Pipe	514	1.2		14.0
TW8	Pipe	444	1.2		13.0
TW9	Culvert	349	5.0	1.90	15.0
TW10	Culvert	-120	5.5	4.5	18.0
TW11	Twin-channel	-268	2x4.0	3.0	185.0
TW12	Twin-channel	-850	2x4.0	3.0	16.0
TW13	Twin-channel	-962	2x4.0	3.0	31.0
TW14	Twin-channel	-1340	2x4.0	3.0	200.0
TW15	Twin-channel	-1940	2x4.0	3.0	497
TW16	Bridge	-1680	30.0	6.0	33.0
TW17	Culvert	4550	3.0	1.35	10
TW18	Pipe	2230	2.0	1.7	2319

1.1.2. Boundary conditions

The computational domain of Mandra FF MM includes 4 liquid boundaries; 2 inflow boundaries, of which one is situated at the northernmost cross-section of s. Soures (LB3) and the other to the northwestern reach of the s. Agia Aikaterini (LB4) The 2 outflow boundaries are located at the estuary of the s. Soures at the s.Sarantapotamos (LB2) and at the s. Mikro Katerini upstream of the city of Elefsina (LB1) (Figure 6.4). For the inflow boundaries the Tsakiris (2017) hydrographs were used, as shown in Figure 6.3.

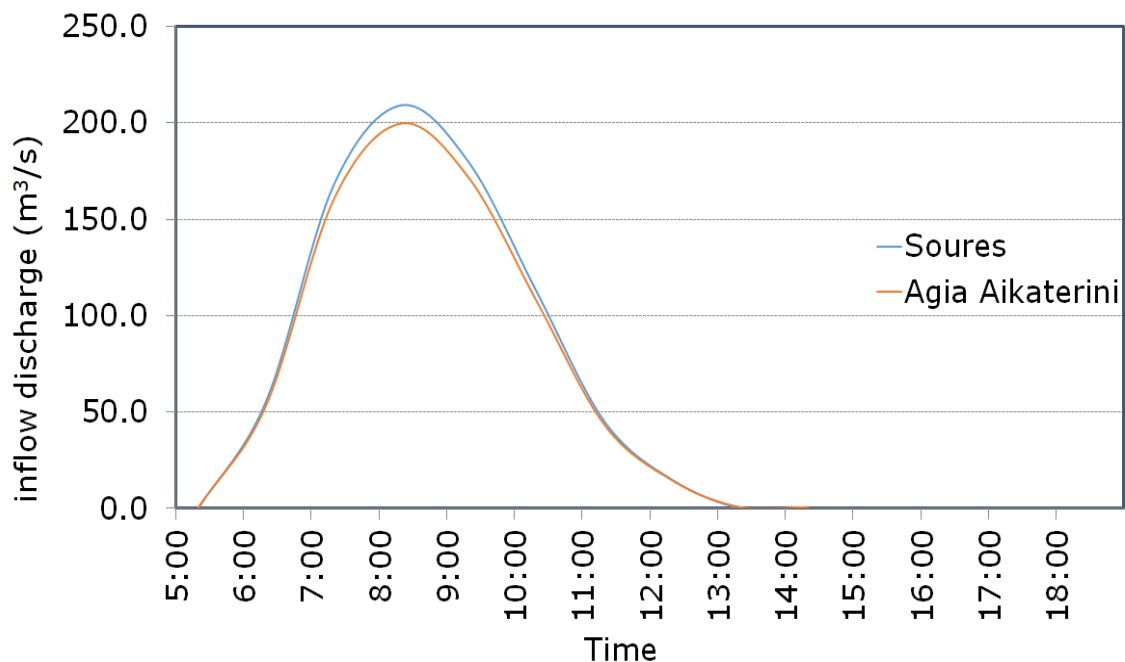


Figure 6.3. Upstream hydrographs (Tsakiris, 2017).

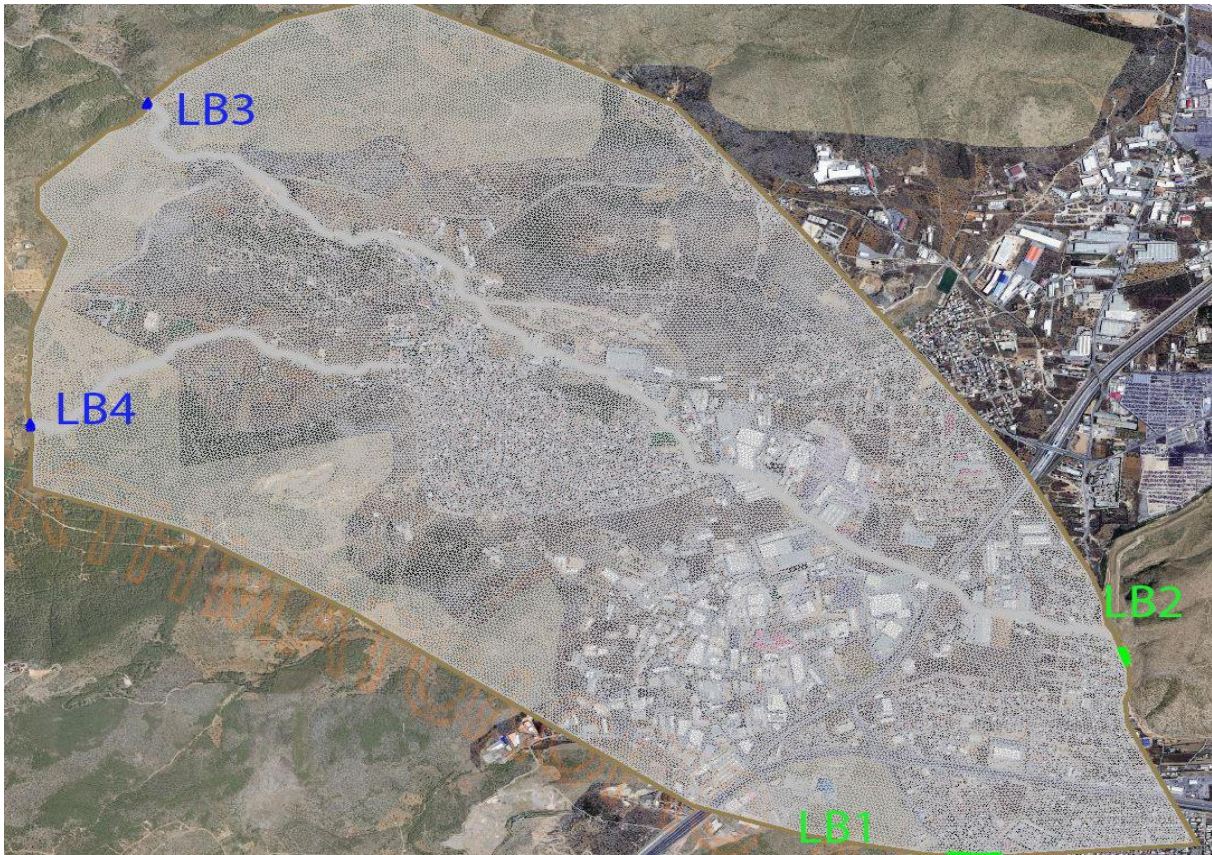


Figure 6.4. Mandra flood MM domain and the liquid boundaries.

6.2. Input data into SISYPHE

6.2.1. Boundary conditions

A common practice in mathematical simulations is to shift the liquid boundaries further away from the area of study in order to sidestep the instabilities introduced by them to the computational domain. This poses a serious challenge in the cases of sediment transport/morphological simulations in riverine environments. Instabilities concerning the velocities in the inflow boundaries frequently result in intense soil erosion, which consequentially results in intense sediment transport downstream, affecting a big part of the area of study. A solution to this problem was suggested by Tassi and Villaret (2014), as well as Villaret et al. (2009). Their approach was to automatically deliver the bedload at the model inflow boundaries, defined in quantity and grain proportions, in order to keep the soil level in these areas constant in time. This also gave an approximation of the inflow sediment flux, which in most cases is unknown. Another approach to this problem is the imposed bed evolution option offered by SISYPHE, through which the user can define the boundary with a fixed bed elevation (zero evolution) in the "liquid boundaries" file. In the diploma thesis simulation, this approach was followed by defining the areas around the inflow boundaries as non-erodable (Figure 6.6). The upstream contribution in sediment generation and deposition processes was not taken into account in the diploma thesis simulation, assuming that these processes take place within the area of study, since it includes the largest part of the water catchment area.

6.2.2. Definition of rigid areas.

The effect of non-erodable areas in the sediment transport and geomorphological processes is an important aspect that should be considered. These rigid areas can be natural, like rocky formations or man-made structures, like buildings and roads. In the water catchment of Mandra, 2 large non-erodable areas were taken into account, Mandra city and the industrial zone. 2 rigid islets were added at the inflow boundaries in order to achieve the imposed bed zero evolution, described previously (Figure 6.5).

The user needs to include the `NOEROD` subroutine in the "user_fortran" file in order to introduce the rigid area effect to the model. Then these areas must be defined in a selafin file along with the geometry of the computational domain and the relative friction ".slf" file. The steps of this procedure can be summed up to the following:

1. Creation of a new ".slf" file (File→ New→ SELAFIN Object)
2. Given name "MANDRA_NOEROD" (Properties→ Meta Data→ Name→NOEROD)
3. Inclusion of BOTTOM and FRICTION meshes in the ".slf" file (the 2 icons should be dragged from the Geometry file and dropped to MANDRA_NOEROD)
4. Creation of the non-erodable mesh (MANDRA_NOEROD→ Add Variables→ Name→ NOEROD)
5. Demarcation of the non-erodable areas (the icon of NOEROD mesh should be dropped in the 2D view icon. Then, a New Closed Line should be drawn around the mesh and saved with the value 100. The same applies for the case of non-erodable areas, but the values given to these lines should be 0 instead)
6. NOEROD mesh update (NOEROD→ Tools→ Map Object→ New Closed Line).

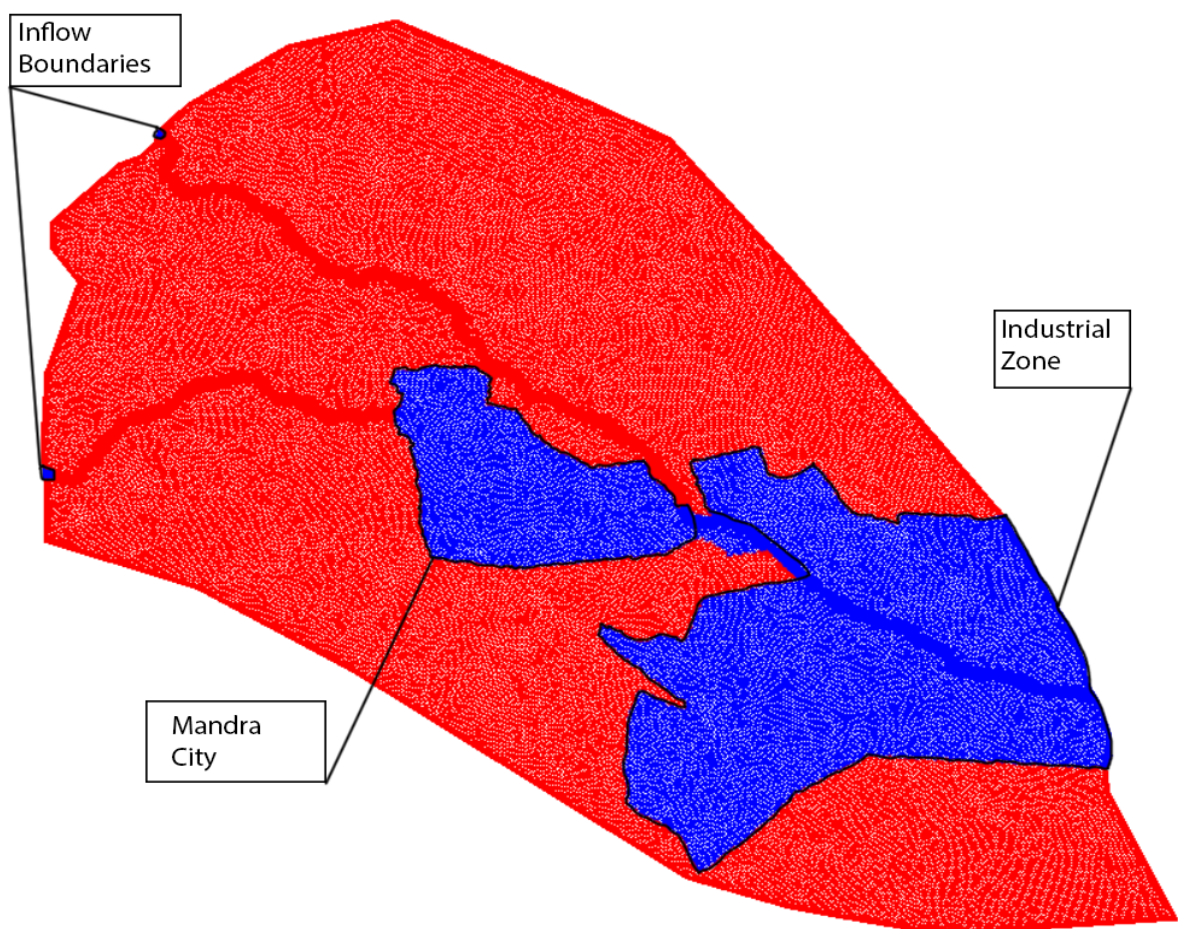


Figure 6.5. Non-erodable areas in Mandra model domain (blue). The area of Mandra city, the industrial zone and the inflow boundaries enclosed by black lines.

6.2.3. Limitations and assumptions

Uniform sediment of 0.63 mm was used for the simulation. The selection of this sediment diameter was considered reasonable and is on the borderline between sand and silt. A representative sediment rating curve was not available for the diploma thesis study. Another limitation was the lack of geological data concerning the soil erodability. The `ACTIVE LAYER THICKNESS` keyword is used in SISYPHE models in order to simulate the soil erodability effect. The selected value was 0.001. The assumption that the soil erosion and sediment transport takes place within the computational domain was made, since it is a big part of the water catchment. Thus, no sediment flux was considered.

6.3. Results presentation

6.3.1. Geomorphological evolution on the upstream part of the s. Soures

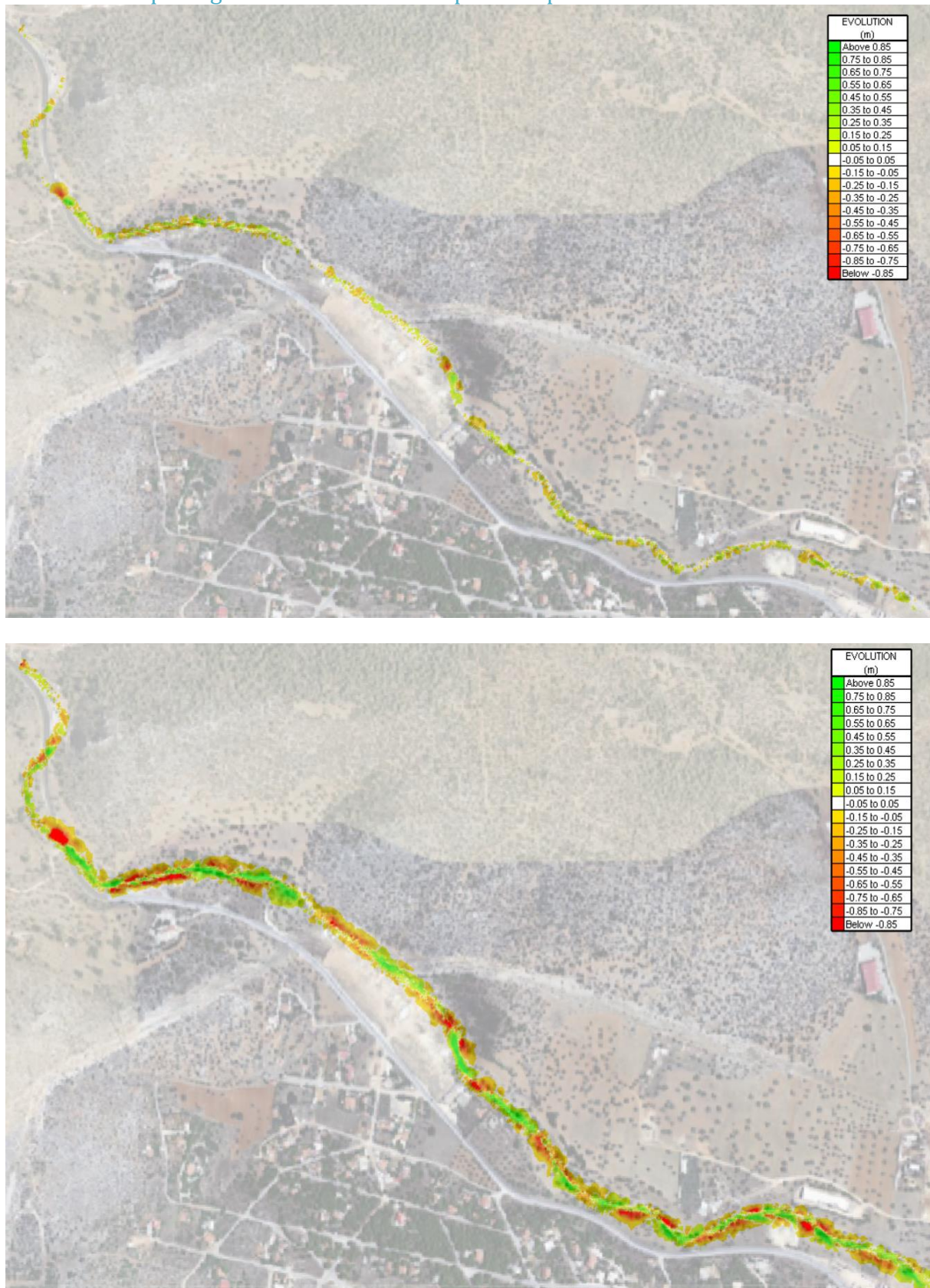


Figure 6.6. Geomorphological evolution due to the flood flows on the upstream part of the s. Soures at 2 hours (above) and 4 hours (below) from the start of the simulation.

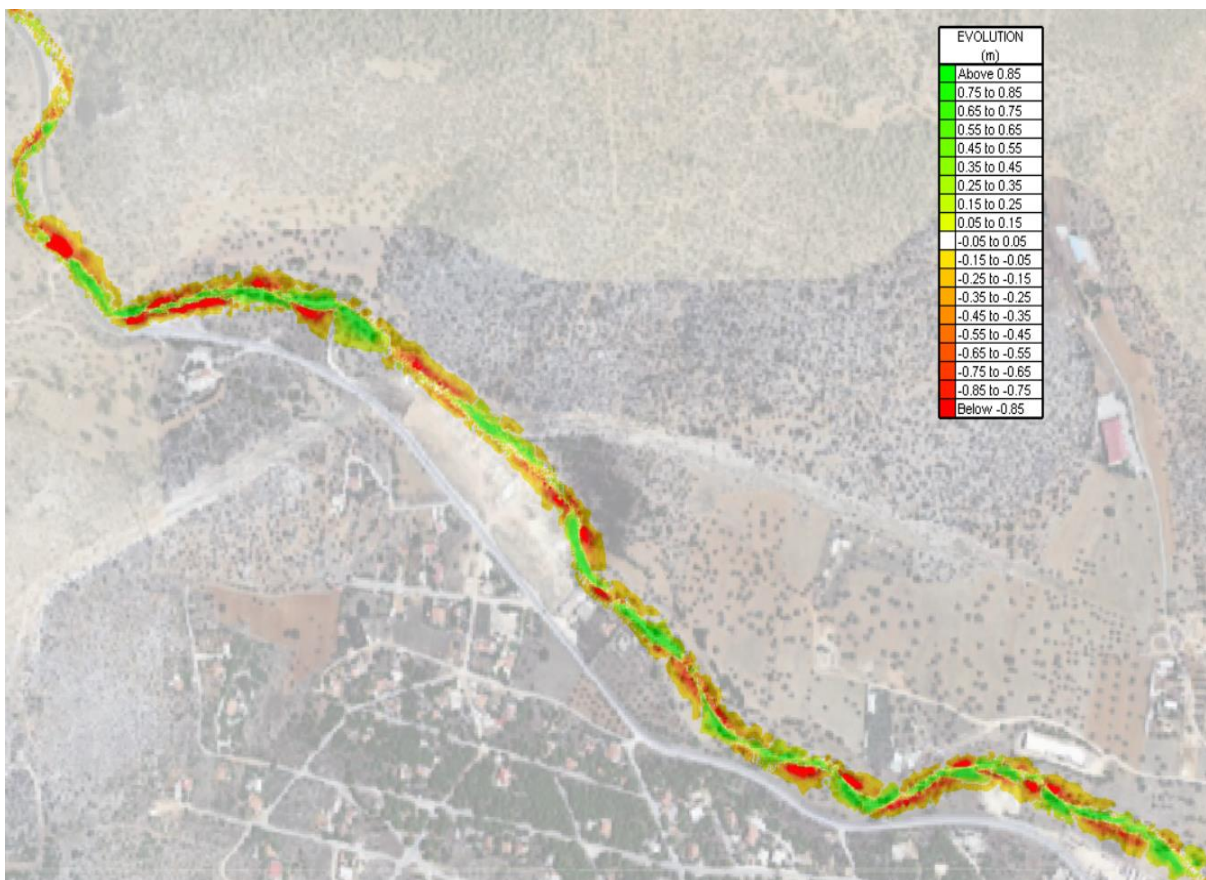
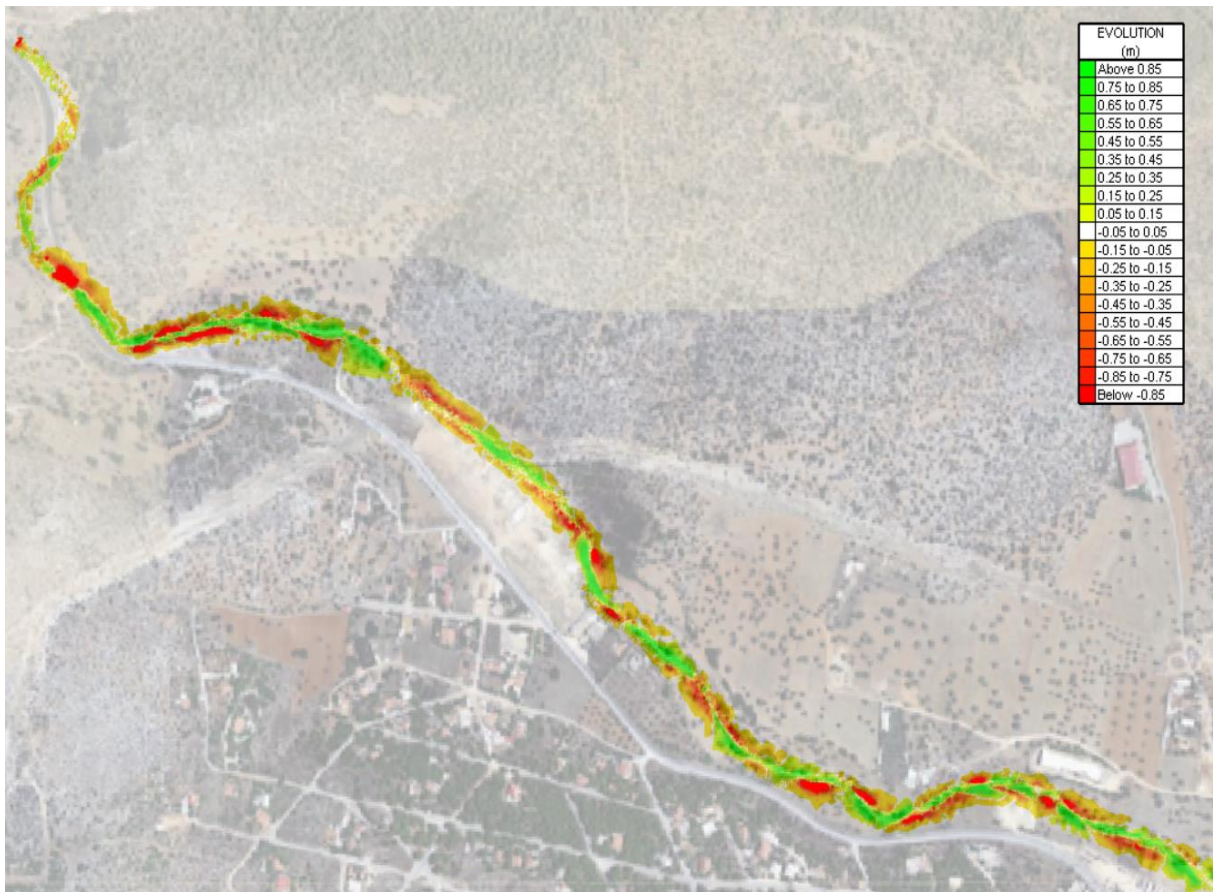


Figure 6.7. Geomorphological evolution due to the flood flows on the upstream part of the s. Soures at 6 hours (above) and 8 hours (below) from the start of the simulation.

6.3.2. Geomorphological evolution on the upstream part of the s. Agia Aikaterini

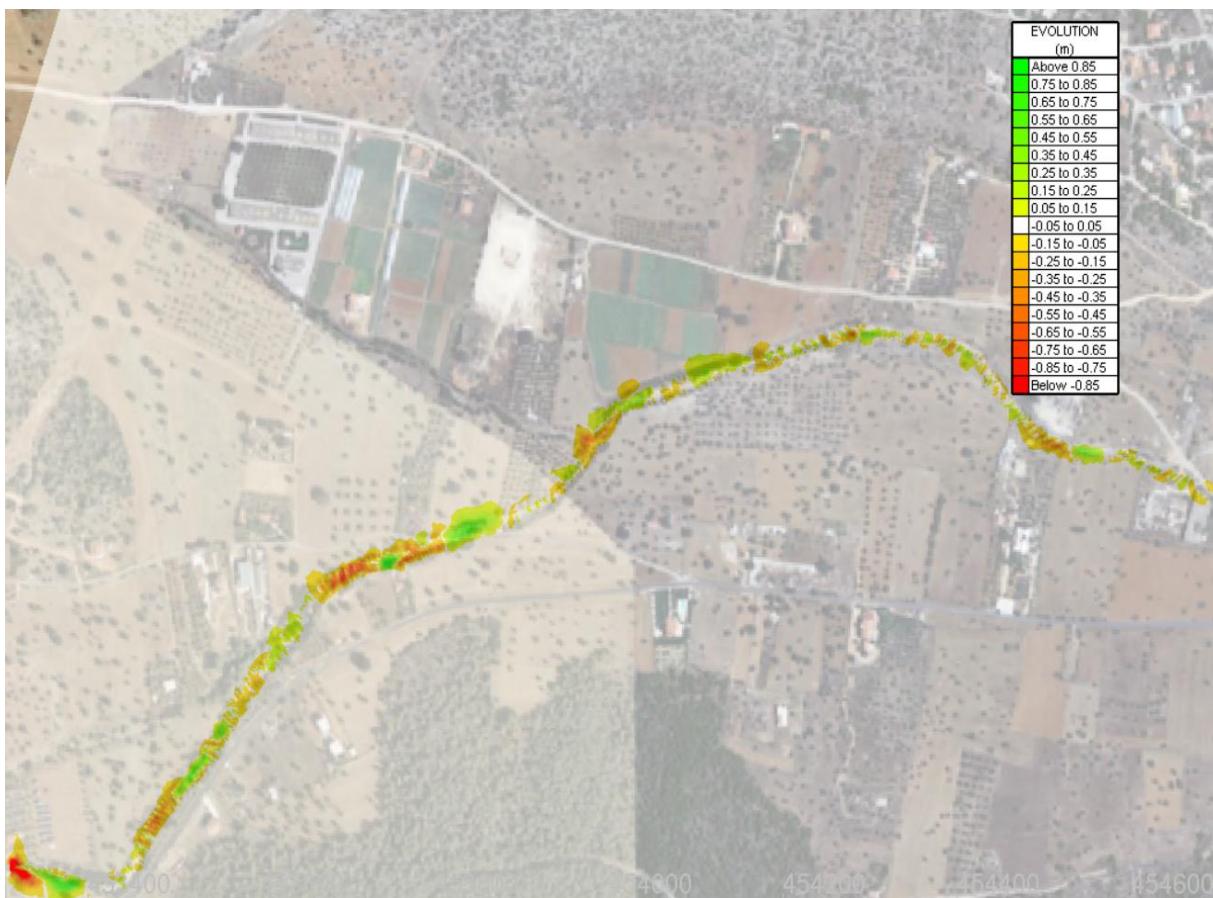
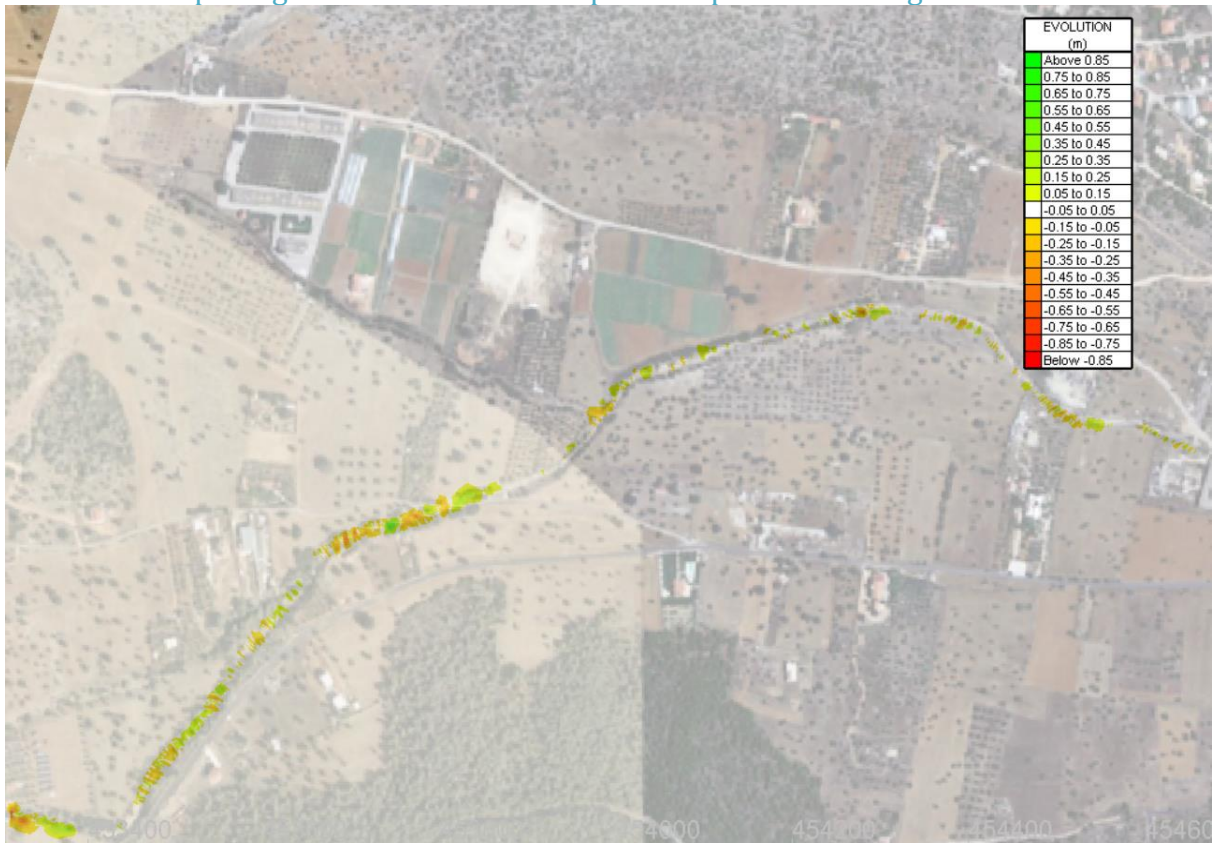


Figure 6.8. Geomorphological evolution due to the flood flows on the upstream part of the s. Aikaterini at 2 hours (above) and 4 hours (below) from the start of the simulation.

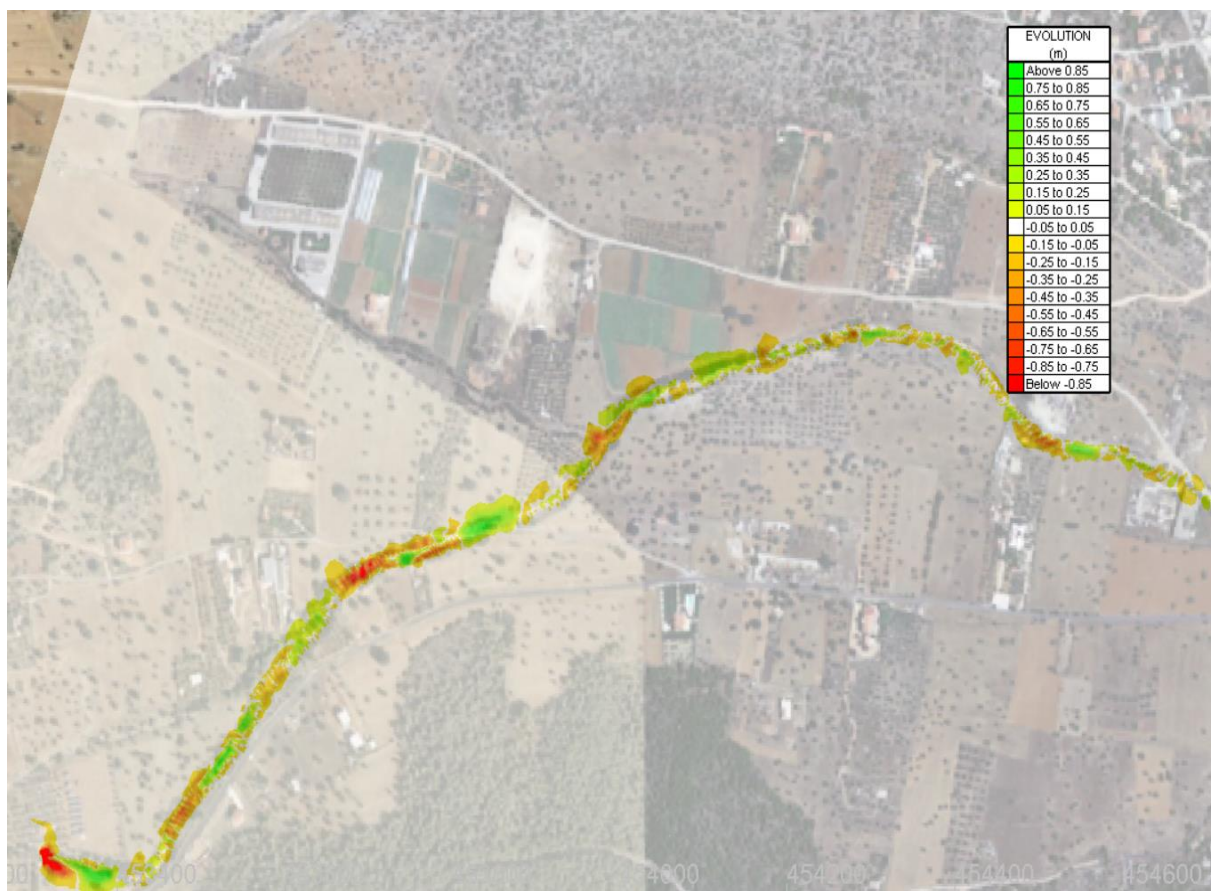
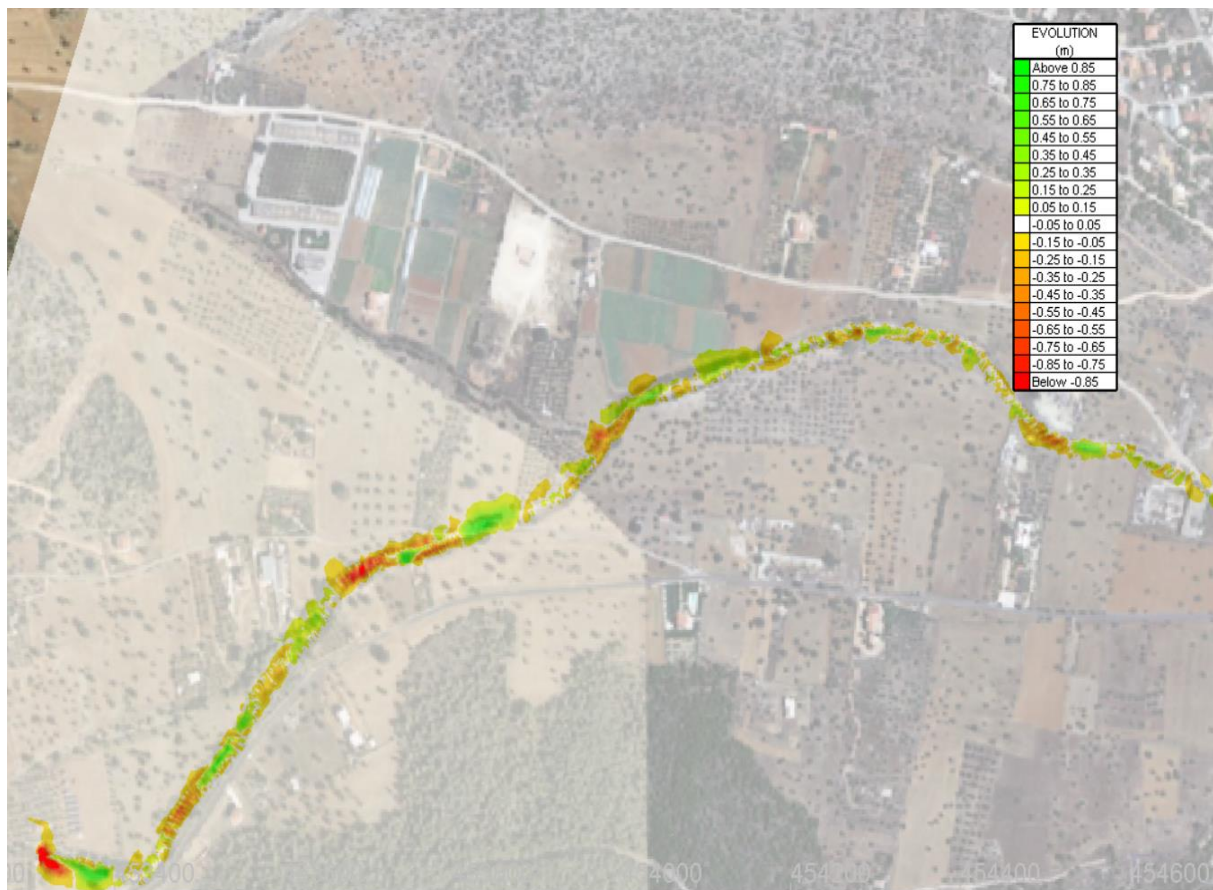


Figure 6.9. Geomorphological evolution due to the flood flows on the upstream part of the s. Aikaterini at 6 hours (above) and 8 hours (below) from the start of the simulation.

6.3.3. Geomorphological evolution of the cross-sectional profiles of Mandra streams

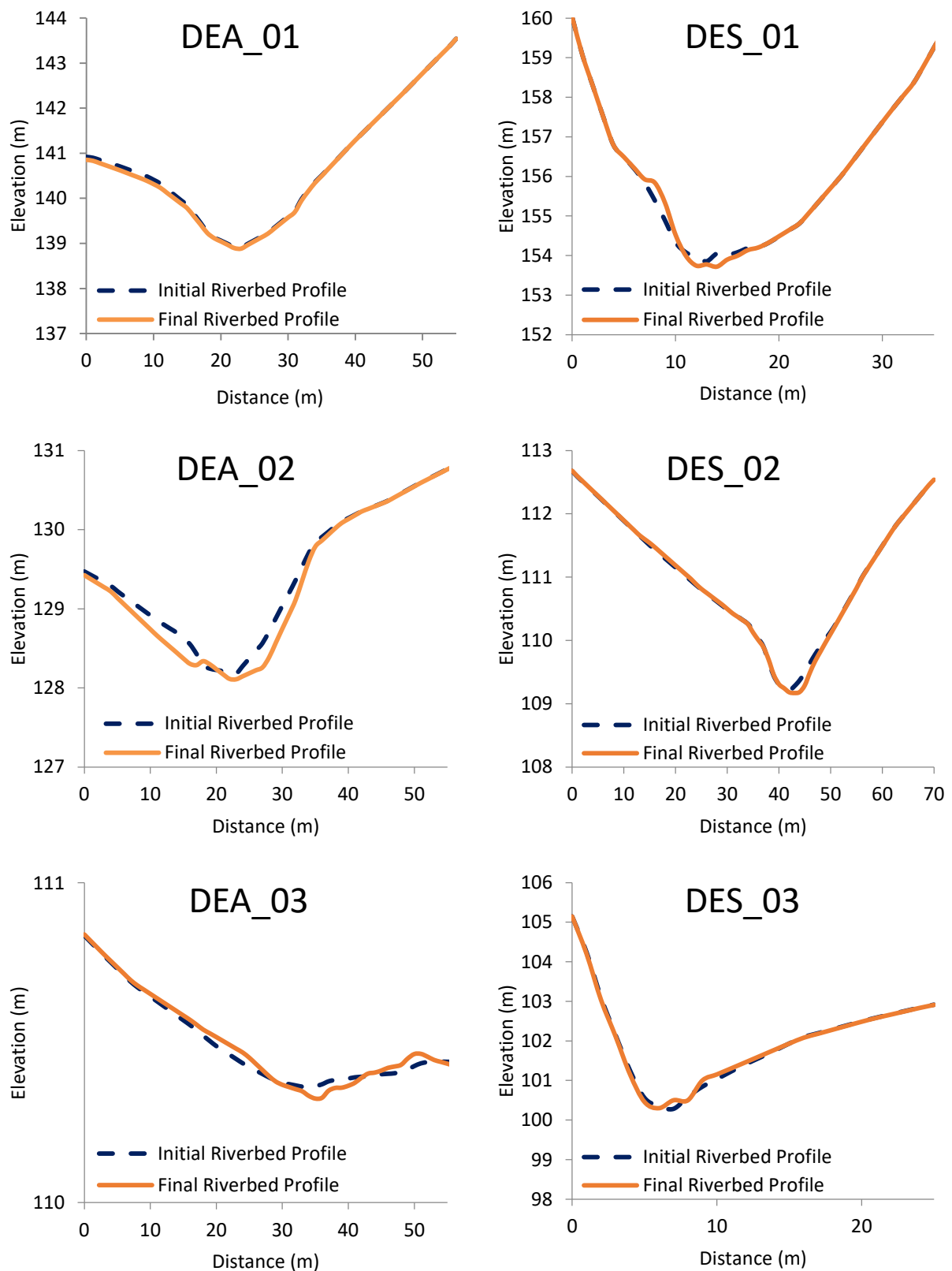


Figure 6.10. Geomorphological evolution due to the flood flow in selected cross-sections of the unregulated parts of the s. Sources (right) and the s. Agia Aikaterini (left).

6.3.4. Integrative model predictions of the flooded area

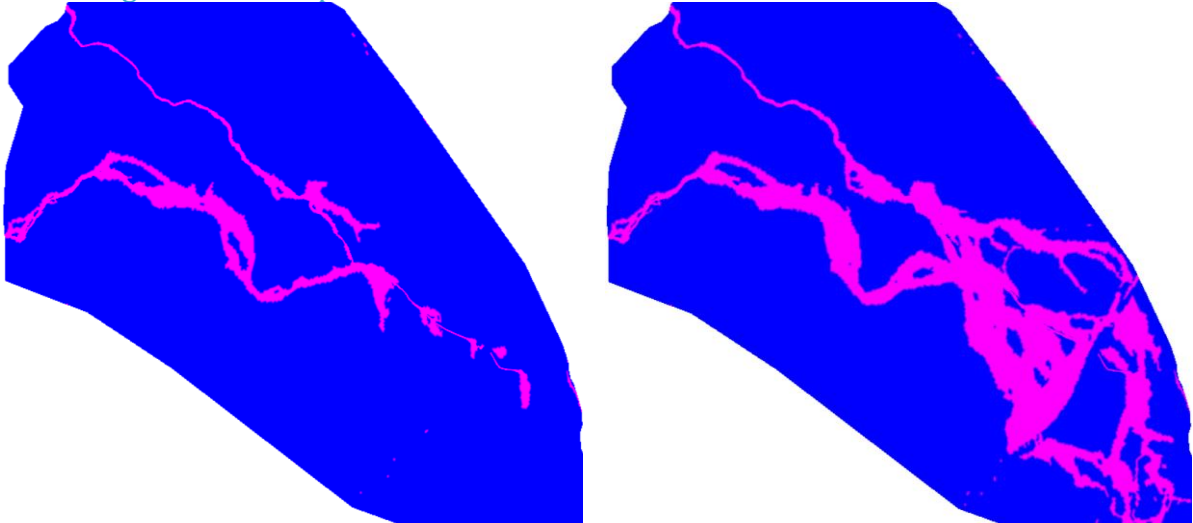


Figure 6.11. The model predictions concerning the flooded area at 2 hours (left) and 4 hours (right) after the start of the simulation.

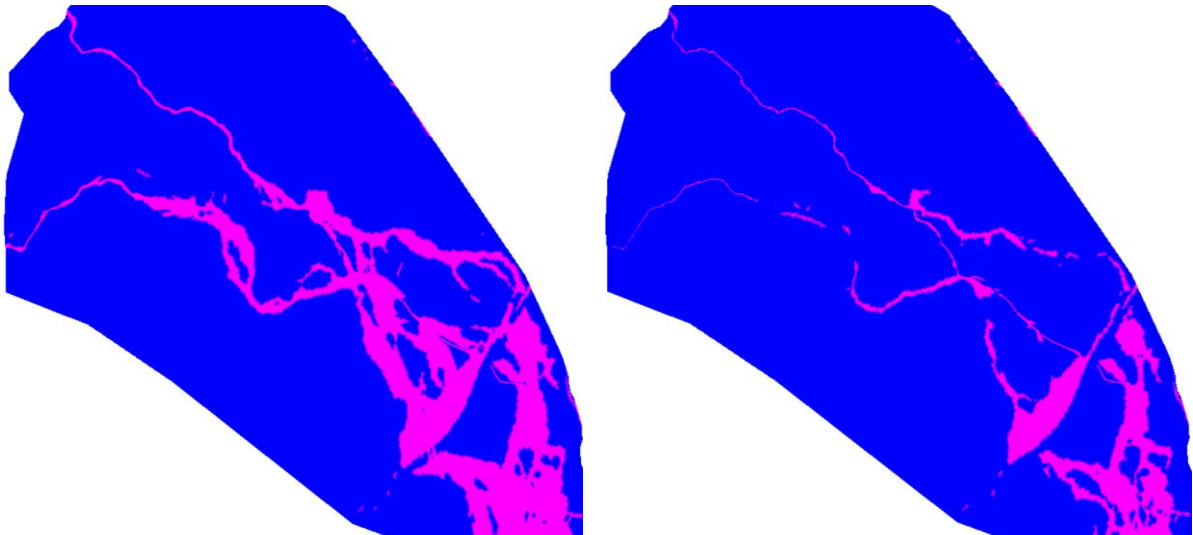


Figure 6.12. The model predictions concerning the flooded area at 6 hours (left) and 8 hours (right) after the start of the simulation.

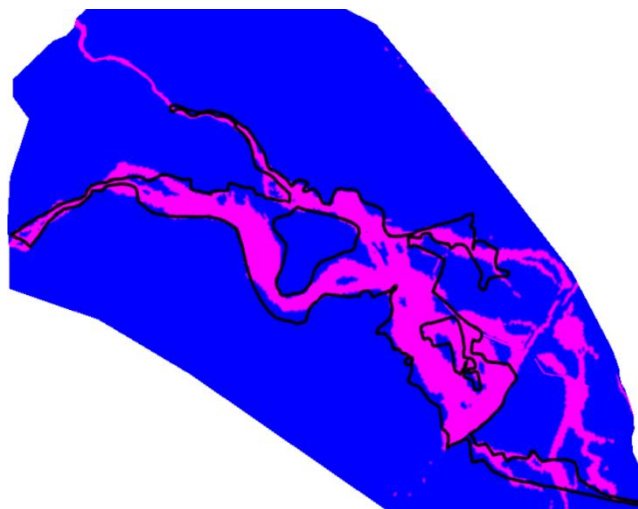


Figure 6.13. Comparison between the model predictions of the maximum flooded area (3.5 hours after the start of the computation) and the in situ measurements (black line).

6.4. Discussion of the results

In the diploma thesis study, the effect of the flood flows on river geomorphology was studied. TELEMAC-MASCARET system (Galand et al., 1991; Hervouet and Van Haren, 1996) was used for a fully coupled TELEMAC-2D/SISYPHE model of Mandra flood. The sediment transport/geomorphology model, currently at a preliminary stage, utilized the Engeland-Hansen & Chollet-Cunge sediment transport formula. Single-grain sediment simulation was conducted due to the lack of sedimentological data. Uniform diameter sediment of 0.63mm was used, corresponding to the borderline between sand and silt. The approach of A. Mendoza et al. (2017) was not followed, since it is recommended for meandering rivers and channel bends. The secondary current effect was not so profound in the flood flows predicted by the model. The Mandra flood integrative model results can be summed up to the following:

1. In the upstream part of the s. Soures intense erosion of the riverbed took place (Figures 6.6 and 6.7), that reached 2 m of scour and 1.5 m of deposition at around 4.5 hours after the start of the simulation.
2. The erosion in the s. Soures was characterized by scour along the stream banks and deposition along the central part of the cross-sections (Figures 6.6 and 6.7). This was less evident in the case of the s. Agia Aikaterini.
3. In the upstream part of the s. Agia Aikaterini (Figures 6.8 and 6.9) the geomorphological changes were smaller compared to the case of the s. Soures, but still substantial. This was attributed to the greater riverbed gradient of the last compared to the s. Agia Aikaterini. The maximum erosion occurred 5 hours after the start of the simulation. Maximum scour and deposition were predicted at 1.2 m and 1 m respectively.
4. There was a considerable lag between the time that maximum velocities and maximum erosion occurred in each area, which was about 1 hour.
5. The model prediction of the maximum flooded area was consistent with the measured one (Figure 6.13).
6. The effects of the geomorphological changes to the flooded area were found to be minimal.

6.5. Conclusions and suggestions for future work

The Mandra flood integrative model results were considered reasonable. The model is currently at a preliminary stage and needs to be validated with measurements concerning the geomorphological changes. Some suggestions about the mathematical simulation of the Mandra flood in future are the following:

1. The contribution of the geomorphological changes in the hydronamic flow regime should be studied, since many researchers (Rickenmann et al., 2015) have recently concluded that this effect may be substantial. This research could be conducted through comparison between predicted water depths and velocities of the clear water and integrative model along cross-sections in the computational domain.
2. Mandra flood erosion processes were characterized by debris flows, an effect that cannot be modelled with the TELEMAC-MASCARET system. Thus, simulations of a debris flow/geomorphological model are suggested.
3. Simulations of a multigrain scenario should be conducted, when sedimentological data are available. In that case a model utilizing Van Rijn sediment transport formula is suggested. Van Rijn formula predictions of the final riverbed morphology were consistent with the measurements in the Yen & Lee (1995) multigrain simulation.
4. Simulations of a mud-sand scenario also should be conducted in order to study the effect of cohesive sediment on the flow and the geomorphological processes.
5. The computational domain should be extended further upstream of the s. Soures in order to include the Kantines area from which sediment/debris flux occurred.
6. The division of the area of study in sub-areas with different sediment diameters corresponding to the geological data is also suggested.

7. Literature

1. Abad J. D., Buscaglia G. C., and Garcia M. H. (2008), 2D stream hydrodynamic, sediment transport and bed morphology model for engineering applications. *Hydrological Processes*, 22(10), 1443-1459.
2. Bui M. D., and Rutschmann P. (2010), Numerical modelling of non-equilibrium graded sediment transport in a curved open channel. *Computers & Geosciences*, 36, 6, 792-800.
3. Karamisheva R. D., Lyness J. F., Myers W. R. C., Cassells J. B. C., and O'Sullivan J. (2006), Sediment transport formulae for compound channel flows. *Proceedings of the Institution of Civil Engineers-Water Management*, 159(3), 183-193.
4. Lee K., Liu Y.L, and Cheng K.H. (2004), Experimental investigation of bedload transport processes under unsteady flow conditions. *Hydrological Processes*, 18(3), 2439-2454.
5. Mendoza A., Abad J. D., Langendoed E. J., Wang D., ASCE M., Wang D., Tassi P., and Abderrezzak K. E.K (2017). Effect of Sediment Transport Boundary Conditions on the Numerical Modeling of Bed Morphodynamics. *Journal of Hydraulic Engineering*, 143(4), 04016099.
6. Recking A. (2010), A comparison between flume and field bed load transport data and consequences for surface-based bed load transport prediction. *Water Resources Research*, 46, 1-16.
7. Rickenmann D., Badoux A., and Hunzinger L. (2016) Significance of sediment transport processes during piedmont floods: the 2005 flood events in Switzerland. *Earth Surface Processes and Landforms*, 41(2), 224-230.
8. Stamou (2018), The Disastrous Flash Flood of Mandra in Attica-Greece and now What? *Civil Engineering Research Journal*, 6(2), 2575-8950.
9. Talmon A. M., Struiksma N., and Van Mierlo M. C. L. M. (1995), Laboratory measurements of the direction of sediment transport on transverse alluvial-bed slopes. *Journal of Hydraulic Research*, 33(4), 495-517.
10. Villaret C., Hervouet J.-M., Kopmann R., Merkel U., and Davies A. G (2013), Morphodynamic modeling using the Telemac finite-element system. *Computers & Geosciences*, 53, 105-113.
11. Vu T. T., Nguyen P. K. T., Chua L. H. C., Law A. W. K. (2015), Two-Dimensional Hydrodynamic Modelling of Flood Inundation for a part of the Mekong River with TELEMC-2D, *British Journal of Environment & Climate Change*, 5(2):162-175.
12. Wang J.-P., and Liang Q. (2011), Testing a new adaptive grid-based shallow flow model for different types of flood simulations. *Journal of Flood Risk Management*, 4(2), 96-103.
13. Xiao Y., Shao X., Wang H., and Zhou G. (2012), Formation process of meandering channel by a 2D numerical simulation. *International Journal of Sediment Research*, 27(3), 306-322.
14. Yilmaz L. (2007), Experimental Study of Sediment Transport in Meandering Channels. *Water Resources Management*, 22(2), 259-275.

Manuals:

- Ata R. (2017), *Telemac2d User Manual*
- Tassi P. (2017), *Sisyphé User Manual*
- Canadian Hydraulics Centre, National Research Council (2011), *Blue Kenue Reference Manual*


```

C
  INTEGER          :: I
  DOUBLE PRECISION :: PHI(NPOIN)
!   DOUBLE PRECISION, PARAMETER :: ACOEFF = 0.004D0 ! Sediment transport
!   param (m^2s^-1)
!
!=====
!
!                               PROGRAM
!=====
!
!
!   CHENG (2002) TYPE
!
  DO I = 1, NPOIN

    PHI(I) = 13.0 * TETAP%R(I) ** 1.5 * EXP(-0.05 / TETAP%R(I) ** 1.5)
    QSC%R(I) = PHI(I)
    QSS%R(I) = 0.D0

  END DO

!
!-----
!
  RETURN
  END

```



```

!
!=====
!=====
!
!                                PROGRAM                                !
!=====
!=====
!
!*****ROTTNER BED LOAD FORMULA*****!

DO I = 1, NPOIN
UTOT(I)=SQRT(U2D%R(I)**2+V2D%R(I)**2)
TERM1(I)=SQRT(GRAV*DENS*DM**3)
TERM2(I)=UTOT(I)/SQRT(DENS*GRAV*DM)
TERM3(I)=0.667*((DM/HN%R(I))**(2/3)-0.14)
PAR(I)=TERM2(I)*TERM3(I)-0.778*(DM/HN%R(I))
QSC%R(I) = TERM1(I)*PAR(I)
QSS%R(I) = 0.D0
ENDDO

!
! EXAMPLE BY VAN RIJN
!
! C1 = DENS * GRAV * DM
! C2 = 0.053D0 * SQRT(DM**3*DENS*GRAV) * DSTAR**(-0.3D0)
!
! DO I = 1, NPOIN
!
!     TRANSPORT STAGE PARAMETER
!
!     IF(TETAP%R(I) .LE. AC) THEN
!         T = 0.D0
!     ELSE
!         T = (TETAP%R(I)-AC)/MAX(AC,1.D-06)
!     ENDIF
!
!     BEDLOAD TRANSPORT RATE
!
!     QSC%R(I) = C2 * T**2.1D0
!     QSS%R(I) = 0.D0
!
! ENDDO
!
! FOLLOWING LINES NEED TO BE COMMENTED OUT
!
c$$$!     IF(LNG.EQ.1) WRITE(LU,52)
c$$$!     IF(LNG.EQ.2) WRITE(LU,53)
c$$$!!
c$$$!52     FORMAT(/,1X,' STOP :',/
c$$$!     &         ,1X,' LE TAUX DE TRANSPORT DOIT ETRE CALCULE DANS QSFORM')
c$$$!53     FORMAT(/,1X,'SISYPHE IS STOPPED : ',/
c$$$!     &         ,1X,' SAND TRANSPORT MUST BE CALCULATED IN QSFORM')
c$$$!     CALL PLANTE(1)
c$$$!     STOP
!
!-----
!
RETURN
END

```



```

DOUBLE PRECISION :: TERM2 (NPOIN) , TERM3 (NPOIN)
DOUBLE PRECISION :: USTAR (NPOIN) , UTOT (NPOIN)
!
!=====
!=====
!
!                                PROGRAM
!=====
!=====
!
!*****KARIM AND KENNEDY TOTAL LOAD FORMULA*****!

DO I = 1, NPOIN
  IF (TOB%R(I) .GT. 0.D0) THEN
    USTAR(I) = (TOB%R(I) / XMVE) ** 0.5
  ELSE
    USTAR(I) = 0.D0
  END IF
  UTOT(I) = SQRT (U2D%R(I) ** 2 + V2D%R(I) ** 2)
  TERM1(I) = (ABS (UTOT(I)) / SQRT (GRAV * DENS * DM)) ** 2.97
  TERM2(I) = (USTAR(I) / XWC) ** 1.47
  TERM3(I) = SQRT (GRAV * DENS * DM ** 3)
  QSC%R(I) = k1 * TERM1(I) * TERM2(I) * TERM3(I)
  QSS%R(I) = 0.D0
END DO

!
! EXAMPLE BY VAN RIJN
!
! C1 = DENS * GRAV * DM
! C2 = 0.053D0 * SQRT (DM ** 3 * DENS * GRAV) * DSTAR ** (-0.3D0)
! DO I = 1, NPOIN
!   TRANSPORT STAGE PARAMETER
!   IF (TETAP%R(I) .LE. AC) THEN
!     T = 0.D0
!   ELSE
!     T = (TETAP%R(I) - AC) / MAX (AC, 1.D - 06)
!   ENDIF
!   BEDLOAD TRANSPORT RATE
!   QSC%R(I) = C2 * T ** 2.1D0
!   QSS%R(I) = 0.D0
!
!   ENDDO
!
! FOLLOWING LINES NEED TO BE COMMENTED OUT
!
!$$$!      IF (LNG.EQ.1) WRITE (LU, 52)
!$$$!      IF (LNG.EQ.2) WRITE (LU, 53)
!$$$!!
!$$$!52    FORMAT (/ , 1X, ' STOP : ', /
!$$$!      &      , 1X, ' LE TAUX DE TRANSPORT DOIT ETRE CALCULE DANS QSFORM')
!$$$!53    FORMAT (/ , 1X, 'SISYPHE IS STOPPED : ', /
!$$$!      &      , 1X, ' SAND TRANSPORT MUST BE CALCULATED IN QSFORM')
!$$$!      CALL PLANTE(1)
!$$$!      STOP
!
!-----
!
RETURN
END

```



```

=====
=====
!
!                                     PROGRAM
!
=====
=====

! ---> Global Parameters
      B=5.D0

      DO I=1,NPOIN

        MI(I)=18*LOG10(12*HN%R(I)/(1.4*DM))
1       / (18*LOG10(12*HN%R(I)/(2.0*DM))

        USTAR(I)=SQRT(TOB%R(I)/XMVE)

        UTOT(I)=SQRT(U2D%R(I)**2+V2D%R(I)**2)

        STR(I)= -0.27*DM*(DENS+1)*XMVE*GRAV/(TOB%R(I)*MI(I))
        QSC%R(I)=B*EXP(STR(I))*DM*USTAR(I)*MI(I)
        QSS%R(I)=0.D0

      END DO

!
!
! EXAMPLE BY VAN RIJN
! C1 = DENS * GRAV * DM
! C2 = 0.053D0 * SQRT(DM**3*DENS*GRAV) * DSTAR**(-0.3D0)
! DO I = 1, NPOIN
!   TRANSPORT STAGE PARAMETER
!
!   IF(TETAP%R(I) .LE. AC) THEN
!     T = 0.D0
!   ELSE
!     T = (TETAP%R(I)-AC)/MAX(AC,1.D-06)
!   ENDIF
!
!   BEDLOAD TRANSPORT RATE
!
!   QSC%R(I) = C2 * T**2.1D0
!   QSS%R(I) = 0.D0
!
! ENDDO
!
! FOLLOWING LINES NEED TO BE COMMENTED OUT
!
!$$      IF(LNG.EQ.1) WRITE(LU,52)
!$$      IF(LNG.EQ.2) WRITE(LU,53)
!
!$$$52   FORMAT(/,1X,' STOP :',/
!$$      &      ,1X,' LE TAUX DE TRANSPORT DOIT ETRE CALCULE DANS QSFORM')
!$$$53   FORMAT(/,1X,'SISYPHE IS STOPPED : ',/
!$$      &      ,1X,' SAND TRANSPORT MUST BE CALCULATED IN QSFORM')
!$$      CALL PLANTE(1)
!$$      STOP
!
!-----
!
RETURN
END

```



```

=====
=====
!
!                                     PROGRAM
!
=====
=====
!

!*****NIELSEN (1992) BED LOAD FORMULA*****!

      COEF=DENS*GRAV*DM*XMVE
      TERM1=SQRT (GRAV*DENS*DM**3)
      DO I = 1, NPOIN
      TERM2 (I)=12.0*TOB%R (I) /COEF-0.05
      TERM3 (I)=SQRT (TOB%R (I) /COEF)
      QSC%R (I) = TERM1*TERM2 (I) *TERM3 (I)
      QSS%R (I) = 0.D0
      ENDDO

!
!   EXAMPLE BY VAN RIJN
!
!   C1 = DENS * GRAV * DM
!   C2 = 0.053D0 * SQRT (DM**3*DENS*GRAV) * DSTAR** (-0.3D0)
!
!   DO I = 1, NPOIN
!
!       TRANSPORT STAGE PARAMETER
!
!       IF (TETAP%R (I) .LE. AC) THEN
!           T = 0.D0
!       ELSE
!           T = (TETAP%R (I) -AC) /MAX (AC,1.D-06)
!       ENDIF
!
!       BEDLOAD TRANSPORT RATE
!
!       QSC%R (I) = C2 * T**2.1D0
!       QSS%R (I) = 0.D0
!
!   ENDDO
!
!   FOLLOWING LINES NEED TO BE COMMENTED OUT
!
c$$$!       IF (LNG.EQ.1) WRITE (LU,52)
c$$$!       IF (LNG.EQ.2) WRITE (LU,53)
c$$$!!
c$$$!52    FORMAT (/ ,1X, ' STOP :', /
c$$$!      &      ,1X, ' LE TAUX DE TRANSPORT DOIT ETRE CALCULE DANS QSFORM')
c$$$!53    FORMAT (/ ,1X, 'SISYPHE IS STOPPED : ', /
c$$$!      &      ,1X, ' SAND TRANSPORT MUST BE CALCULATED IN QSFORM')
c$$$!      CALL PLANTE (1)
c$$$!      STOP
!
!-----
!
RETURN
END

```



```

!
!=====
!=====
!
!                                PROGRAM                                !
!=====
!=====

! ---> Global Parameters

      Alfa   = 1/(3*DM)
!      RhoSW  = Me%Density / Me%ExternalVar%WaterDensity

      if (DSTAR.GT.60.) then
        Vn = 0.00
        Va = 0.17
        Vm = 1.78      ! 1.5 in 1973 version
        Vc = 0.025
      else
        Vn = 1.-0.56*Log10(DSTAR)
        Va = 0.14+0.23/(SQRT(DSTAR))
        Vm = 1.67+6.83/DSTAR                                ! 1.34+9.66
/DSTAR in 1973 version
        Vc1= 2.79*Log10(DSTAR)-0.98*(Log10(DSTAR))**2.-
3.46 ! 2.86*Log10(DSTAR)-(Log10(DSTAR))**2.-3.53 in 1973 version
        Vc = 10.**(Vc1)
      endif

      ! ---> Sediment Mobility (Fgr)

DO I=1,NPOIN

  USTAR(I)=SQRT( (TOB%R(I)/XMVE)
  UTOT(I)=SQRT( (U2D%R(I)**2+V2D%R(I)**2)

  Fgr1(I) = USTAR(I)**Vn/(SQRT(GRAV*DM*DENS))
  Fgr2(I) = SQRT(32.0)*Log10(Alfa*HN%R(I)/DM)
  Fgr(I) = Fgr1(I)*(UTOT(I)/Fgr2(I))**(1-Vn)

! ---
> Sediment Transport (Ggr e m3/s de sedimento por m3/s de fluxo de agua)

  Ggr1(I) = Fgr(I)/Va
  if (Ggr1(I).GE.1.) then
    Ggr(I) = Vc*(Ggr1(I)-1)**Vm
    S1(I)=(USTAR(I)/UTOT(I))

!Me%TransportCapacity(i, j) = Ggr*RhoSW*Me%D35%Field2D(I,J)/S
! (m)
1   QTR(I) = Ggr(I)*DM/S1(I)                                ! (m)

! [m3/s/m] = [m/s]*[m]
  QSC%R(I) = UTOT(I) * Ggr(I)

  else
    QSC%R(I) = 0.D0

```

```

endif

QSS%R(I) = 0.D0

end do

!
! EXAMPLE BY VAN RIJN
!
! C1 = DENS * GRAV * DM
! C2 = 0.053D0 * SQRT(DM**3*DENS*GRAV) * DSTAR**(-0.3D0)
!
! DO I = 1, NPOIN
!
!     TRANSPORT STAGE PARAMETER
!
!     IF(TETAP%R(I) .LE. AC) THEN
!         T = 0.D0
!     ELSE
!         T = (TETAP%R(I)-AC)/MAX(AC,1.D-06)
!     ENDIF
!
!     BEDLOAD TRANSPORT RATE
!
!     QSC%R(I) = C2 * T**2.1D0
!     QSS%R(I) = 0.D0
!
! ENDDO
!
! FOLLOWING LINES NEED TO BE COMMENTED OUT
!
!$$     IF(LNG.EQ.1) WRITE(LU,52)
!$$     IF(LNG.EQ.2) WRITE(LU,53)
!
!$$$2   FORMAT(/,1X,' STOP :',/
!$$     &       ,1X,' LE TAUX DE TRANSPORT DOIT ETRE CALCULE DANS QSFORM')
!$$$3   FORMAT(/,1X,'SISYPHE IS STOPPED : ',/
!$$     &       ,1X,' SAND TRANSPORT MUST BE CALCULATED IN QSFORM')
!$$     CALL PLANTE(1)
!$$     STOP
!
!-----
!
RETURN
END

```



```

!
!=====
!=====
!
!                                PROGRAM
!
!=====
!=====
!
!*****YANG LIM TOTAL LOAD FORMULA*****!

DO I = 1, NPOIN
  USTAR(I)=SQRT(TOB%R(I)/XMVE)
  UCR(I)=SQRT(TAUP%R(I)/XMVE)
  TERM(I)=(USTAR(I)**2-UCR(I)**2)/XWC
  IF (USTAR(I).GT.OCR(I)) THEN
    QSC%R(I) = k2*(DENS+1)*TOB%R(I)*TERM(I)/(XMVE*DENS)
  ELSE
    QSC%R(I)= 0.D0
  END IF
  QSS%R(I) = 0.D0
ENDDO

!
! EXAMPLE BY VAN RIJN
!
! C1 = DENS * GRAV * DM
! C2 = 0.053D0 * SQRT(DM**3*DENS*GRAV) * DSTAR**(-0.3D0)
!
! DO I = 1, NPOIN
!
!   TRANSPORT STAGE PARAMETER
!
!   IF(TETAP%R(I) .LE. AC) THEN
!     T = 0.D0
!   ELSE
!     T = (TETAP%R(I)-AC)/MAX(AC,1.D-06)
!   ENDIF
!
!   BEDLOAD TRANSPORT RATE
!
!   QSC%R(I) = C2 * T**2.1D0
!   QSS%R(I) = 0.D0
! ENDDO
! FOLLOWING LINES NEED TO BE COMMENTED OUT
!
c$$$!      IF(LNG.EQ.1) WRITE(LU,52)
c$$$!      IF(LNG.EQ.2) WRITE(LU,53)
c$$$!!
c$$$!52    FORMAT(/,1X,' STOP :',/
c$$$!      &      ,1X,' LE TAUX DE TRANSPORT DOIT ETRE CALCULE DANS QSFORM')
c$$$!53    FORMAT(/,1X,'SISYPHE IS STOPPED : ',/
c$$$!      &      ,1X,' SAND TRANSPORT MUST BE CALCULATED IN QSFORM')
c$$$!      CALL PLANTE(1)
c$$$!      STOP
!
!-----
!
RETURN
END

```